

Building Pathology and Rehabilitation



João M. P. Q. Delgado *Editor*

Building Rehabilitation and Sustainable Construction

 Springer

Building Pathology and Rehabilitation

Volume 23

Series Editors

Vasco Peixoto de Freitas, University of Porto, Porto, Portugal

Aníbal Costa, Aveiro, Portugal

João M. P. Q. Delgado , University of Porto, Porto, Portugal

This book series addresses the areas of building pathologies and rehabilitation of the constructed heritage, strategies, diagnostic and design methodologies, the appropriateness of existing regulations for rehabilitation, energy efficiency, adaptive rehabilitation, rehabilitation technologies and analysis of case studies. The topics of Building Pathology and Rehabilitation include but are not limited to - hygrothermal behaviour - structural pathologies (e.g. stone, wood, mortar, concrete, etc...) - diagnostic techniques - costs of pathology - responsibilities, guarantees and insurance - analysis of case studies - construction code - rehabilitation technologies - architecture and rehabilitation project - materials and their suitability - building performance simulation and energy efficiency - durability and service life.

More information about this series at <https://link.springer.com/bookseries/10019>

João M. P. Q. Delgado
Editor

Building Rehabilitation and Sustainable Construction

 Springer

Editor

João M. P. Q. Delgado
CONSTRUCT-LFC
Department of Civil Engineering
Faculty of Engineering
University of Porto
Porto, Portugal

ISSN 2194-9832

ISSN 2194-9840 (electronic)

Building Pathology and Rehabilitation

ISBN 978-3-030-95486-4

ISBN 978-3-030-95487-1 (eBook)

<https://doi.org/10.1007/978-3-030-95487-1>

© The Editor(s) (if applicable) and The Author(s), under exclusive license to Springer Nature Switzerland AG 2022

This work is subject to copyright. All rights are solely and exclusively licensed by the Publisher, whether the whole or part of the material is concerned, specifically the rights of translation, reprinting, reuse of illustrations, recitation, broadcasting, reproduction on microfilms or in any other physical way, and transmission or information storage and retrieval, electronic adaptation, computer software, or by similar or dissimilar methodology now known or hereafter developed.

The use of general descriptive names, registered names, trademarks, service marks, etc. in this publication does not imply, even in the absence of a specific statement, that such names are exempt from the relevant protective laws and regulations and therefore free for general use.

The publisher, the authors and the editors are safe to assume that the advice and information in this book are believed to be true and accurate at the date of publication. Neither the publisher nor the authors or the editors give a warranty, expressed or implied, with respect to the material contained herein or for any errors or omissions that may have been made. The publisher remains neutral with regard to jurisdictional claims in published maps and institutional affiliations.

This Springer imprint is published by the registered company Springer Nature Switzerland AG
The registered company address is: Gewerbestrasse 11, 6330 Cham, Switzerland

Preface

Building pathology is the systematic treatment of building defects, causes and consequences. The type of defect may vary widely, from a minor crack to a major collapse. Obviously, the last one implies a failure and the termination of required use. Building rehabilitation is an important subject to alert all the stakeholders for the need for preservation and rehabilitation of the built heritage, and to alert them for the most current causes of building pathologies associated with incorrect design and construction deficiencies. This knowledge is crucial to recognize the most important building pathologies, determine their possible causes and define the corresponding rehabilitation solution. To provide resilient solutions, a simple optimization of individual technologies will not be sufficient. Each system interacts with others on different scales, i.e., materials, components, buildings, cities; and domains such as ecology, economy and social. More precisely, at this time of knowledge, building rehabilitation should be always linked with sustainable construction.

Sustainable construction is the practice of creating a healthy environment that is based on ecological principles. In other words, the main goal of sustainable construction is to reduce the industry's impact on the environment by utilizing sustainable development practices, employing energy efficiency and taking advantage of green technology. There are two things that go into sustainable construction: the materials used and the methods employed.

The main purpose of this book, *Building Pathologies and Sustainable Construction*, is to provide a collection of recent research works related to building pathologies, recycled materials, case studies and practical advice on the implementation of sustainable construction.

The book is divided in seven chapters that intend to be a resume of the current state of knowledge for benefit of professional colleagues, scientists, students, practitioners, lecturers and other interested parties to network. At the same time, these topics will be going to the encounter of a variety of scientific and engineering disciplines, such as civil, mechanical and materials engineering.

Porto, Portugal

João M. P. Q. Delgado

Contents

Application of Indo-Saracenic Style in Architectural Design Process	1
Prafulla Parlewar	
Design of Structure for Steam Turbine Generator	13
Prafulla Parlewar	
Fiber Optic Sensors to Perform Structural Health Monitoring of Concrete Structures Affected by Internal Swelling Reactions	29
K. K. Santos Silva, F. A. N. Silva, T. Mahfoud, A. Khelidj, A. C. Azevedo, and J. M. P. Q. Delgado	
Evaluation of Lime Solution in Kneading Water for the Preparation of Roughcast and Plaster Coating	55
A. M. Santos, A. J. Costa e Silva, J. M. Freitas Mota, J. M. P. Q. Delgado, F. A. N. Silva, and A. C. Azevedo	
Technological Performance of Cellulose Fibre Reinforced Cement-Based Mortars	83
E. C. L. Rezende, A. J. Costa e Silva, J. M. P. Q. Delgado, and A. C. Azevedo	
Use of Construction Waste to Replace Conventional Aggregate in Reinforced Concrete Production	109
F. A. N. Silva, M. T. A. Silva, F. A. F. Lopes, J. M. P. Q. Delgado, and A. C. Azevedo	
Thermal Performance of Dwellings: Comparative Study Between Simulation Methods with NBR 15,575 (2013) and NBR 15,575 (2021)	123
M. M. Barbosa, P. E. Silva de Oliveira, A. J. Costa e Silva, J. M. P. Q. Delgado, and A. C. Azevedo	

Application of Indo-Saracenic Style in Architectural Design Process



Prafulla Parlewar

Abstract The heritage architecture in British period in Asia was influenced under the Indo-Saracenic architecture style. This style was also known as Neo-Gothic style of architecture. It was used by British engineer and architects in many buildings during colonial period. The famous British architect George Wittet designed Gateway of India, General Post Building and Prince of Wales Museum in Mumbai (Bombay), India. In his design he used design parameter of Indo-Saracenic architecture. But, after the independence, buildings were rehabilitated for new uses. Particularly, the Prince of Wales Museum is now adapted into new galleries as per the modern requirements. In this rehabilitation process, original architecture style is lost. The chapter here illustrates a project of design of gallery in which the original Indo-Saracenic style of architecture was conserved in the rehabilitation process of the building. The research here illustrates what is the Indo-Saracenic style of architecture? What is architectural design process? How to apply the Indo-Saracenic style of architecture in the architectural design process? Thus, the research illustrated the methods to conserve the historic buildings by retaining the original styles of architecture.

Keywords Building pathology · Architectural design process · Rehabilitation · Indo-Saracenic style

1 Introduction

The historic building rehabilitation has been a challenging design task for the engineers and architects. The rehabilitation of historic building requires a complex knowledge of the building pathology. This includes investigation and research on the structural and architectural condition of the building during colonial period. Many historic buildings have complex structural systems and innovative architecture of the historic period. These innovations of engineering and architecture make the heritage building unique and impose challenges for rehabilitation. One such project was planned for

P. Parlewar (✉)
City Development Corporation (P) Ltd., Mumbai, India

Chhatrapati Shivaji Maharaj Vastu Sangrahalaya (Prince of Wales Museum) in Mumbai, India. The Prince of Wales Museum was designed by British architect George Wittet. The museum was designed in year 1909. The building was constructed in the memories of visit of Prince of Wales to India. Architect George Wittet was also assigned to design famous Gateway of India and General Post Building in Fort, Mumbai, India. The significant part of this design was the use of Indo-Saracenic architecture in the building.

As the time passes, the historic buildings have changes in uses, utilities and design. Hence, the Prince of Wales museum underwent many changes in construction of new galleries and exhibition places and museum stores. The project includes a design of the new gallery in an open area used for circulation to connect various areas in the first floor of the museum. The design vision of the gallery was to keep the natural ventilation of the building. Importantly, the rehabilitation process was designed with a concept of reusing the existing style of indo-Saracenic architecture. Yet, the gallery was to integrate with modern architecture and services.

Alexander in his books “The timeless way of building” and “A pattern language” has introduced a theory and practical approach to architectural and urban design (Alexander 1977a and 1979b). For architecture to occur, the properties of formal composition need to be strongly influenced by the social context of space. The presence of the presence of the human body brings events, circulation sequence, procession, presence and occupation into architectural syntax (Plowright 2014). Even in education of architectural design, the knowledge of design process and applying various innovative methods are researched by many authors. The design studio is concerned with the definition of design education, its problems, relations and contents at sociological level and its relation to other disciplines at epistemological level (Demirbas 2003). So, it is important to understand the architectural design process and develop pedagogy in it. Pre-design, schematic design, and design development are the three phases of the design process implemented in educational design studios of architectural design courses. The construction of documents phase is implemented through working and drawing courses. The negotiation and construction phases are not implemented in educational studios (Soliman 2017). Thus, understanding the architectural design process is an major area of research in architectural education and practice.

2 Historic Building Rehabilitation

The rehabilitation of historic building includes complex understanding of the engineering and architecture. This includes a process to understand the original architectural language of the building for modern adaptive reuse. Many of the historic buildings are designed by original architect with innovative material and technology of original times. So, the methods for rehabilitation of historic building includes: (a) conditional basement of structural system, (b) existing vitalities of heritage and (c) adaptive reuse of the building. The conditional assessment of the building includes

identifying the structural stability of the building for future sustainability. Most of the historic building undergoes deterioration due to natural forces. So, stability analysis provided knowledge of the condition of the building. This stability analysis is many times undertaken through the non-destructive test like rebound hammer test, ultrasonic pulse velocity test, concrete core sample test, load test and others.

In the second part, it is important to access the architecture style of the building. More importantly, one has to understand the vitalities of the existing architecture. These vitalities includes the architectural style, the spatial system and construction technology inside the building. In the process of adaptive reuse, the vitalities play a significant role in rehabilitation the building. So, many times the rehabilitation can be undertaken by adaptive reuse of the similar style in new design. This approach conserves the original architecture. Thus, it also merges old design with the new rehabilitation.

3 Indo-Saracenic Architecture

The Prince of Wales Museum was designed with the Indo-Saracenic style of architecture in year 1909. Indo-Saracenic style also refers as Neo-Gothic style. Generally, the concept of Indo-Saracenic refers to represent the element of local architecture. So, the building designs suitable to local context. The architect George Witted vision of the design of the Indo-Saracenic style of architecture includes similar vision to reflect the local context of design.

Generally, before 1857, European classical style originated from Greek and Roman period was used in design by the architects. These may be some time similar to renaissance architecture. Many architects used monumental style of building similar to Greek architecture and influence them to become major landmarks. Particularly, these gave an impression of colonial power and status. Hence, the old design principals significantly defined a different style of architecture.

The buildings built in India by Indo-Saracenic style of architecture were built according to advanced British structural engineering standards of the 1800's including infrastructures of iron, steel and poured concrete. These type of buildings were employed with domes, pointedarch, vaulted roofs, pinnacles, minarets, pierced open arcade and open pavilions. It is an indispensable overview to one of civilizations most resplendent artistic traditions (Sheeba et al. 2018). Basically, it was an attempt by the colonial administration to "Orientalise" typically Western tastes and forms in the hope that it would appeal in the Indian subjects. It was particularly prominent in Madras (Now Chennai) and later spread to other parts of India. However, Indo-Saracenic buildings were much prized in the communities in which they are built. This could have been due to their innovative and "magical" appearance or, by comparison to native secular architecture, a style which seemed to incorporate a grand use of European and Indian elements. The appeal rested on the twin functions of association and sensual effect. Indo-Saracenic architect, like sculpture, struck popular imagination by the size of its building, mass space, color and texture. These

buildings are confined to public spaces like government offices, municipalities, law courts, colleges, museums and art galleries and therefore enjoyed great visibility (Baweja 2018). An assertive character permeates Indian architecture throughout the recognized periods in history and each period has seen a conscious mixing of styles and the creation of a new hybrid architecture. One such initiative, gave birth to the Indo-Saracenic Architecture style, an eclectic mix of European, Hindu and Mughal building elements. Despite being a symbol of colonialism, the Indo-Saracenic architecture was “modern” and incorporated much of the taste of its time. The style has been an inspiration to a lot of public and administrative architecture of the post independent India (Choudhary et al. 2018). In the Law Courts of Madras, India this structure was inspired by the functional layout of the Gothic Law courts of London, but designed as a celebration of the Indo-Saracenic style, taking forward the ideas of Chisholm at the Senate House. This building was initially designed by J. W. Brassington and developed by Henry Irwin; modifications were incorporated by the supervising engineer J. H. Stephens during construction. Begin in 1889, it took four years to be completed (Grover 2014).

In India during the colonial period, the public structures reflect the British imperial position as rulers. The main purposed of the design of these building was the representation of empirical rules in the colonies. The British colonies thus took substantial link of the Mughal political system to dominate the locals. So, the architecture was developed with mix of British, Hindu and Mughal architecture elements. The overall objective of the architect was to design the building which can dominantly show the British rules, yet, provide and local use of technically and styles. Thus, the Indo-Saracenic architecture was introduced by many architect like Robert F. Chisholm, Charles Mant, Henry Irwin, William Emerson, George Wittet and others. The Indo-Saracenic style of architecture include following element of design (1) British, (2) Hindu and (3) Mughal design elements.

The Prince of Wales Museum is designed with a British architecture style by use of grand scale structure to represent monumentality. Apparently, monumentality represents colonial grandness and rule over India. Secondly, monumental scale makes the building look landmark in surrounding. Symmetry was an important principle of design with use of large central lobby. It has two wings to balance the three dimensional massing and two dimensional planning in the building. Architecture of building also incorporates the axial design system. Complete form of the building is designed on two axis like x and y. This axial pattern is followed in many small and medium design elements to make a visually dominant, yet simple architecture for human vision (Parlewar 2021a, b).

The geometry and axis are the major features of colonial principals of planning as they have to indicate the monumentality. So, in Prince of Wales Museum, it is found that the geometry (Fig. 1) is developed by design of central lobby and two large wings for gallery in both side of the building. The geometry is developed in modular forms. The square grid is evident in plan and elevations. This geometry has reached in architecture right form the period of golden means in architecture. Second part of the design ideas are use of axis like x and y in to get the complete building symmetrically organized structurally for making easy load transfer. Also, the axial pattern helps the

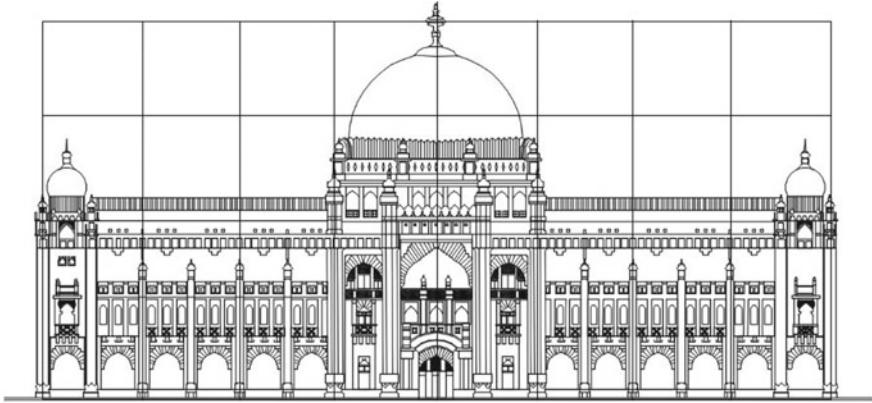
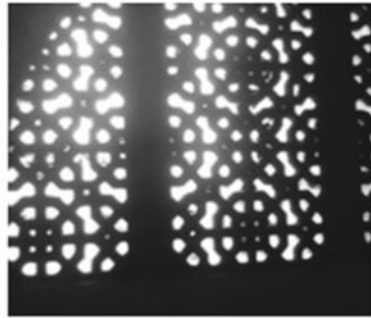


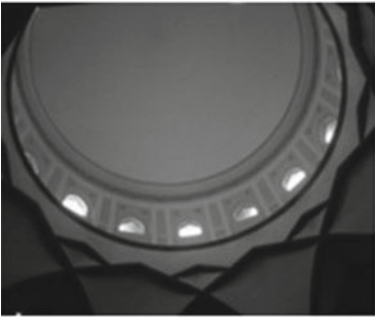
Fig. 1 Elevation of building showing Indo-Saracenic architecture



a



b



c



d

Fig. 2 a Hindu arches, b Islamic grid pattern, c Gothic dome, and d Islamic pointed arches

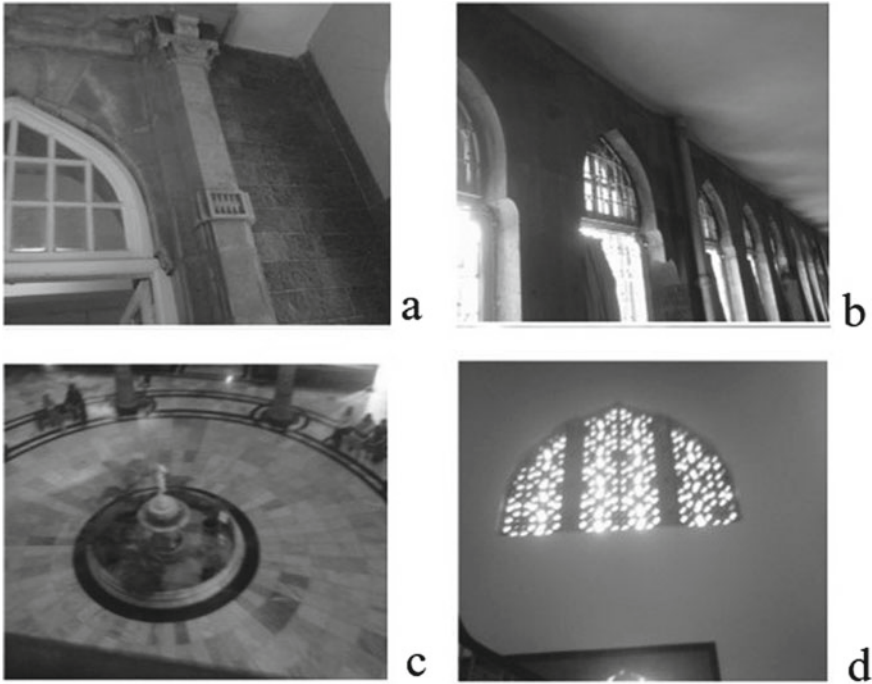


Fig. 3 a Hindu temple columns, b Islamic pointed arches, c Central lobby and d Islamic grid

moment of the person inside the building. It allows strength, moment and visibility of the objects inside the building (Fig. 8). Third part of the colonial design principal is the scale of the building. To, indicate the imperial rule, the architects used grand scale element giving visibility of the building from long distance. The monumental scale is designed to make impression of the building in public area. This scale is evident in design in two dimensional plan and exteriors of the building.

Prince of Wales Museum is organised with large open lobby with a monumental dome in center. Once a person enter the lobby (Fig. 3c), a dominant colonial architecture is viewable to visitors (Fig. 2a and c). The lobby ceiling is designed with pointed arch support as found in the Gothic architecture. The construction technology of the dome is unique with use of pointed buttress, rings in windows and main dome (Fig. 2c). Generally, the dome construction technology requires innovation in the bottom support. Because it connects the circular part with rectilinear part. This Gothic arch construction provide an innovative construction technology (Fig. 4a). The use of pointed support on bottom gives a unique interior of Gothic patterns inside the building. Thus, many more elements are found inside the building that indicates the use of colonial style elements.

The second part of the Indo-Saracenic architecture is use of the Hindu architecture elements inside the building. In Prince of Wales Museum, architect has used

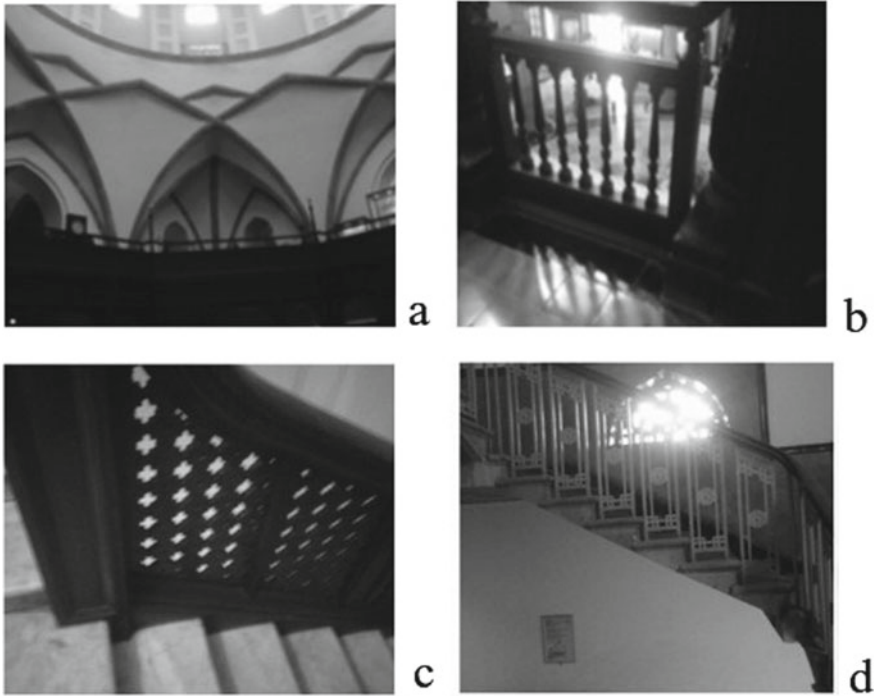


Fig. 4 a Gothic arch dome support, b Hindu wooden railing, c Islamic pattern railing, and d Islamic pattern railing

wooden frame railing in the main entrance lobby (Fig. 2a). This architectural style is predominantly found in the Indian palaces and residential typologies. Generally, this wooden technology is used to support the spaces. In many palace and residential typologies this construction is used to support the slab and court yards. Thus, use of the wooden support has been an innovative style of the medieval period in Hindu architecture. The Hindu construction technology was mainly based on the used of wooden structure elements during the medieval period. In many residential typologies wooden railing with vertical conical bars was used in architectural style (Fig. 4c). This style is also combined in many places in the Prince of Wales Museum. The early Indian temple architecture styles is also evident in the corbelled supports (Fig. 5a). The Indian temple architecture was mainly based on the stone construction technology. These supports are used in the exterior of the building. This stone corbelled support provides support to the main beam. They are also used to support the rain water canopies (Fig. 6a). Not the least, but the Hindu temple architecture columns are used in the interior columns of the building (Fig. 3a).

The Islamic architecture and construction technology was very much dominant with used of pointed arches. The typical Islamic pointed arched are used in various parts of the building (Figs. 2a, 3b and 5b). This style is also reflected in balustrade

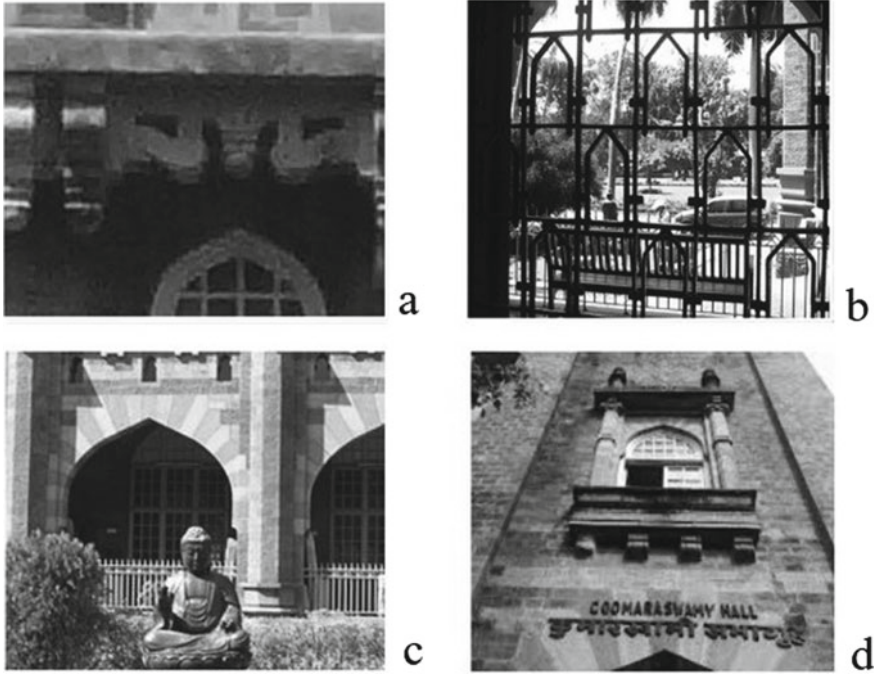


Fig. 5 a Hindu temple stone architecture corbelling, b Islamic pattern grills, c Gothic pointed stone masonry arches and d Islamic balcony pattern

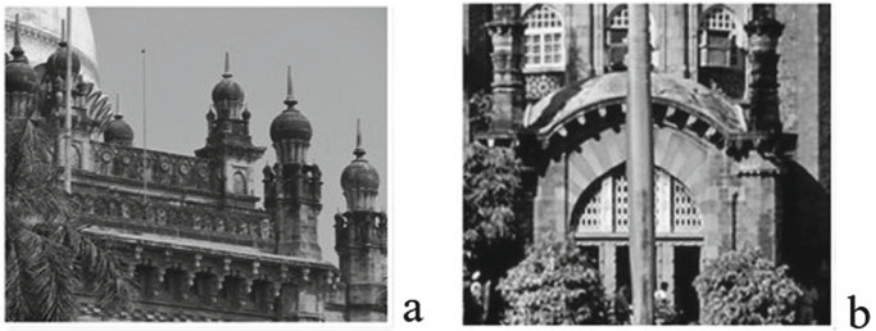


Fig. 6 a Islamic architecture turrets and b Islamic dome design

(Fig. 4a) and grills (Fig. 5b) in the building. The dome exterior is similar to the exterior of Taj Mahal. It has similar shape, scale and patterns. This similar design is used by the architect to represent a monumental design. The provision of the domes turrets at the end is an important requirement of the load bearing construction technology. The Islamic architecture style turrets domes are designed in the building (Fig. 6a). On various forts of Islamic times, the balcony projects were used in the building (Fig. 5a). This similar style of architecture is found in the exterior of Prince of Wales Museum. The main entrance is also dominated by use of (Fig. 6b) Islamic construction dome system. Thus, the combination of local style architecture made the Indo-Saracenic architecture of Prince of Wales Museum.

4 Gallery Design

The project involved design of gallery for painting Western artist. This gallery was designed to revitalise the exiting architecture. Yet, it had to be modern and attractive to visitors. It was proposed with the central circulation and display system on both the side of walls. Generally, the gallery design in museum involves following process: (a) identification the requirement of display, (b) moment of visitor, (c) adaptive reuse, (d) conservation of heritage, (e) display system, (f) ventilation system, (g) lighting and (h) various allied services.

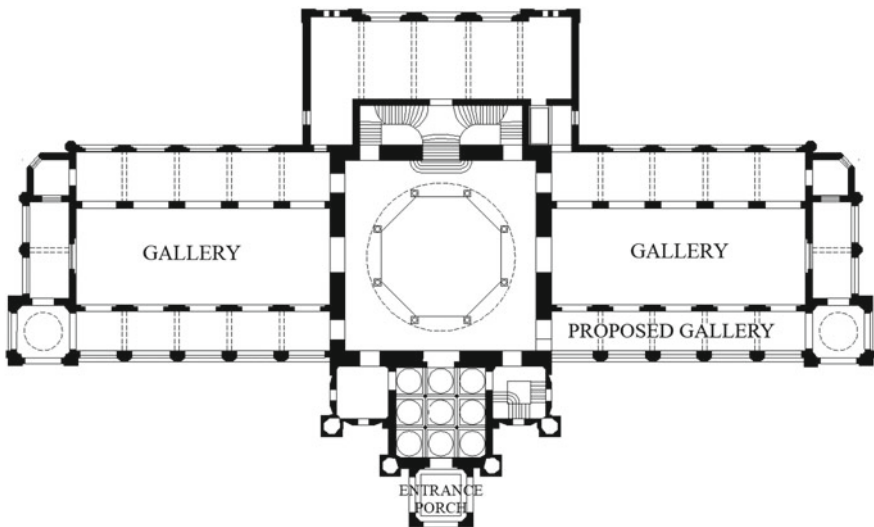


Fig. 7 Plan of building

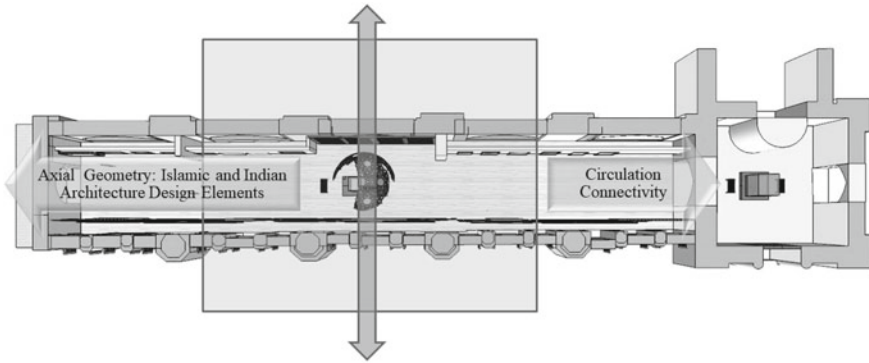


Fig. 8 Proposed gallery

4.1 Application of Style

In the design of the gallery various India-Saracenic style of were applied to revitalize the original architecture of Prince of Wales Museum. The gallery design is proposed with an axial concept for circulations and visibility of the objects (Fig. 8). These axial patterns connected one space to the other space in the gallery. The Islamic architecture patterns are famous for the use of the gird patterns (Fig. 9). This grid pattern style represents the lotus in the Islamic architecture. The purpose of gird pattern is also to provide air circulation in the hot and humid climate (Fig. 10). These grid panels were proposed inside the walling along the display. The main purposed of this grid pattern was to integrated the original architecture and allow the wind movement to maintain ventilation inside the gallery. Thus, the new gallery designs were applied with the various Indo-Saracenic architecture elements in the architectural design process.



Fig. 9 View of proposed gallery



Fig. 10 View of prosed gallery

5 Conclusions

The historic building rehabilitation includes the understanding of the original architectural style and construction technology of the building. The Indo-Saracenic architecture style was prominently used in the Prince of Wales Museum. As, the new galleries were constructed, the museum developed various contemporary design. It is indeed important to revitalize the original architectural style of building in the rehabilitation process. So, the project developed an innovative idea to use the existing Indo-Saracenic style for the construction of new gallery. Significantly, the application of Indo-Saracenic style in architectural design process revitalize the original architecture. Similar, approach can be adopted for the rehabilitation of various historic buildings. Also, such approach can revitalize the architecture and provide accurate adaptive reuse of the historic buildings. This research further opens new ideas on applying similar methods to rehabilitate historic buildings in different styles.

References

- Alexander, C. (1977). *A pattern language*. New York, NY, USA: Oxford University Press.
- Alexander, C. (1979). *The timeless way of building*. New York, NY, USA: Oxford University Press.
- Aruna Ramani Grover (2014) Indo-Saracenic architecture: Indigenous Ingredients For Imperial Intent Humanities and Social Sciences Review 03: 05. 305–326 December
- Baweja, V. (2018). Indo-Saracenic architecture. *Traditional Dwellings and Settlements Review*, 30(1), 111–112.
- Choudhary, A. S., Pipralia, D. S., & Kumar, D. N. (2018). Energy efficiency assessment of Indo-Saracenic buildings in India. In The 3rd International Conference on Energy Efficiency in Historic Buildings (EEHB2018), Visby, Sweden, September 26th to 27th, 2018. (pp. 199–206). Uppsala University.
- Demirbaş, O. O., & Demirkan, H. (2003). Focus on architectural design process through learning styles. *Design Studies*, 24(5), 437–456.

- Parlewar, P. (2021a). Prince of wales Museum: Revitalization of European painting store. In: J. Delgado (Eds.), Case studies in building constructions. Building Pathology and Rehabilitation (Vol. 15). Cham: Springer.
- Parlewar, P. (2021b). Rehabilitation of historic chancery building, Yangon, Myanmar. In: J. Delgado (Eds.), Case studies in building rehabilitation. Building pathology and rehabilitation (Vol. 13). Cham: Springer.
- Plowright, P. D. (2014). *Revealing architectural design: methods, frameworks and tools*. Routledge.
- Sheeba, J., & Dhas, J. T. M. (2018). A study of Indo-Saracenic architectural heritage. *International Journal of Pure and Applied Mathematics*, 118(22), 1737–1742.
- Soliman, A. M. (2017). Appropriate teaching and learning strategies for the architectural design process in pedagogic design studios. *Frontiers of Architectural Research*, 6(2), 204–217.

Design of Structure for Steam Turbine Generator



Prafulla Parlewar

Abstract The structure for Back Pressure Steam Turbine Generator of 6.0 Mw is designed in structural steel and Reinforced Cement Concrete (R.C.C.) for a petroleum refinery. This structure included a composite arrangement of structural steel build form and R. C. C. structure to support the turbine generator. This structure was having complex loading of steel structure and dynamic loading of the turbine generator. The research here looks into the questions like how to design a composite technical structure? How vibration affects the design criteria for design of technical structure? What are the design criteria of design of R.C.C. structure for turbine generators? The project included design to facilitate the operation and maintenance of the steam turbine generator. The research looks into the complete cycle of structure of steam turbine generators. The cycle of designing the structure included the loading, aesthetic, functionality of the structure. Similar approaches can be used to design structures under various dynamic loading in industries and refineries.

Keywords Machine foundation · Steel structure · Technical structure · Steam turbine generator

1 Introduction

A structure in Reinforced Cement Concrete (R.C.C.) and structure steel is designed for a Back Pressure Steam Turbine Generator at petroleum refinery. The structure consists of turbine generators of 22000 Kg. The structure was designed as per the operation of the turbine generator and its related functions. This technical structure is designed with R.C.C. structure for turbine generator and structural steel for operations and control. The two structures are isolated by an isolation joint to avoid transfer of vibration from one structure to another. It is also provided with an Electrical Overhead Travelling (EOT) crane for installation and maintenance of the generator. The research here looks into question like how to design composite technical

P. Parlewar (✉)
City Development Corporation (P) Ltd., Mumbai, India

structure? What are the design criteria for design of structure for turbine generators? The research illustrates the complete cycle of the design and implementation of the composite structure. Furthermore, the research illustrated the loading criteria, functionality and aesthetic for the design of the technical structure.

The project is designed for a petrochemical industry as a consultant. The methodology included the study of the site inspection, loading criteria, design of structure for generator in R.C.C. and for operations in structural steel. The site was located in very narrow plot. A size of 18.02 x 12.15 m was taken for the design of the structure. The general design criteria for the building included use of Indian Standards (IS) of Bureau of Indian Standards (BIS) for live load, dead load, wind load, seismic load and all other necessary loads for the design of the structure. Steam turbine is a heat engine that converts heat energy of the high temperature and pressure steam to kinetic energy and then kinetic to mechanical energy in two stages and/or electrical energy with alternators (Karakurt 2017).

Due to the requirements of process layout, the steam turbine generator foundation is a complex space frame structure system. As the capacity of power plant units continues to expand, the vibration requirements are getting higher and higher. Moreover, understanding of vibration on existing steam turbine generator foundation and their interconnection is significant for estimating the foundation vibration in an effective way (Zhang et al. 2020). Dynamic behaviors of the foundation play an important role in providing normal operating conditions for the supported turbo-machine. The main source of dynamic forces in the turbo-machine is mass eccentricity, when center mass of rotating parts does not coincide with the center of rotation. Unbalanced masses of the rotor produce centrifugal forces that lead to vibrations of the rotating turbo-machine foundation (Livshits 2008).

2 Project Profile

The project is located in a petroleum refinery. It was designed as a consultant for petroleum refinery. The technical requirements for Back Pressure Turbine Generator were studied and analysed before designing the structure. The project is a structure of the size 18.02 x 12.15 m with height of 14.16 m. The structure is designed at two levels. First level is at 1.5 m and second level is at 6.5 m. The project is planned with ground level area for maintenance and lube storage. The generator was placed on the second level with R.C.C. The structure included a large size EOT crane for installation of the generator. The total weight of the generator was 22000 kg. The EOT crane was designed at level 12.10 m. The entire structure was designed for easy operation of EOT crane. The foundation of the machine was designed in a raft of size 10.40 x 4.90 m. The structure was provided with the facility of grated flooring to remove and maintain the parts of the generator. Further, the structure was designed with exterior panels with an aluminium composite panel system. As the vibration of the structure will affect the structure, walls were not provided in most part of the building. The ground floor was designed such that it is easy for the movement of the

fork lifts and loading or unloading of the trucks. The roof design was designed in arch truss in tubular frame. The roof was covered with metal sheets. The gable of the roof was covered with metal sheet.

The Back Pressure Steam Turbine Generator was a multi stage, horizontal spindle, axial flow, and impulse steam turbine generator with power of 6.0 Mw. It had a speed of 5500/1500 R.P.M and steam flow of 120 TPH (Max.). The total weight of turbine and gear box was 2500 Kg. The static load for the turbine and gear box was 2500 Kg at ten points on the foundation. The dynamic load was considered 1.5 times of the static load.

3 Building Operations

The technical structures main operation was installation and maintenance of the generator. The generator was installed at level with concrete structure. The remaining structure was designed with structural steel. The structure was designed such that the operation and installation of the generator was easy. Also, it provided access inside the structure through EOT crane. The generator level was provided with two large opening of size 3.0 x 3.0 m from the two sides of the structure. Similar opening were also provided on the ground level for installation of the generator. The two levels were connected with a large grated opening of the site 6.0 x 6.0 m for allowing the equipment shifting from one level to the others.

The technical structure main operation was installation and maintenance of the generator. The generator was installed at level with concrete structure. The remaining structure was designed with structural steel. The structure was designed such that the operation and installation of the generator was easy. Also, it provides access inside the structure through EOT and hydraulic cranes.

The installation process of the generator involved organized scheduling, positioning and installation inside the industrial complex. The part of the generator were moved inside the first level and installed on the concrete pedestal. After, completing the installation of various parts, the operation connectivity was completed for the generator. Further the maintenance of the operation of the generator was very important in the structure.

The ground level for the technical structure was designed for office, lube tanks and movement of the vehicles. The offices included the maintenance supervisor and other office staff for undertaking operations and maintenance of the generator. The lube tanks play an important role for continues fluid cycle of the lube. These tanks were design with piping connectivity at all levels of the structure.

The most important part of the operation was the movement of the vehicle at ground level. This movement of the vehicle included the movement of forklifts, trucks and other vehicles. So, the flooring was designed with load capacity to handle these vehicle at ground level. A R.C.C. slab of 150 mm thick was planned to sustain this load of vehicles. The vehicles movement was also important to provide accessibility for maintenance. During the maintenance operation, the small or medium parts of the

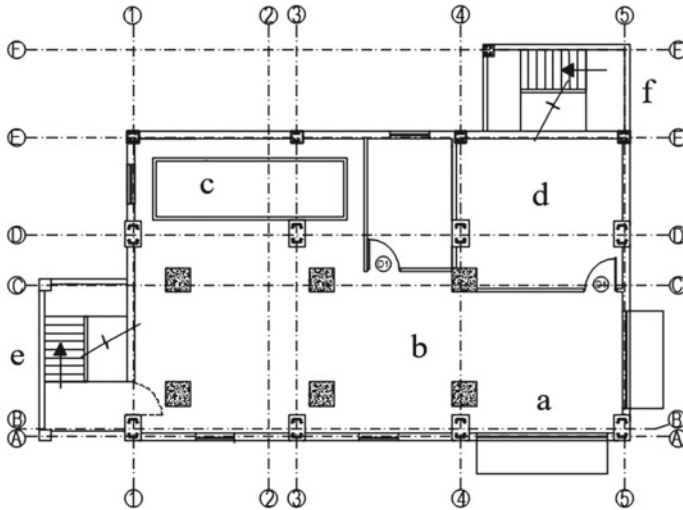


Fig. 1 Plan at ground level **a** 3.0 wide opening, **b** loading and unloading area, **c** lube tank, **d** control room, **e** stair for generator, **f** stair for operation

generator, equipment, panels, and electrical of others need to be replaced from time to time. Hence, this vehicles movement on ground provided easy transportation of these equipment and materials. The large connected opening in the floor of the R.C.C. slab at the generator level provide connectivity for all the maintenance operations. This opening is covered with steel grated flooring for further functionality of the floor at the generator level. The ground floor also comprised of battery room and air pressure high tension control room.

The generator level is located at 6.5 m. Along with the generator, the structure is composed of air condition control room the rooms for the central staff (Figs. 1 and 2). The circulation arrangement in the technical structure was an important design criterion. The circulation of the control room and office for the technicians was planned separately. A mild steel staircase was planner separately for the circulation of the control room staff. Another staircase was planned for the technical maintenance person for the maintenance of generator.

Sufficient consideration was given for the design of interior and building services for the structure. The flooring at the various levels was designed as per the requirement of the usages. The ground floor was typically designed for the vehicle movement. So, R.C.C. floor was prominently used for the movement of vehicles like trucks and forklifts. The industrial epoxy flooring system was used for the purpose of flooring at the generator level. This was particularly important for the maintenance of the equipment. The industrial epoxy also provides effective maintenance of the flooring. The control room were providing with the good quality vitrified tile for the easy working, cleaning and aesthetic of the interior.

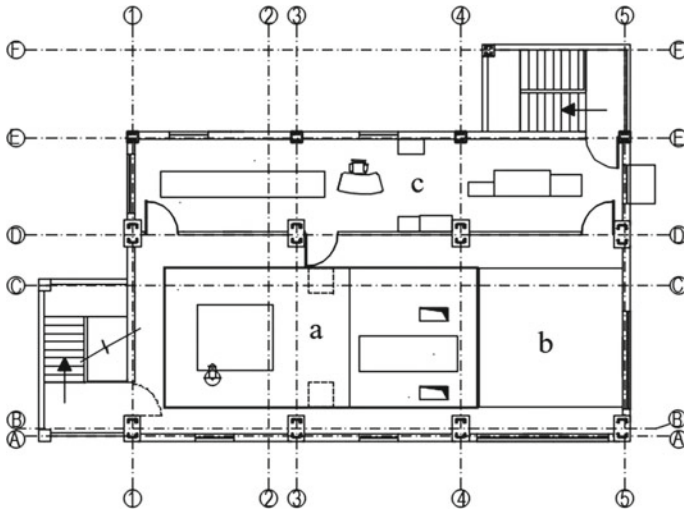


Fig. 2 Plan at first floor level a Generator slab, b Grated area, and c Control room

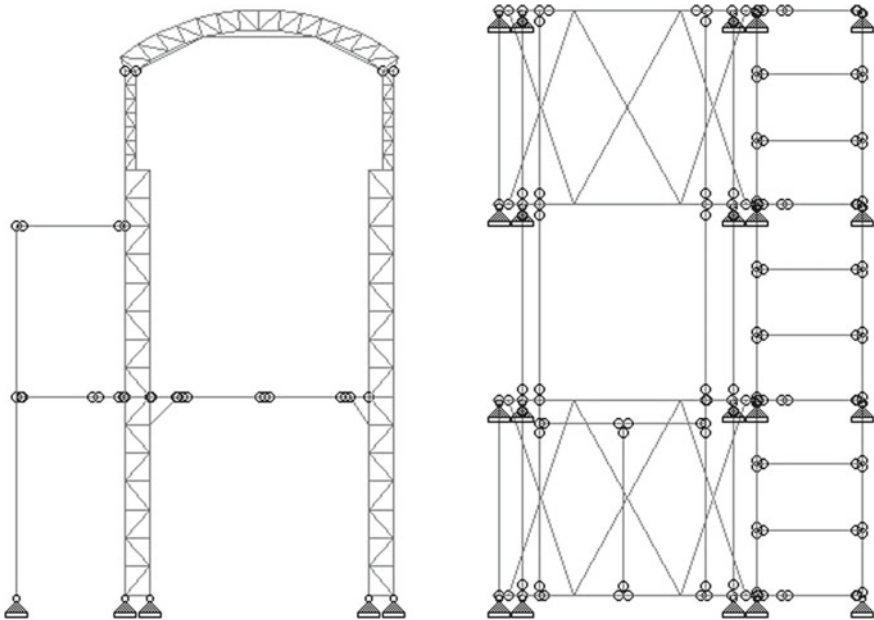


Fig. 3 Section and plan

The internal partition system was designed with construction of light weight blocks. The load of these was rested with the structural beam. The structural design criteria includes the loading of walling with blocks. The internal partition walls were plaster and painted with high quality epoxy paint.

False ceiling was designed with use of metal ceiling system in Armstrong material. This includes the 600 x 600 mm panel with metal suspender at the ceiling. The design of ceiling is designed carefully in the control room. Because in case the ceiling panel's falls, it will not damage the computers or panels. So, an Armstrong "K" type system was specially designed in the control room. The Armstrong "K" type ceiling system keep the ceiling pane hanging in the ceiling with grove system. Thus, in any event the ceiling panels do not fall down. The ceiling was further providing with the internal air condition, cabling, alighting and firefighting system.

The lighting system was designed with LED lights for reducing the electrical consumption. The firefighting system was carefully designed with the use of wet and dry system. The dry system was used in the control and panel rooms. The firefighting system includes complete system of fire alarm, heat detector, smoke detector etc.

The design of EOT crane for the operation of building is supported on the main structural columns. The EOT crane is provided for installation and maintenance of the turbine generator and equipments in the structure. Cranes are frequently needed for material handling in metal buildings. A building crane is a complex structural system that consists of the actual crane with trolley and hoist, crane rails with their fastenings, crane runway beams, structural supports, stops, and bumpers. A motorized crane would also include electrical and mechanical components. Several types of cranes are suitable for industrial metal building systems, the most common being bridge cranes (either top-running or under hung), monorail, and jib cranes. Occasionally, stacker and gantry cranes may be required for unique warehousing and manufacturing needs (Mythili 2015). The mechanical EOT crane was designed inside the structure.

4 Load Design

The load criteria for design of turbine foundation includes: dead load, operation load, torque load, frictional load, normal machine unbalance force, temperature load, bearing failure load, seismic load and wind load. IS:2974(Part I)-1982 provides the design basis for the foundation and concrete structure. The foundation of the turbine has to be designed with consideration of impact and vibration characteristic. Also, the property of soil under dynamic condition plays an important role. Many of the criteria for the turbine foundation are provided by the manufacturer (Fig. 4).

In consideration of natural frequencies of the initial design of the turbine generator foundation model possible resonances of the first two natural frequencies of columns with first harmonic of the generator were identified. Therefore, this became the design objective, while design variables were dimensions of columns cross section. Results showed that natural frequencies of the optimized columns lay out of the critical frequency range, what proves the accuracy of the applied procedure.

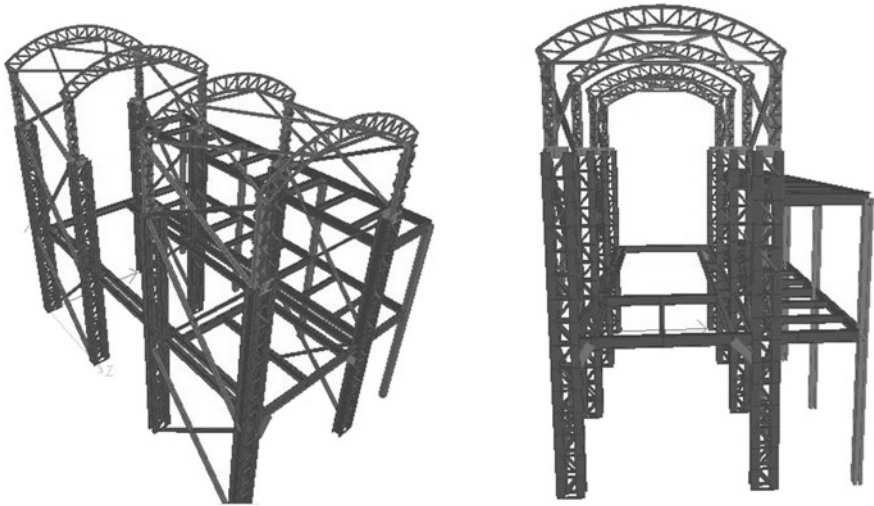


Fig. 4 3D views of structure

Furthermore, the proposed method is suitable not only for the design optimization of the analyzed example but of an every structure subjected to frequency constraints, which can be represented with a similar analytical model (Stimac 2011). Basic mode mainly manifests as spatial modes and for some order shapes of vibration take the form of platen's global vibration. These vibrational modes that are dominated by whole translation and swing do relatively less harm to unit shafting (Lu et al. 2017) (Figs. 5, 6, 7).

A good turbo generator foundation should have following criteria: The machine itself should run smoothly, The foundation supporting the equipment is capable of sustaining the various loads coming from the turbine under operations well as those that could develop due to the vagaries in nature or otherwise like earthquake, thermal, electrical faults, short circuits etc. The turbine generator industry invests great effort in the design of machines in order to increase their efficiency and reliability. Such requirements have led to a demand of high quality, reliable machine foundation which has to provide safe and continuous machine operation (Tripathy et al. 2015). Approach normally used for the design of rotating equipment foundation, which seeks to provide large stiffness (and mass) to the foundation to remove their natural frequencies of the critical speeds of the turbine and minimize the interaction between the equipment and the foundation (Vicencio 2012). Structural responses to dynamic loads are influenced by soil to a greater degree, compared to elevated space-frame type turbine-generator foundations (Bose et al. 2018). The dynamic analysis of turbine generator foundations needs attention to detail both in modelling and interpretation of the results and also to consider the issues on mathematical modelling of structure, soil and machine for dynamic analysis (Madhu et al. 2016). Wind or earthquake

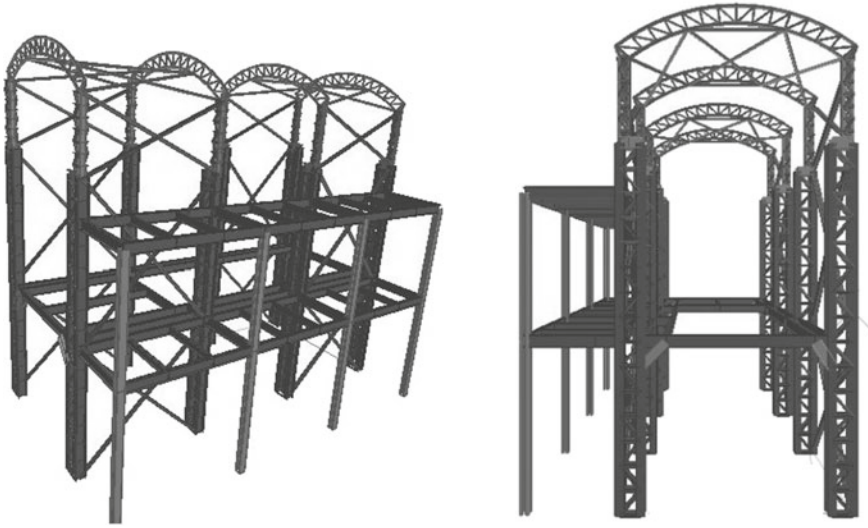


Fig. 5 3D views of structure

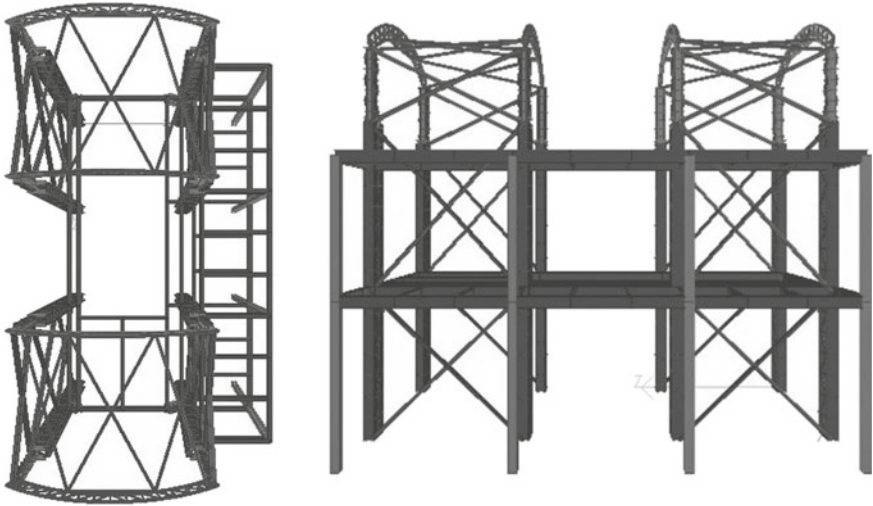


Fig. 6 Top and side views of structure

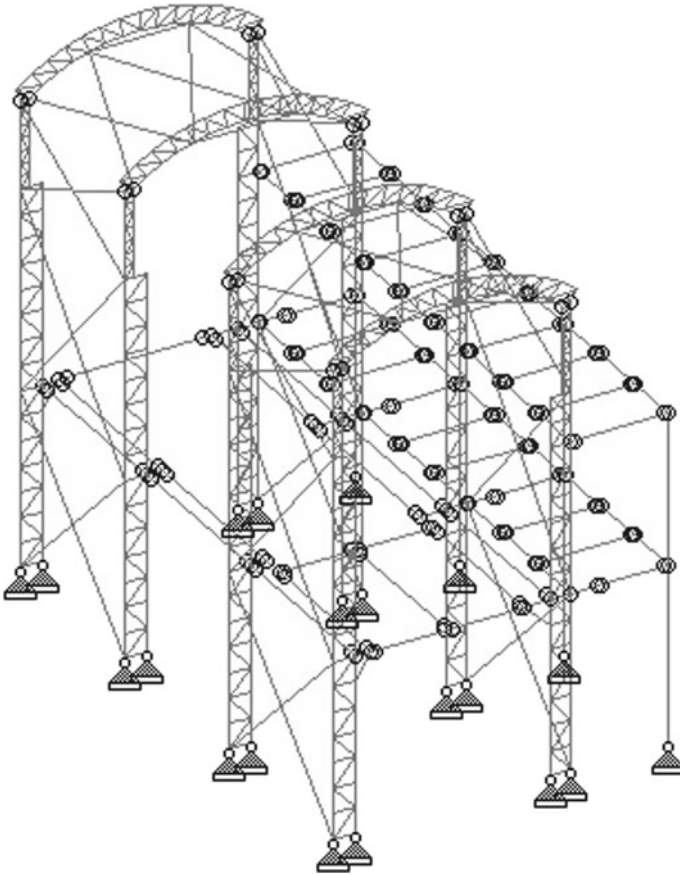


Fig. 7 STAAD model of structure

forces cannot be assumed to occur simultaneously of the building. Also, the effect of temperature and shrinkages are neglected on the buildings. Live load on the building was estimated as per the IS: 875-1964 (Parlewar 2021) (Fig. 8).

5 Building Components

The complete building was designed in R.C.C. and structural steel. To maintain support in the generator, R.C.C. raft was designed with a raft and concrete floor. The raft was 1.0 m thick and the floor bed was 1.2 m thick. The columns for support of the concrete were designed on 900 x 900 mm. As per the generator requirement the total weight of the generator was 22000 Kg (Fig. 1). The structure was designed for reducing vibrations. Hence, the design of two structures for the generator and

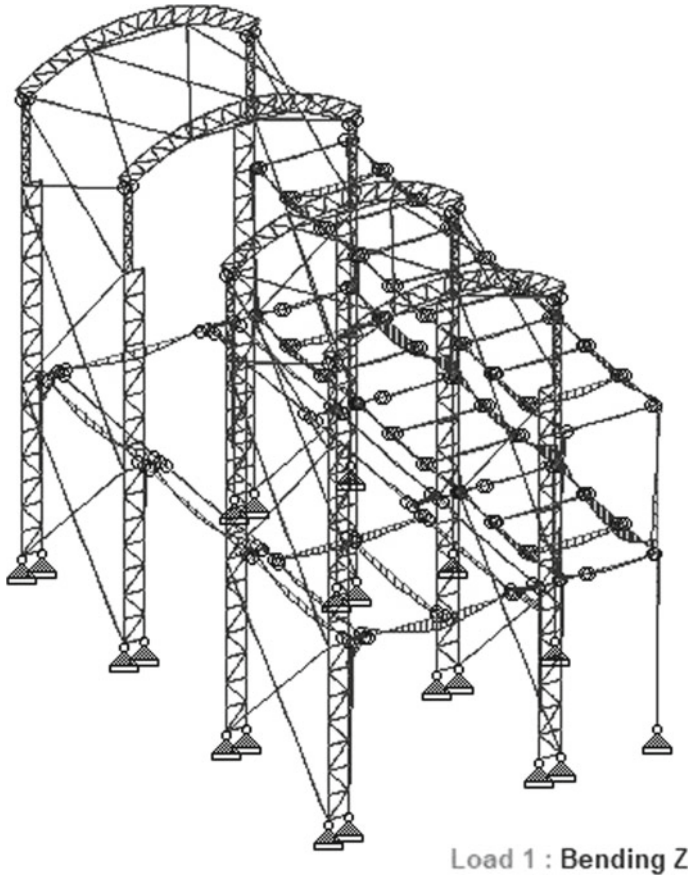


Fig. 8 Model showing bending moments

structure for the operation were separated from each other with a 100 mm joint. Both the raft columns, beams and pedestal were located from the main operation structure. So, the vibration produced by the generator does not reach into the structure columns of two structures. The steel design for the generator pedestal was 20 diameter at 150 center to center main bars and 10 diameter at 150 center to center diameter bars. The steel estimation was developed based on the loading. The major part of the structural steel design is illustrated in steps in Figs. 9 and 10. The overall sequence of construction of the structure is illustrated in the first step which shows how the main foundation was erected at site. Then the beams were erected for the main structure. The complete steel structure was fabricated in this foundation. In the next step, the raft for the generator was constructed and complete structure for the generator was erected on the site. Next steps included the construction of super structure with columns in vertical W-356 x 171. The fabrication and erection of these super structure elements included fabrication of beams for flooring in super structure. After erection

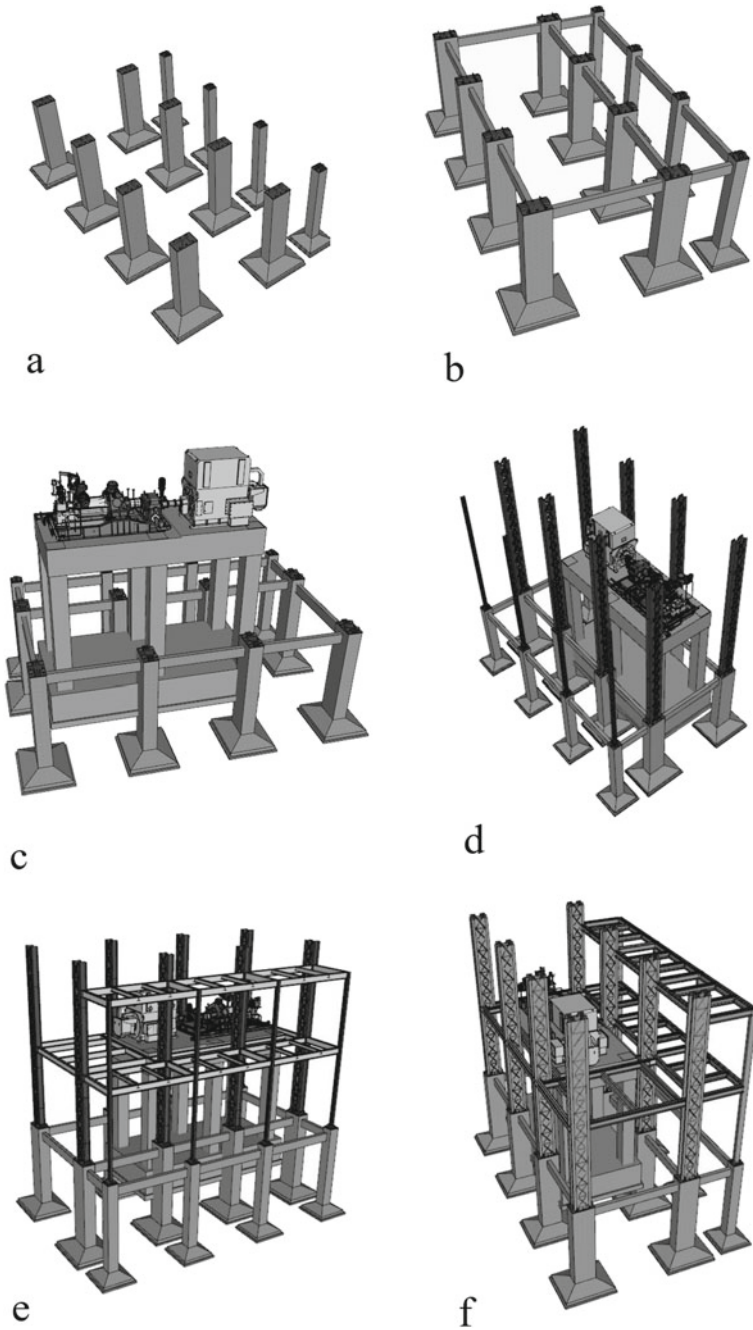


Fig. 9 Structure installation sequence—**a** Foundation, **b** Plinth beams, **c** R.C.C. foundation and pedestal for steam generator, **d** Fabrication and erection of steel columns, **e** Fabrication and erection of beams, and **f** Application of cementous fire proofing

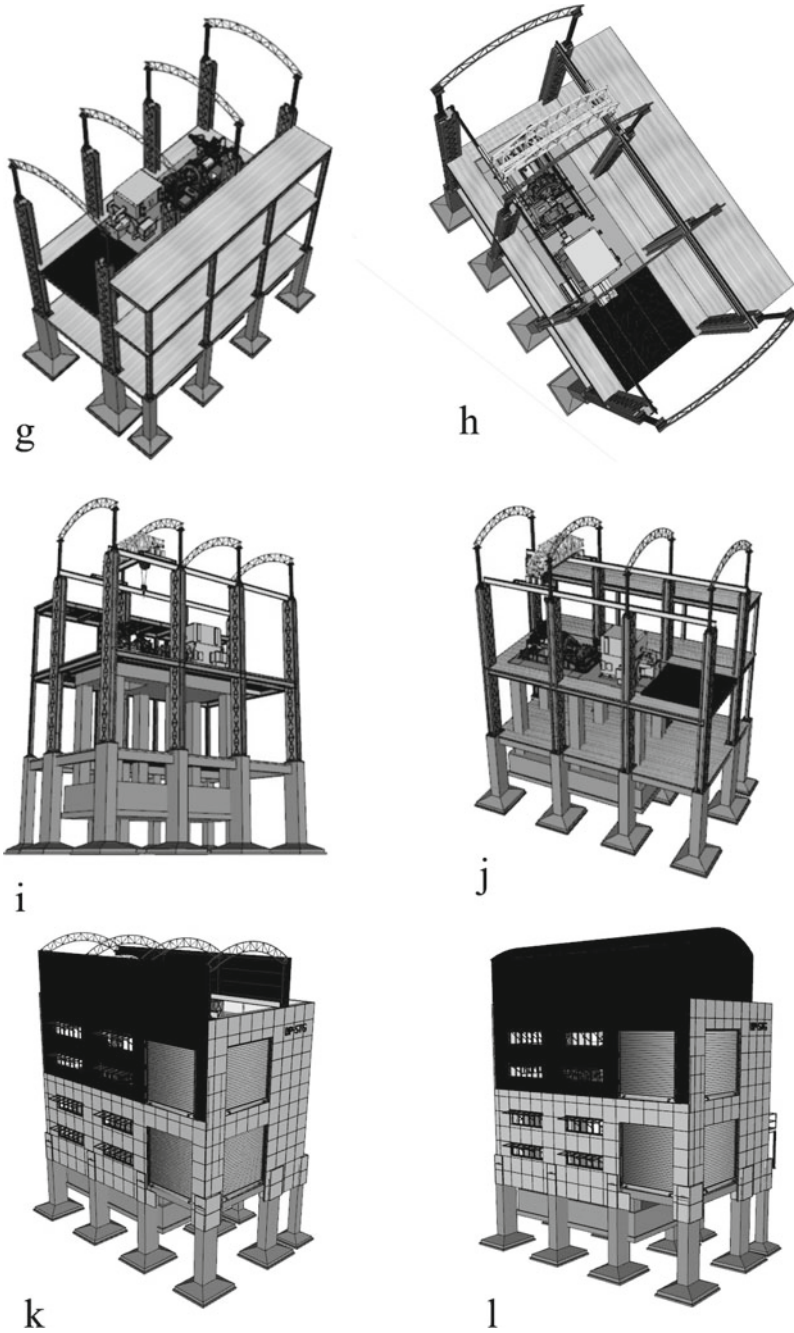


Fig. 10 Structure installation sequence—**g** Construction of flooring, **h** Erection of grated flooring, **i** Fabrication and erection of arch trusses, **j** Installation of EOT crane, **k** Installation of wall panels and exterior APC panel, and **l** Erection of roofing

of beams and columns, the roof truss plays an important role in the structure. The roof truss was designed as an arch, so it can be fabricated and erected easily on site. After this the EOT crane was installed on the proposed steel buttress of the generator. Last and important part of the structure includes the panelling system, wind bracing and aluminium, composite pane. The internal wind bracing were designed such that the whole structure is stable from the wind. Also, the structure is provided with windows for ventilations. So, the wind bracing is carefully designed to provide the support along with the openings

As the structure is dynamic structure and the generator will have major vibration transformed from one point to the other, two side of structure were kept with panels. Remaining two side of the structure was having the modular blocks wall construction. This gave an opportunity to make the structure aesthetically appealing. So, toward the modular blocks aluminium composite panel were erected to give a good aesthetic appearance to the structure. The ACP panel with metal silver finish was added to the overall aesthetic of the structure. Hence at last the wall panelling and the ACP panels was completed for the structure (Fig. 1).

6 Fire Safety of Structure

The complete structure was designed with high safety of fire. So, cementous fireproofing was applied to the structural steel. Generally, this cementous fireproofing is supplied by various companies. One such company is Cafco FENDOLITE. This fireproofing is a lightweight cementous spray. It provides protection against highly severe fire. It can protect the structure from hydrocarbon pool fire and jet fires. It is a monolithic coating able to withstand the high intensity hydrocarbon fire. As this coating is low density, it significantly reduces the dead load. It is highly durable and does not crack even after the heavy impact. It has following advantages: (a) The structural steel protected from cementous fire proofing can provide fire resistance upto 240 min, (b) During the fire, it does not release any toxic or hazardous fire, and (c) It can have float finish to look aesthetically good.

Along with the cementous fire proofing the complete structure was provided with all necessary firefighting requirements like wet and dry sprinkler system. The dry sprinkler system was used in the server rack room and other similar locations. The system was used for locations like open passages or open circulation areas. The structure was also provided with all the necessary firefighting systems like heat detectors, smoke detectors, fire alarms etc.

7 Conclusions

The composite technical structure for the steam turbine generator was designed as structure in R.C.C. and structural steel. The steam turbine generator was installed on the concrete structure and the steel structure is used as an envelope for operational purposes. The design criteria for both structures are different. The structural steel members are affected by live, dead, wind and seismic load. The concrete structure is mainly affected by the vibration load. Also, dead load and wind load are considered while designing the R.C.C. structure for the steam generator. The important part of the design of the structure is effective operation and maintenance of the steam generator. The structure was designed with a large EOT crane for installation and maintenance of the generator. A grated opening was also provided to exchange of the parts during maintenance. Some of the important design criteria are as follows:

(a) The composite structure required accurate consideration for dynamic design from vibration of the generator. As the generator vibration shall not enter into the complete structure, careful consideration was taken to separate the structures. Also, to reduce the effect of vibration on the steel structure wall panelling was designed such that it reduces the effect of vibration.

(b) The load design is the most important criteria for the structure. The load design included design of the dynamic load for the structure. The load criteria included dead load, live load, wind load, seismic load and others.

(c) The aesthetic was an integral part of design of structure. So, the exterior panelling was provided with Aluminium Composite panels to make the structure look aesthetically appealing.

(d) The design criteria include accurate design for the operations and maintenance of the structure. The installation of the steam generator was an important process of the design. So, the entire structure was planned for technical installation of the turbine generator.

The design of the technical structure in industrial complexes is particularly important due to the loading of the equipment. This approach can also be used to design similar technical structures for various types of turbine generators.

References

- Bose, J., Saini, J. S., Liu, H., Elkhoraibi, T., & Ostadan, F. (2018, April). A Case Study on the Dynamic Analysis of a Combustion Turbine Generator Foundation Using Different Soil Modeling Approaches. In Structures Congress. (2018). *Bridges, transportation structures, and nonbuilding structures* (pp. 432–443). Reston, VA: American Society of Civil Engineers.
- Karakurt, A. (2017). Performance analysis of a steam Turbine power plant at part load conditions. *Journal of Thermal Engineering*, 3(2), 1121–1128. <https://doi.org/10.18186/Thermal.298611>.
- Livshits, A. (2008, July). Dynamic analysis and structural design of turbine generator foundations. In Proceedings, European Built Environment CAE Conference.

- Lu, B., & Qu, T. (2017, June). Experimental study on dynamic characteristics of foundation for large turbine-generator set. In 2017 6th International Conference on Energy and Environmental Protection (ICEEP 2017) (pp. 1–5). Atlantis Press.
- Madhu Priya, M., Chandru, P., Vijaya Sarathy, R., & Jose Ravindra Raj, B. (2016). Dynamic analysis and structural design Of Turbo generator frame foundation—A review. *International Journal of Advances in Engineering Research*, e-ISSN, pp 2231–5152.
- Mythili, T. D. (2015). Analysis and comparative study of conventional steel structure with PEB structure. *International Journal of Science and Research (IJSR)*, ISSN (Online), pp. 2319–7064.
- Parlewar, P. (2021). Design of blast resistant buildings. In: Delgado J. M. P. Q. (Eds.) *Case studies of building rehabilitation and design. Building Pathology and Rehabilitation*, vol. 19. Springer, Cham.
- Stimac, G., Braut, S., & Zigulic, R. (2011). Structural optimization of turbine generator foundation with frequency constraint. *Strojarstvo: casopis za teoriju i praksu u strojarstvu*, 53(5), 389–398.
- Tripathy, S., & Desai, A. K. (2015). Dynamic analysis of turbo generator frame foundation using SAP: 2000 v 17.1 software? In Fiftieth Indian geotechnical conference.
- Vicencio, F., Cruz, E. F., & Valdivia, D. (2012). Evaluation of Different Modeling Options for Seismic Analysis of Large Turbine-Generator Systems and their Foundation. In *Fifteenth World Conference on Earthquake Engineering*.
- Zhang, Q., Chen, J., & Lu, Z. (2020, February). A comparison of the mechanical vibration evaluation standards of steam turbine generator foundation. In *IOP Conference Series: Earth and Environmental Science* (Vol. 455, No. 1, p. 012046). IOP Publishing.

Fiber Optic Sensors to Perform Structural Health Monitoring of Concrete Structures Affected by Internal Swelling Reactions



K. K. Santos Silva, F. A. N. Silva, T. Mahfoud, A. Khelidj, A. C. Azevedo, and J. M. P. Q. Delgado

Abstract Structural Health Monitoring (SHM) on concrete structures is an important issue in controlling its performance during its service life. Data obtained using this technology can provide valuable information for decision making about the needs for corrective interventions that can ensure the integrity and safety of concrete structures. When concrete structures exhibit internal expansions due to the several types of swelling reactions a strong surface mapping cracking process appears that can significantly affect its durability and performance. The paper presents the state-of-art of the use of fiber optics sensor to monitoring concrete structures with focus in the researches related with its use. Background of the theory regarding fiber optics sensors and advantages and limitations are also discussed.

Keywords Fiber optic sensors · Internal swelling reactions · Concrete structures

K. K. S. Silva · F. A. N. Silva
Civil Engineering Department, Universidade Católica de Pernambuco, Recife, Brazil
e-mail: klayne.dos-santos-silva@2020.icam.fr

T. Mahfoud · A. Khelidj
GeM Laboratory, University of Nantes, Saint Nazaire, Nantes, France
e-mail: mahfoud.tahlaiti@icam.fr

A. Khelidj
e-mail: abdelhafid.khelidj@univ-nantes.fr

A. C. Azevedo · J. M. P. Q. Delgado (✉)
Departamento de Engenharia Civil, CONSTRUCT-LFC, Universidade Do Porto, Rua Dr. Roberto Frias, s/n, 4200-465 Porto, Portugal
e-mail: jdelgado@fe.up.pt

A. C. Azevedo
e-mail: antonio.costaazevedo@fe.up.pt

1 Introduction

Concrete is one of the main structural materials, widely used worldwide and it is used in diverse types of works and construction projects. Good durability and performance to carry mechanical loads are some issues that justify its spread use. As a heterogeneous material, made with elements from different origins, concrete structures may present pathologies manifestations throughout their useful life due to applied loads and also due to its interaction with the environment. Over time, an important scientific understanding of the nature of this material has been developed, including the perception that certain problems may cause changes in its micro and macro structure with possibility of generating an early deterioration and even the failure of the material (Tseng 2002; Surahayo 2019a, b). The occurrence of such problems may result from inappropriate selection aggregates types and cement to make concrete mixtures or it can arise from some hydration products. Regarding the development of its compressive strength along the time, some concretes may show pathologies due to environmental action, unforeseen stresses and external loads or due to changes in its micro structure that can lead to a cracking process that reduce its durability and performance (Sims 2017).

Structural health monitoring (SHM) with a focus on concrete structures emerged with the need to increase the safety of structures and provide guidelines for efficient and cost-effective maintenance plans. Currently for the SHM approach, several point sensors are used, however, due to the complexity of the concrete structures, it often ends up being necessary to use a large number of sensors. Fiber optic (FO) technology is being increasingly implemented for monitoring concrete structures, as it can provide integrated detection of a high degree of sensitivity, durability and stability (Bukenya et al. 2014; Sakiyama et al. 2019).

Internal swelling reactions (ISR) describe chemical phenomena that have physical implications for concrete structures. These expansion mechanisms can be broadly classified as alkaline aggregate reaction (RAA) and delayed ettringite formation (DEF), which lead to the expansion of the affected concrete elements that generate a cracking process on concrete surface that propagate through or around aggregate particles and/or cement paste (Noel et al. 2017).

Currently, there are several test methods used to describe the behavior of structures affected by internal swelling reactions (ISR). On the other hand, they do not take into account that in real situations the concrete element is subjected to mechanical loads or what effects that loading produce in the expansion levels. Retrofitting or rehabilitation works on the concrete structural element, affected by expansion reactions, in spite being very expensive, are sometimes performed without even knowing whether the expansion has stopped or not (Selier et al. 2017). To evaluate the behavior of concrete structures under normal loading conditions and during their use, it is essential to use safe monitoring strategies that allow obtaining material quality indicators to make decisions on possible intervention processes before the damage process increases. A deeper understanding of concrete expansion levels and the loads applied to material

is needed, as well as finding cost-effective means of monitoring concrete structures. Over time, new technologies have been investigated being one of the most promising fiber optics sensors (Noel et al. 2017; Selier et al. 2017).

2 Internal Swelling Reactions

Currently, a large number of concrete structures around the world are affected by internal swelling reactions. Several reactions can cause internal expansions on concrete and the most common ones are: the alkali-aggregate reaction (AAR) and the internal reaction of sulfate (hereinafter used to designate the delayed ettringite formation—DEF). One of the main steps to develop means of rehabilitation or retrofitting works of concrete structures is to have a comprehensive assessment of structural implications of ISRs (Noel et al. 2017; Custodio and Ribeiro 2019).

2.1 Alkali-Aggregate Reaction

The reaction between the aggregate and the alkalis has been called the “alkaline-aggregate reaction”. AAR’s first records were reported in the state of California in the 1930s by Thomas Stanton of the California State Highways Division. The identification of the problem was reported by the same researcher in 1940 (Stanton 1940). Stanton identified the expansion of the mortar bars and observed that this expansion was influenced by the alkaline content of the cement, the type and amount of reactive silica present in the aggregate, the presence of moisture and also the temperature levels (Sims and Poole 2017; Thomas et al. 2013).

The most common AAR in concrete is the alkali-silica reaction. It is a chemical reaction that occurs between amorphous silica present in reactive ions and hydroxyl in porous solution aggregates. ASR is a complex reaction three conditions must be met for it to occur: the presence of reactive aggregate, a high level of alkalis, cement component and enough moisture, around 80% in the concrete pores. Without one of these conditions, ASR will not occur. Initially the gel formed does not cause damage to the concrete because it fills existing pores, however over time this gel can increase in volume significantly and can generate internal stresses in the concrete structure, sufficient to break the affected aggregate and, consequently, the surrounding cement paste (Pan et al. 2012; Comi et al. 2012).

For the occurrence of AAR, water is a primary factor, as water works not only as a means of transport, but actively participates in the expansion process, considering that the silica gel absorbs water and expands (Martin et al. 2012).

2.2 *Delayed Ettringite Formation*

Although AAR and DEF have similar effects and they can appear in the structure in a combined way, these types of expansive reactions have completely different origins. The first reported cases of DEF occurred in some precast concrete elements subjected to heat treatment inadequate to the concrete composition and the environment. The main reported cases of DEF worldwide include railway sleepers and components with large volumes of solid concrete. Most of the reported cases also include bridges. The parts damaged by DEF were mainly solid structural elements (pillars, beams or pillars, etc.) in contact with water or subject to high humidity. The sulphate activity that occurs when concrete undergoes a thermal process in the early ages is known in several countries and has been the subject of several studies worldwide (Noel et al. 2017; Godart and Divet 2013; Godart 2017).

The formation of ettringite occurs naturally in the cement hydration process, when the tricalcium aluminate (C3A) reacts with gypsum and forms the primary ettringite. When all the gypsum is consumed, the ettringite can react even more with the remaining C3A and form monosulfate in the first days. Ettringite can re-form later, after months or years, as long as there is a new source of sulfate is present in the solution of the cement paste pores. This way we have the so-called “delayed ettringite formation”—DEF—, which is usually associated with a damage sulphate attack on concrete (Yu et al. 2016).

The chemical reactions that lead to DEF occur among several ionic species available in the pore solutions of concrete when the preliminary ettringite was inhibited by high temperature (above 70 °C). This temperature may be due to steam curing processes or the cement hydration process itself, which is an exothermic reaction (Karthik et al. 2016; Bouzabeta et al. 2012).

2.3 *Effects of ISR's on the Mechanical Properties of the Concrete*

What justify the widespread use of concrete are its good properties of strength and deformation, namely: tensile strength, compressive strength and Young's module. These properties change when there are internal swelling reactions in the material. On a macroscopic scale, the damage caused by AAR and DEF is considered to be similar, as they usually manifest disorderly cracks that resemble a map, although restrictions due to loads or structural reinforcements can modify the observed crack pattern. Regarding the mechanical behavior, the tensile strength and the elastic modulus of the concrete can be severely reduced with the development of the expansion, while the compressive strength is generally little affected (Comi et al. 2012; Bouzabata et al. 2012).

The ISRs generate a decrease in Young's modulus in the first moments of the expansion. After it is observed an increase in modulus because both the hygroscopic

gel formed by AAR and the etringite crystals formed by DEF fill the cracks formed, stiffening, this way, its structure. Regarding the compressive strength, AAR and DEF exhibit different effects. AAR occurs more slowly and the gel can promote the healing effect that can be efficient to stabilize or increase the compression strength of the concrete. DEF expansions occur more quickly and the healing process must not be able to fill in the cracks, leading to a decrease in compressive strength (Martin et al. 2012; Brunetaud et al. 2018).

3 Fiber Optic Sensors (FOS) for Health Monitoring of Concrete Structures

The occurrence of cracks in the concrete directly affects its useful life and durability. Structural health monitoring (SHM) becomes more and more necessary for concrete structures because it is, in fact, a way to complement the visual inspection that is often performed in concrete structures, but it is most of the time subjective and it is a good possibility to overcome such limitations. Monitoring concrete structures is extremely important to early identify problems and adopt the most appropriate recovery measure. In recent years, several SHM techniques have been developed for concrete structures using fiber optic sensors, piezoelectric materials and radioactive materials (X-rays and G-rays) (Hu et al. 2013; Sakiyama et al. 2019).

The use of fiber optic sensors is shown to be increasingly promising because they are characterized by their high sensitivity, durability, stability and small size when compared to traditional sensors. In addition, they can withstand high temperatures and other aggressive environments, which make them ideal for SHM of large concrete structures (Bao and Chen 2012).

3.1 Basic Concepts on Fiber Optic Sensors

Fiber optics sensors are basically an optical waveguide, which consists of the joining of filaments, which can be made of glass or polymers, and are used as a means of propagating light. It consists basically of a fiber optic interrogator that emits light down the FO cable and a photodetector that measures the light that comes back (Hisham 2018; Barrias et al. 2016).

Optical fibers are composed of three layers: the core, the cladding, and the coating (Fig. 1). The core has a high refractive index and is coated with polymeric layers whose refractive index is lower, so that total internal reflection occurs and losses do not occur during the process. The cladding, in addition to protecting against losses, also works to protect the core from contaminants and incorporates mechanical resistance to the material. The coating is used to prevent the occurrence of physical

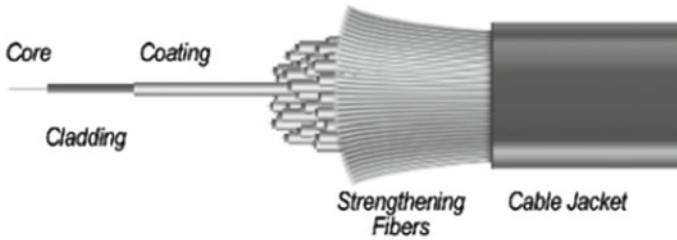


Fig. 1 Representation of the parts of fiber optics (Hisham 2018)

damage, considering that it is a fragile material (Hisham 2018; Giles and Spencer 2015).

The intensity of the light that passes or is reflected by the fiber optic is generally known and controlled by the emitter. A sudden decrease in the intensity of the light can indicate the appearance of a failure in the real structure, it can even indicate the break of the fiber due to the real damage of the structure (Giles and Spencer 2015).

3.2 *Types of Fiber Optic Sensors*

Optical fibers have properties that allow for different approaches with regard to the design of optical sensors. Currently, there are several types of fiber optic sensors that can be classified into basically three different categories: localized sensors distributed and multiplexed. These categories are based on the detection methods for each sensor (Kesavan et al. 2010).

Lau (2003) describes these categories one by one as follows:

- (a) Localized sensors or point sensor: Localized sensors, as the name suggests, determine the use of a specific segment of an optical fiber, and are similar to voltage or temperature meters applied. The specific detection of the intensity modulation refers to the losses of light intensity that are directly related to the flexion or the micro curvature of optical fibers along any length extension. In this type of sensor, the active luminescent material at the distal end of the fiber responds to a temperature change applied to the optical fiber;
- (b) Distributed sensors: The sensors can be designed to be able to make measurements in a spatial way, that is, the variable to be measured can be determined along the length of the fiber itself, this type of method is called distributed detection. The distributed sensors make full use of optical fibers, as each element of the optical fiber is used for measurement and data transmission purposes. These sensors are more suitable for application in large structures, as they have multi-point measurement capabilities. A distributed sensor allows the measurement of a desired parameter as a function of length along the entire fiber;

- (c) **Multiplexed sensors:** Are generally built by combining several sensors to measure disturbances in a large structure, that is, the information is interpreted at specific points along the length of an optical fiber network. It is a complex technique where several researchers create innovative methods for the development of multiplexed fiber optic sensors. The most widely used multiplexed detection technique for measuring delays in the propagation time of light traveling in the fiber based on the change induced by measurement in light transmission. An optical time domain reflectometer (OTDR) is used primarily for this purpose. In this type of sensor, a pulsed light signal is transmitted to one end of the fiber, and the light signals reflected by several partial reflectors (splices) along the length of the fiber are recovered by the same end of the fiber.

As noted, there are several types of optical fiber sensors used in engineering for the most diverse purposes, among them the extrinsic Fabry–Perot Interferometric (EFPI) sensors and the Fiber Bragg Grating (FBG) sensors are being used more for long-term / structural monitoring of concrete structures (Kesavan et al. 2010).

3.3 Fabry–Perot Interferometric Sensor

The Fabry–perot fiber sensor is an in-line sensor device, which makes it very useful for a variety of applications. It is basically an optical cavity (called the FP cavity) that has high reflectivity mirrors with the reflective surfaces facing each other. Due to the high reflectivity, the transmission is spectrally selective and serves as an interference filter (Meggitt 2010).

In sensors of this type, light is reflected partially at the sensor input and then again at the distal end of the sensor (Fig. 2). If the light returning to the fiber entrance is in phase with the light being reflected at that point, constructive interference occurs. If the light is in the antiphase phase, destructive interference occurs. Adjusting the

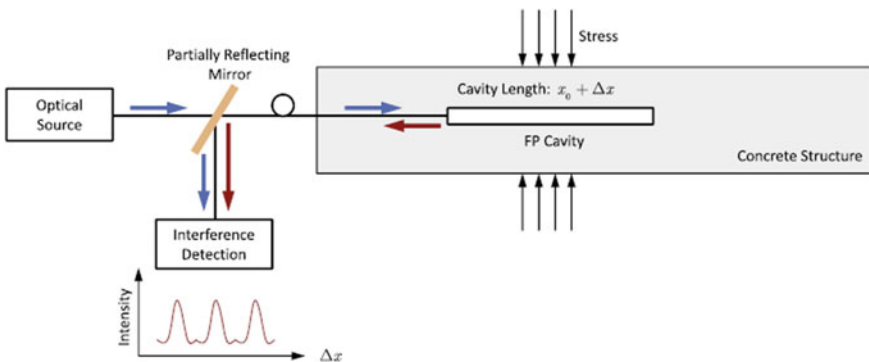


Fig. 2 Fabry–Perot Interferometric sensor (Yehia et al. 2014)

reflection coefficients at the sensor's final limits allows the sensor to be designed so that the light makes several passes. When all of these passages combine with the same phase, strong reflection occurs (Michie 2000).

The optical cavity changes in length when any voltage is applied to the structure in which the FOS is inserted. From the moment the light is injected into the cavity, this change in length causes a change in the pattern of interference of the optical signal coming out of the sensor, linking the structural deformation to the variations received in the optical intensity. FP-based sensors are very sensitive to changes in the length of the optical cavity and therefore are more sensitive to small structural changes than other FOS techniques (Yehia et al. 2004).

3.4 Fiber Bragg Grating Sensor

Among fiber optic sensors (FOS), Bragg fiber sensors, called FBG, are widely used and versatile. Basically, an FBG is a periodic variation in the refractive index along the fiber. This variation occurs due to the exposure of the nucleus to an intense pattern of optical interference (Taheri 2019).

Generally, the FBG's monitoring system consists of monitoring the wave of the "Bragg" response signal as a function of the variable being measured, such as temperature, voltage and others. The system has gratings in its composition (Fig. 3), which are a fundamental part of this type of sensor, because when a spectral source injects light into the fiber, these are Bragg grating that reflect, in response, a narrow spectral component corresponding to the measurement performed by each grating (Fig. 4) (Grattan and Sun 2000).

The main reason why FBGs are widely used is that, through this type of sensors, temperature and tension can be measured at a series of points along a fiber line, and have several advantages over conventional sensors (Pei et al. 2014).

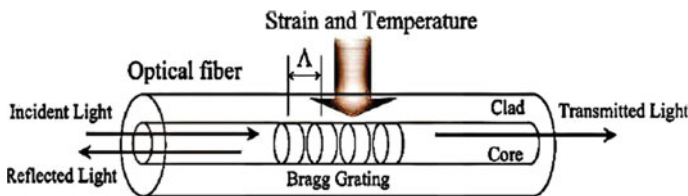


Fig. 3 Representative scheme of Fiber Bragg grating (Ramakrishnan et al. 2016)

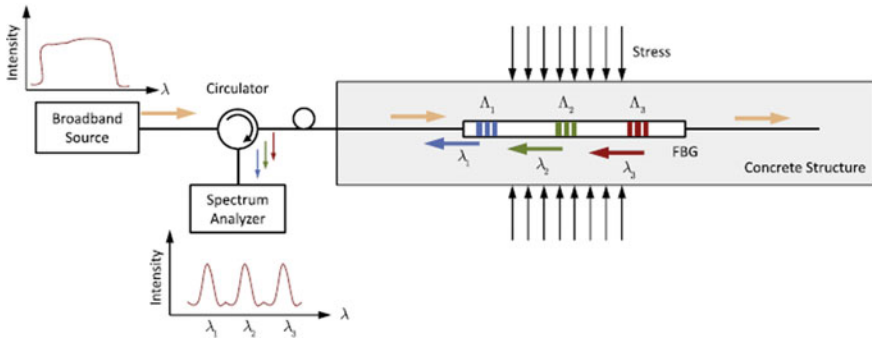


Fig. 4 Sensor representation of Fiber Bragg grating in a concrete element (Yehia et al. 2014)

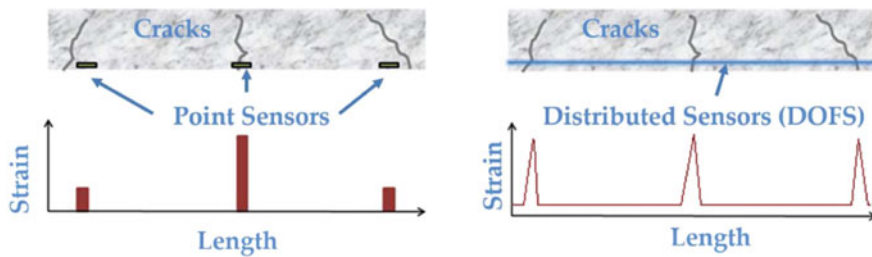


Fig. 5 Distributed sensor for crack detection (Barrias et al. 2018)

3.5 Practical Application of Fiber Optic Sensors in Concrete Structures

In the case of concrete structures, there are numerous places where cracks can occur, so that, in order to analyze the structure in a global way, the use of localized sensors becomes impractical, as it would require a very large number of point sensors, in this case, it becomes more appropriate to use sensors distributed (Bao et al. 2010) as shown in Fig. 5.

4 Tests with Embedded FOS in Concrete

4.1 Strain, Crack and Temperature Monitoring

The work developed by Yehia et al. (2014) used optical fibers to measure deformations due to physical changes, such as heat of hydration, as well as deformations due to cyclical and torsional loads. Concrete cylinders of 15 × 30 cm and beams of 175 cm in length and with a cross section of 35 × 55 cm were used. Fiber optic sensors

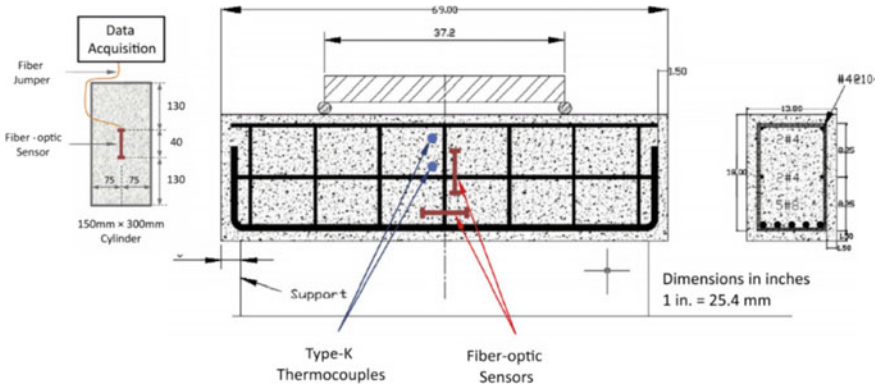


Fig. 6 Experimental setup: cylinder testing and beam testing (Yehia et al. 2014)

were inserted in the cylinders (1 in each) and in the beams (2 in each) as shown in Fig. 6. The FOS sensors used in the experimental investigation were the embedded fiber-optics (EFO), temperature-compensated and strain gauge for cylinder and beam testing, respectively. The sensors are based on Fabry–Perot interferometry.

To identify temperature variations during the hydration of the concrete, thermocouples were incorporated in the middle and on the surface of the beams, the embedded sensors could detect temperatures between 40 and 100 °C. All sensors were connected to the data acquisition system right after molding to record deformations due to the heat of hydration and also the shrinkage of concrete. The same procedure was used for both beams and cylindrical specimens. Monitoring was performed continuously during 7 days (Yehia et al. 2014).

In Fig. 7, it is possible to observe the performance of tests with cylindrical samples and concrete beams, and in the Figs. 8, 9 and 10, it is possible to see the results provided by the sensors, for each test performed on the concrete samples, as a function of time.

As a result, in the test made by Yehia et al. (2014) it was possible to observe in all tests, the FOS sensors showed instantaneous response to any changes in loading as well as temperature changes, which indicate the sensitivity and the ability of the FOS



Fig. 7 Cylindrical specimen and beams during tests (Yehia et al. 2014)

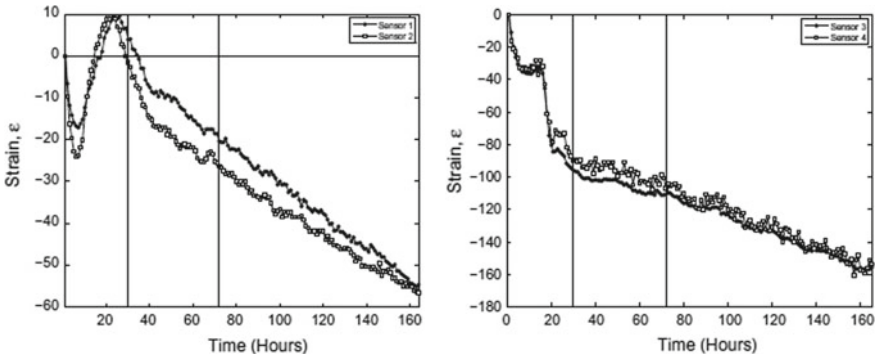


Fig. 8 Deformation result in the four cylindrical concrete samples presented by FOS (Yehia et al. 2014)

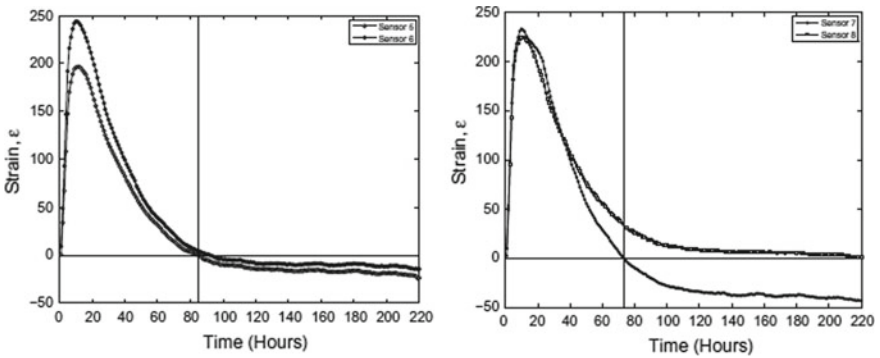


Fig. 9 Result of deformation in beams presented by FOS (Yehia et al. 2014)

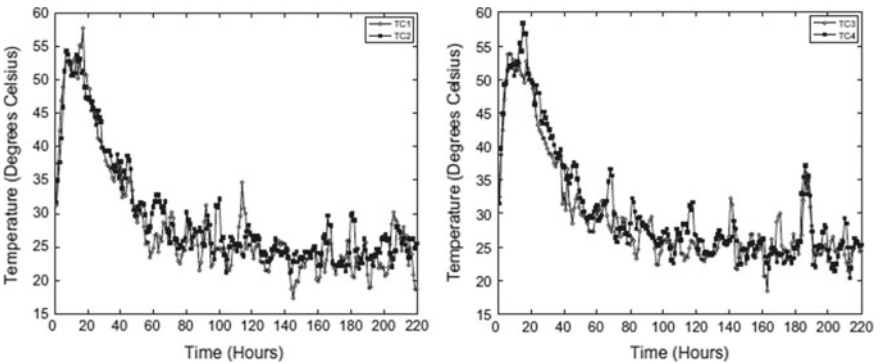


Fig. 10 Result of temperature variation in beams (Yehia et al. 2014)

sensors to record responses from the samples of concrete due to loading or during hydration.

Another work that uses FOS to analyze concrete strains is the work of Sienko et al. (2018). In this work, fiber optic sensors are used to investigate strains and cracks in a reinforced concrete element during a load test. Deformations are measured by analyzing the cracks that occurred during the load application. The crack dimensions were calculated based on the fiber deformation data obtained.

The FOS used were of the type single-mode telecommunication optical fibre SM 9/125 in a tight jacket (outer diameter of 0.9 mm), precisely to analyze the viability of this specific type of fibers, widely used in telecommunications, in the study of concrete structures.

The studied concrete element is $77 \times 110 \times 1050$ mm (see Fig. 11a) and a 16 mm diameter steel bar inside, located in the middle of the cross section (see Fig. 11b). The optical fibers were placed along the length of the limb in six different positions (see Fig. 11c).

After processing the raw data, the author defined measurement bases in post-processing. The length of the bases taken was 10 mm and the distance between successive bases was 5 mm. This means that the sensor bases overlapped by half their lengths (see Fig. 12d).

Figure 12 shows the changes (deformations) of the fibers individually, according to each measurement base defined by the author (Pei et al. 2014), before the concrete cracked. It can be observed that the fibers B, D and F show greater variations in relation to the others, this is due to the fact that they are located close to the surface of the element, where due to the natural internal stresses, the surface shrinks.

The tensile stress was applied in an eccentric way, so that cracks were initially formed in the upper part of the element where there was the greatest stress and due to the progressive redistribution of the concrete they gradually developed on the lower surface. It was observed that all critical cracks appeared in the element up to a load

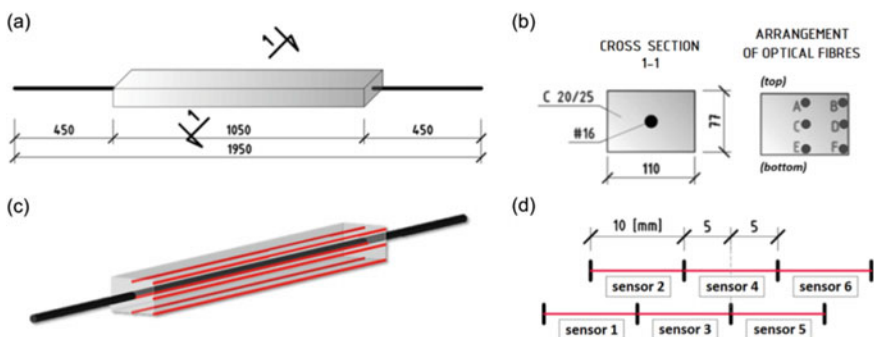


Fig. 11 a Specimen dimensions, b Cross section with the locations of optical fibres, c View of the member analyzed and d Arrangement of sensor bases along the length of the fibre (Sienko et al. 2018)

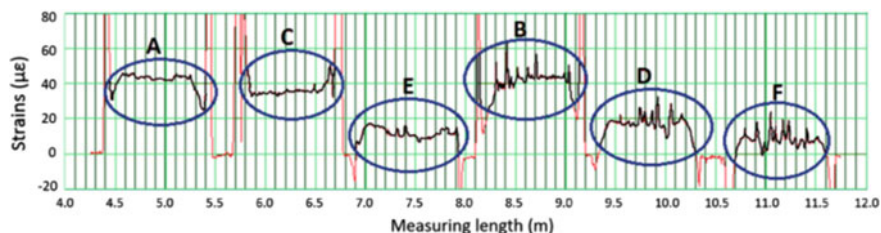


Fig. 12 Optical fibre strains recorded within individual measurement sections before the concrete became cracked (Sienko et al. 2018)

of 10 kN. From this information, the graphs referring to the behavior of the fibers for two load levels (6 kN and 10 kN) are shown in Fig. 13.

Significant changes in the signal presented by the fibers represent internal changes in the structural element. Figure 13a and b, are used as deformations measured by fibers closest to the most elastic surface (A and B). Note that there is a load of 6 kN, there are three characteristic locations of large deformations, confirming or appearing three cracks.

A load of 10 kN, the number of cracks identified by the doubled strain local ends. The measurements also show that the deformations that occur between a crack and another are very small.

In Fig. 13b for cracks 1 and 2, where the extreme stress values occur at the load level of 6 kN, but for load 10 kN, these deformations were smaller, but cover a wider area in the vicinity of the cracks. According to the author this occurs due to slipping on the surface where the contact between the fiber layer and the concrete is maintained, as well as between the jacket and the optical glass core.

The Fig. 13c shows the changes in the tension of the fibers glued to the steel bar. Figure 13d shows the changes in fiber tension in the middle of the element. Figure 13e and f shows deformations on a less elastic surface.

These deformations are positive or negative, depending on the degree of crack development along the shortest edge of the cross section. Based on the measured deformations (Fig. 13), the elongations of the fibers were determined on the measurement bases provided with a length of 10 mm (Fig. 14).

This work (Sienko et al. 2018) confirmed the usefulness of fiber optic technology to identify very small cracks (about 0.01 mm). This conclusion is of significant practical importance, as it refers to cracks that are difficult to identify using other methods. In addition, the research also confirmed the usefulness of optical fiber strain measurement technology for analyzing larger cracks and visible to the naked eye.

In another work, knowing the possibility of implementing the FOS in concrete, Horch et al. (2015) went beyond the existing laboratory studies and used sensors in the foundation element of a tall building. In the work in question, a system called "Backscattered Optical Reflectometry" (OBR) was used.

In this work (Horch et al. 2015), the configuration of the sensor system used has a spatial resolution of 5 mm, a temporal resolution of 50 Hz and a maximum detection

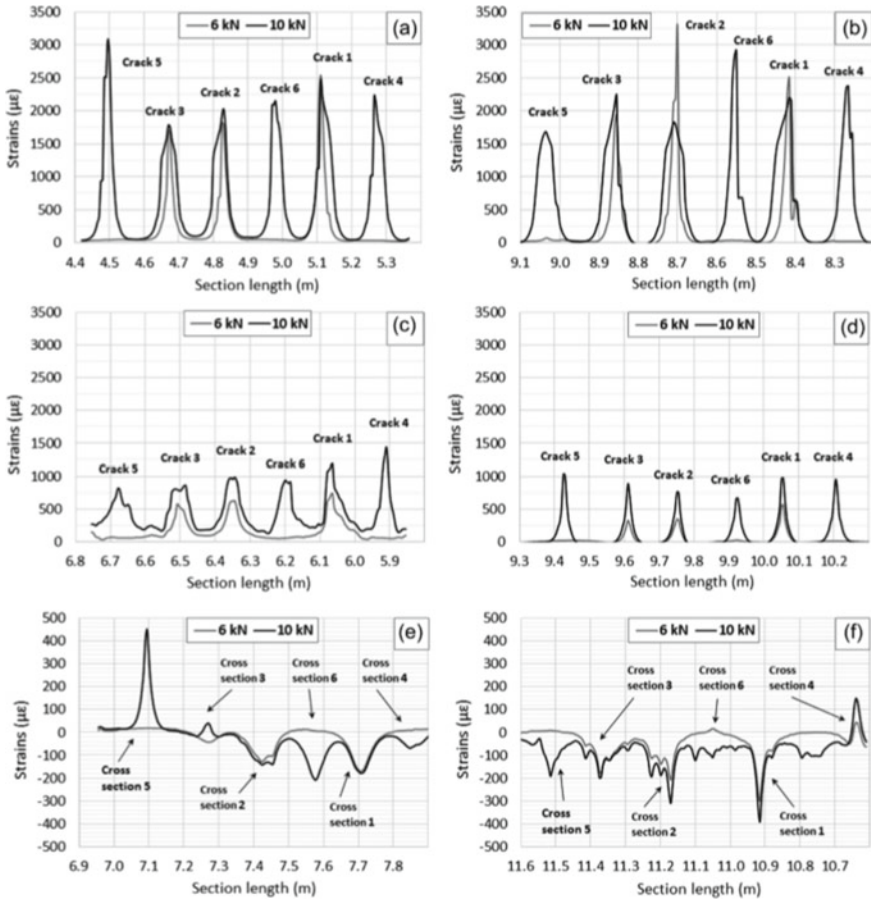


Fig. 13 Changes in FOS strains measured during the test: **a** Top center, **b** Top right, **c** On the reinforcing bar, **d** Center right, **e** Bottom center and **f** Bottom right (Sienko et al. 2018)

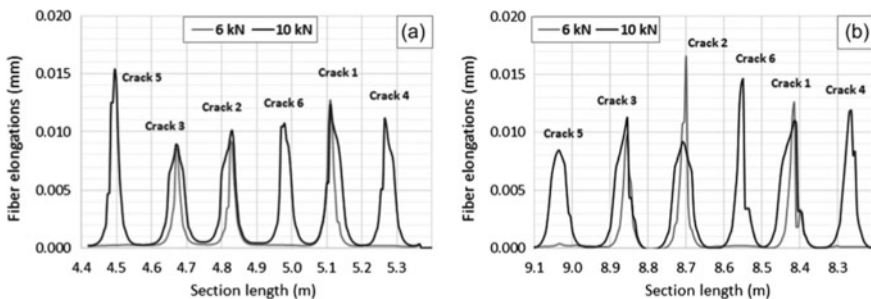


Fig. 14 Changes in elongations of selected FOS: **a** Top center and **b** Top right (Sienko et al. 2018)



Fig. 15 Three different sensor cables attached to the reinforcement (Horch et al. 2015)

of 20 m. As the structural element was 32 m. Altogether, 12 fibers were used coupled to the reinforcement (see Fig. 15), 8 for strain measurement (blue cables) and 4 for temperature (red cables). Regarding the 8 sensors, 4 had cables with a diameter of 3.2 mm and 4 with a diameter of 7.2 mm, in order to also compare the influence of the size of the cables in obtaining the results. The system is described in the Fig. 16.

After pouring, the reference measurement was made when the structure was 18 weeks old, then a reading was taken at 26 weeks and finally another reading at 34 weeks after pouring. For each measurement, temperature changes were measured once.

Regarding temperature measurement, according to the author, as the expected strain values are in the range of $10 \mu\text{m} / \text{m}$, it is necessary to compensate the levels of thermal expansion of the concrete. Temperature sensitive fibers were used for this reason basically.

The values obtained from temperature presented in Fig. 17 presented large ranges of oscillation (noise), analyzed by the author as not consistent with reality, considering that the deformations did not show similar behavior, therefore, it was taken into account some alteration coming from the cables or the machine.

On the other hand, the temperature values oscillate around a constant average value throughout the foundation slab. The two horizontal lines in Fig. 17 show these average values. The author used these means to compensate for thermal expansion, so a constant stress displacement is calculated from the average temperature and subtracted from the measured strain values.

Figure 18 shows the values corresponding to the deformations after temperature compensation. It is seen that the absolute value of the voltage seems to increase. This is natural, as the load on the foundation increases as construction progresses.

For Horch et al. (2015) the purpose of the work was to demonstrate the use of fiber optic sensors distributed inside a real building as opposed to a laboratory installation. With the application in a real structure, some difficulties were observed, both in terms

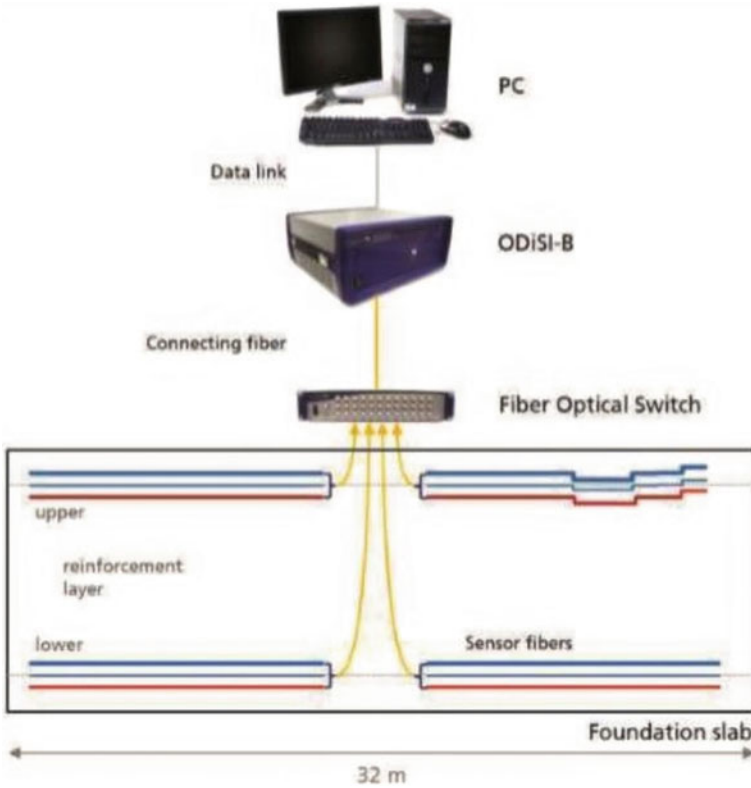


Fig. 16 Location of the sensor cables in the foudation slab and experimental setup (Horch et al. 2015)

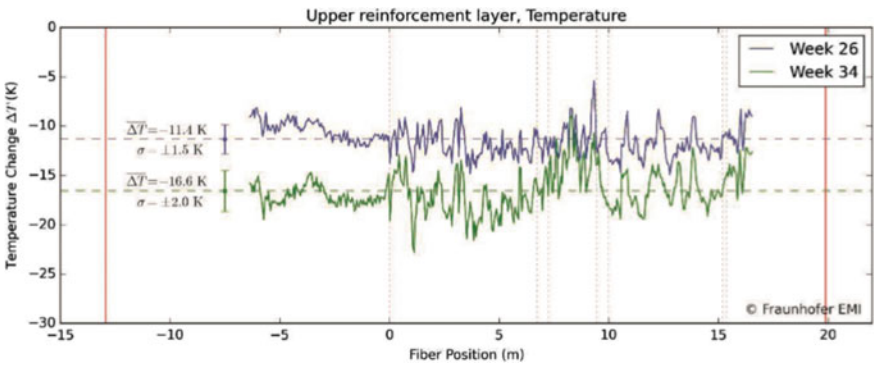


Fig. 17 Results of temperature measurements. The horizontal lines show the average of the temperature curves. The solid red lines indicate the dimensions of the foundation slab. Position 0 is the position where the fibers leave the slab. The dotted gray lines mark vertical sections of the sensor cable (Horch et al. 2015)

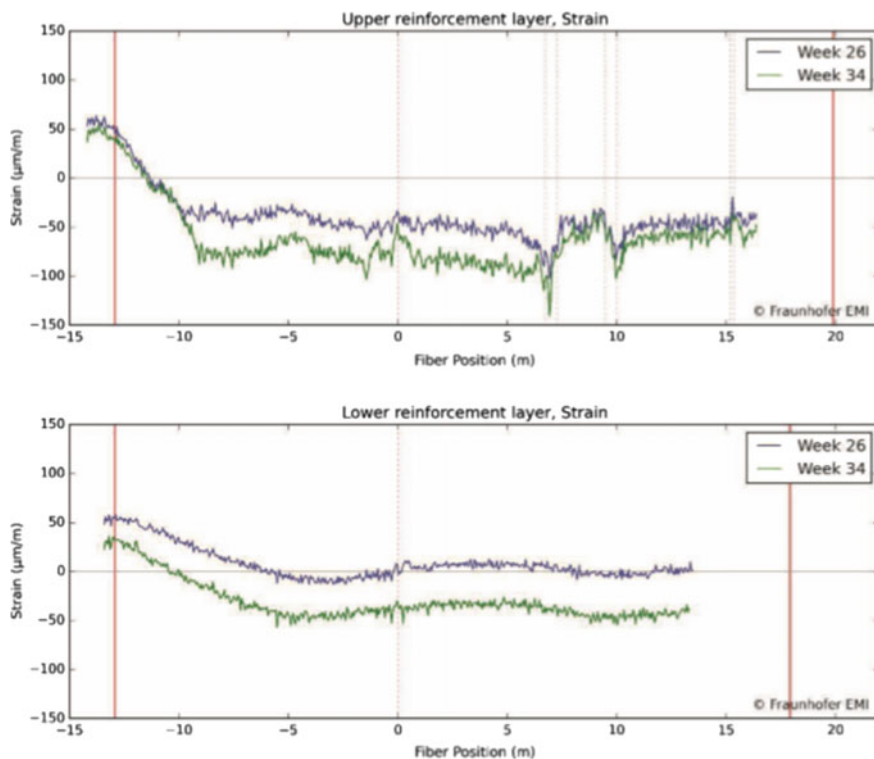


Fig. 18 Results of strain measurements at the upper and the lower reinforcement layer after compensation of temperature (Horch et al. 2015)

of logistics and in obtaining the results. The author states that the data should be better determined and that the factors related to the temperature and the influence of the different dimensions of the cables should be studied, considering that there was no coherent conclusion found by the author for these factors.

4.2 ISR's Monitoring

Fiber optic sensors can be used to measure deformations in concrete elements. It is well known that internal swelling reactions cause deformations due to the stresses caused by the hydration products (expansive gel, ettringite crystals, etc.). The use of FOS specifically for the analysis of structures that present these types of pathology (AAR or DEF) is still very scarce.

One of the works that uses FOS to analyze one of the internal expansion reactions is the work of Dunant & Scrivener (2012). In this work it was performed an experimental study using sensors embedded in reactive and non-reactive concrete samples, with



Fig. 19 Samples in the loading frame (Horch et al. 2015)

the samples loaded in modified creep frames. In the concrete mixture procedures, reactive and no-reactive coarse aggregate were used. The concrete was cured at a temperature of 20° for 28 days. After that time the concrete was placed in a room with a controlled temperature of 38°. It is important to highlight that the reaction (ASR) was not accelerated. After this cure, the samples were placed in creep frames and subjected to 0, 5, 10 and 15 MPa stress levels.

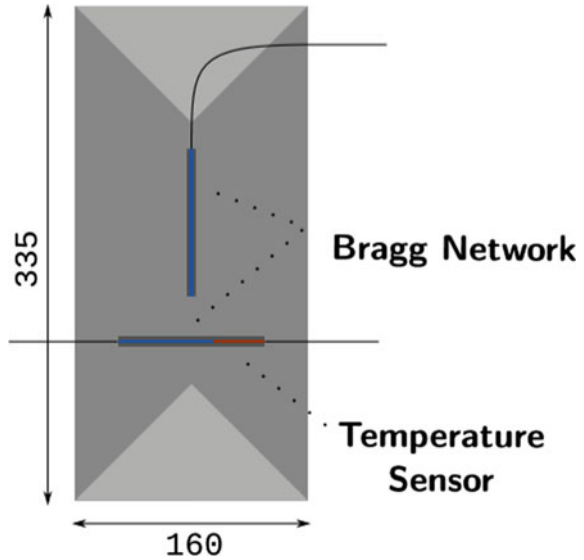
Three standard cylindrical concrete specimens—height 335 mm, diameter 160 mm—were loaded in creep. In each column: a non-reactive sample on top and two reactive samples at the bottom (see Fig. 19). The load in each column was kept constant by hydraulic pressure, and the non-reactive samples allowed us to distinguish strains due to creep from the expansion induced by ASR.

For FOS monitoring the sensors embedded in each sample placed in the loading frame were:

- A temperature sensor;
- The elongation is measured using a *Fiber Bragg grating sensor* (length 67.5 mm);
- The temperature sensor allows the correction of small strain fluctuations due to variations of the ambient temperature.
- A longitudinal strain gauge (optical fibre length 100 mm) which functions in the same way as described above, but without a temperature sensor.
- A computer which logged the sensor values every 20 min. The resolution of both captors is 0.001 mm.

The scheme for installing the sensors in concrete is shown in Fig. 20. During the tests the samples were undisturbed and strain variations due to temperature fluctuations could be compensated. The low dispersion can be explained by the scale at

Fig. 20 Schematic of the sample instrumentation (Dunant and Serivener et al. 2012)



which cracking occurred. As the aggregates used are slow reacting aggregates, the cracks caused by the reaction are all micro-cracks in the aggregates and in the cement paste. No macroscopic cracks were observed at the surface of the samples during the duration of the experiments.

Figure 21 a and b show how deformations occur, both due to the applied loads and the presence of ASR, simultaneously. Under load, a clear direction of propagation is favored: parallel to the load. When the load is further increased, the longitudinal expansion goes to 0, but the lateral expansion increases. This behavior is at odds with the idea of a “redistribution” of the expansion.

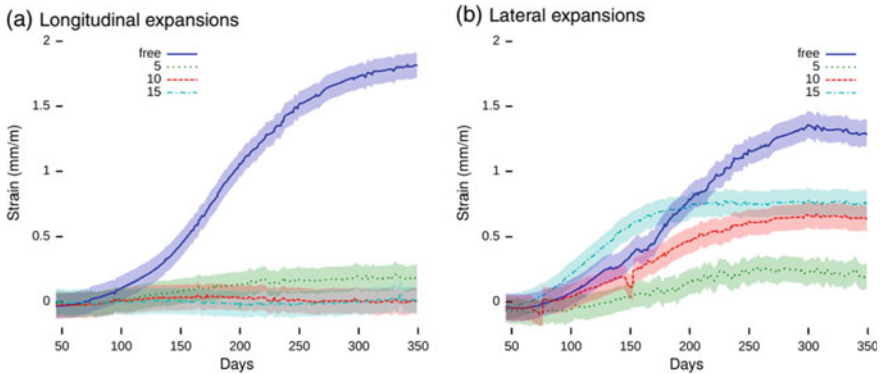


Fig. 21 A Longitudinal and b Lateral and expansions of samples due to ASR and load application (Dunant and Serivener et al. 2012)

Under the 5 MPa stress level, the cracking is more pronounced and its onset began often on the aggregate. Notable features of the crack patterns are that damage concentration are immediately around gel pockets, a network of cracks connecting the gel pockets. A dense pattern of short radial cracks immediately around the aggregates and relatively few main cracks which will grow to the edge of the samples.

The effects of uni-axial stress on the expansion of ASR reactive concrete were linked to the orientation and development of micro-cracks in the aggregates and paste. It is notably found that the expansion is not redistributed, but the applied load forces the orientation of the micro-cracks at the micro-structural level.

The expansions observed experimentally at 5 MPa is probably due to the very specific combination of mechanical properties of the materials, the aggregate type and the morphology of the cracks formed. As the strength of the material was not measured, this result does not indicate that the concrete is less damaged at this load.

Another experimental work that uses FOS to analyze one of the internal swelling reactions is the work of Rocha et al. (2013). This work was developed in two stages, in a laboratory and in a real structure. For laboratory tests, 12 samples of potentially reactive mortar were made for analysis of AAR. The specimens were made in metallic molds and had dimensions of $0.10 \times 0.10 \times 1.40$ m. Before molding, optical fiber sensors were inserted into the molds, as shown in Fig. 22. A total of 12 fiber optic segments were placed: 6 sensing cables segments and 6 tight buffer segments.

The sensors used were distributed optical fiber strain sensors (DTSS). The prepared mortar was composed of potentially reactive aggregate and standard cement. Molding of specimens the mortar was prepared in a standard mechanical mixer with a trait of mixing 1: 2.24: 0.47.

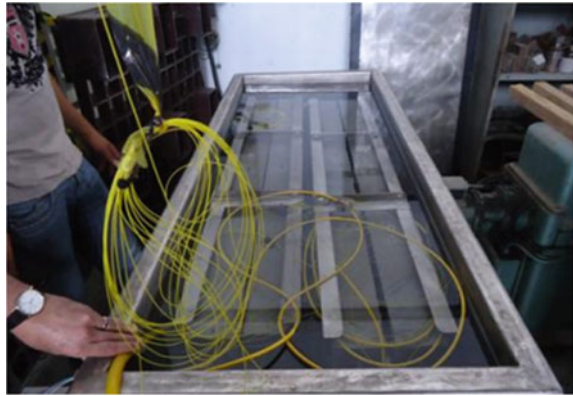
The forms were filled with mortar carefully to avoid damage to the sensors. Demolding occurred after 7 days. To perform external measurements, metal pins were fixed on the lateral surface of each sample. Each group of pins was fixed at least 50 cm apart. External measurements were made to compare with internal optical fiber measurements (Rocha et al. 2013).

After demolding, the specimens were placed in a metal structure that facilitates handling and then in a tank with a 1 N NaOH solution (see Fig. 23) to accelerate



Fig. 22 Installation of the sensors in the molds (Rocha et al. 2013)

Fig. 23 Specimens in the tank (Rocha et al. 2013)



the reaction and a constant controlled temperature of 80 °C during the experiment. External measurements were made daily for 30 days (the duration of the experiment) and internal measurements, with the fiber optic system, were made every 30 min (Rocha et al. 2013).

In his work, Rocha et al. (2013) observed cable degradation due to the aggressiveness of the NaOH solution at high temperature. Although these factors are not considered in field installations, it is relevant in the analysis of laboratory tests, as it affects the condition of connection between sensors and the surrounding expansion mortar.

The results of the tight buffer data are not reliable after 10 days of measurement, while the cable, which is a more protected element, shows consistent results up to the 15th day of measurements (see Fig. 24). After these periods in each case, the information obtained is not relevant.

However, it was observed by the author that the expansion detected within the period in which the measurements were possible, is consistent with the measurements of the external pins. Its magnitude is smaller as expected, due to the gradient of deformation from the outer surface to the center of the sample. However, the important result is evidence of its ability to detect the evolution of AAR.

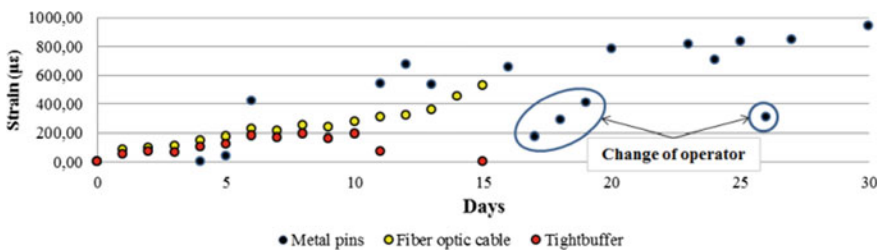


Fig. 24 Comparison of measurements of a large specimen—external metallic pins and optic sensors (Rocha et al. 2013)



Fig. 25 Peti Dam (Rocha et al. 2013)

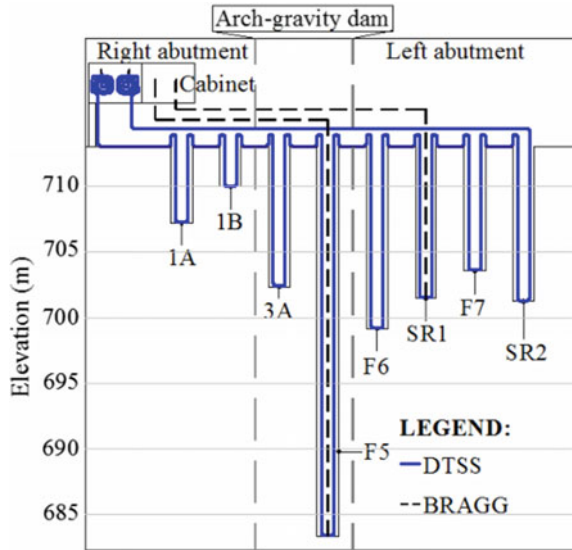
According to the authors (Rocha et al. 2013), the first part of the experiment, carried out in the laboratory, served as a basis for understanding the measurement system that incorporates FOSs and only after the laboratory tests, the study began in a real structure. The structure in question is the Peti dam (see Fig. 25) that is located in the state of Minas Gerais, Brazil and was built between 1941 and 1945.

Unlike the studies previously presented in this work, in the case in question the installation of optical fiber sensors was done after the element already built. In this dam, structural abnormalities have been observed due to the reaction of the alkaline aggregate (AAR) since 1972. Eight preexisting vertical wells, with different depths, were instrumented with fiber optic sensors, with a depth of 3 to 30 m, distributed along the dam. One limitation encountered was the possibility of installing only in one direction. The column regions and the central section were instrumented, with a greater number of sensors on the left column, where greater degradation was reported. In this particular region, the DTSS and FBG sensors were applied. A schematic distribution of the DTSS cable is shown in the Fig. 26. The FBG sensors were installed on the left column next to the DTSS sensors in holes F5 and SR1.

For the installation of the sensors, some interventions were made in the holes, such as cleaning the well, anchoring the cable at the bottom and completely filling the well with a mixture of cement mortar.

Rocha et al. (2013) was observed that the Peti Dam is still showing evidence of a slow and continuous expansion due to the AAR. The installation of DTSS and FBG sensors in this structure offers a great opportunity for validating the use of optical fiber sensors for evaluation of expansions due to internal expansion reactions. Data readings can be taken in a few hours and are taken from a single point for the entire

Fig. 26 Distribution of fiber optic sensors (Rocha et al. 2013)



installation. Also according to the authors, high spatial coverage and information density may be the main advantage of using FOS technology.

Finally, although no studies have been found using fiber optic sensors only for evaluation and monitoring of expansion by DEF, it is important to consider that although the origin of AAR and DEF are different, the effects on structures on a macroscopic scale are basically the same, both cause expansion in concrete elements, and often occur simultaneously. From the studies presented, it is possible to state that regardless of the internal reaction existing in the structure, the expansions can be detected through the FOSs.

5 Conclusions

FOSs technology has been successful for monitoring several types of concrete structures. The application of this type of technology has been increasingly frequent and promising. These are complex studies that need to be planned and done in a conscious way for the results to be valid. Most of the existing tests for this type of use of FOSs are made in the laboratory, however there are already tests on real structures, mainly on bridges and viaducts, and some tests on buildings (according to Horch's work (Barrias et al. 2018)), but on real scale there are important factors to be considered and the analysis of the results tries to be even more complex.

The aforementioned works highlight the potential in monitoring the performance of reinforced concrete structures with the use of FOSs. On the other hand, there are important challenges to be overcome, especially the aspects related to data processing

and the need for a clearer and more objective presentation of the results to the academic community.

Moreover, the information about the equipment used and a justification for choosing the same ones is not always well detailed in the existing works. This fact greatly limits the possibility of reproduction of the same tests in lab or use this approach in real concrete works.

From the bibliographical review performed, one can say that there are currently several types of fiber optic sensors available on the technical market. These are usually sensors for multiple purposes and they have been effective in several works investigated, especially in the study of deformations of concrete elements.

Internal expansion in concrete may come from different internal swelling reactions and the investigation of FOSs to measure such expansion in an open filed to research—few studies have been found on this topic, although its use is promising. Most studies were conducted to measure deformations due, almost exclusively, to mechanical loads imposed on concrete specimens.

References

- Bukenya, P., Moyo, P., Beushausen, H., & Oosthuizen, C. (2014). Health monitoring of concrete dams: a literature review. *Journal of Civil Structural Health Monitoring*, 4(4).
- Bao, T., Wang, J., & Yao, Y. (2010). A fiber optic sensor for detecting and monitoring cracks in concrete structures. *Science China Technological Sciences*.
- Bao, X., & Chen, L. (2012). Recent progress in distributed Fiber optic sensors. *Sensors*, 12(7), 8601–8639. MDPI journal.
- Barrias, A., Casas, J. R., & Villalba, S. (2016). A review of distributed optical Fiber sensors for civil engineering applications. *Sensors (Basel, Switzerland)*, 16(5).
- Barrias, A., Casas, J., & Villalba, S. (2018). Embedded distributed optical fiber sensors in reinforced concrete structures—A case study. *Sensors*, 18.
- Bouzabata, H., Multon, S., Sellier, A., & Houari, H. (2012). Swellings due to alkali-silica reaction and delayed ettringite formation: Characterisation of expansion isotropy and effect of moisture conditions. *Cement and Concrete Composites*, 34.
- Brunetaud, X., Divet, L., & Damidot, D. (2018). Impact of unrestrained delayed Ettringite formation-induced expansion on concrete mechanical properties. *Cement and Concrete Research*, 38(11), 1343–1348.
- Comi, C., Kirchmayr, B., & Pignatelli, R. (2012). Two-phase damage modeling of concrete affected by alkali-silica reaction under variable temperature and humidity conditions. *International Journal of Solids and Structures*, 49(23–24), 3367–3380.
- Custódio, J., & Ribeiro, A. B. (2019). Evaluation of damage in concrete from structures affected by internal swelling reactions—A case study—The 3rd International Conference on Structural Integrity ICSI.
- Dunant, C. F., & Scrivener, K. L. (2012). Effects of uniaxial stress on alkali-silica reaction induced expansion of concrete. *Cement and Concrete Research*, 42(3), 567–576.
- Giles, R. K., & Spencer Jr. B. F. (2015). Development of a long-term, multimetric structural health monitoring system for a historic steel truss swing bridge.
- Godart, B., & Divet, L. (2013). Lessons learned from structures damaged by delayed ettringite formation and the French prevention strategy. Fifth international conference on Forensic Engineering, Institution of Civil Engineers.

- Godart, B. (2017). Pathology, assessment and treatment of structures affected by Delayed Ettringite Formation. *Structural Engineering International*, 27(3).
- Grattan, K. T. V., & Sun, T. (2000). Fiber optic sensor technology: introduction and overview—Optical Fiber Sensor Technology: Fundamentals, chapter 1, Springer Science+Business Media.
- Hisham, K. H. (2018). Optical Fiber sensing technology: Basics, classifications and applications. *American Journal of Remote Sensing*, 6(1).
- Hu, B., Kundu, T., Grill, W., Liu, B., & Toufigh, V. (2013). Embedded piezoelectric sensors for health monitoring of concrete structures. *ACI Materials Journal*, 110(2), 149–158.
- Horch, C., Hupfer, J., & Schäfer, F. (2015). Distributed Fiber optical sensing inside the foundation slab of a high-rise building. AMA Conferences, Nürnberg, Germany.
- Karthik, M. M., Mander, J. B., & Hurlebaus, S. (2016). ASR/DEF Related expansion in structural concrete: model development and validation. *Construction and Building Materials* 128.
- Kesavan, K., Ravisankar, K., Parivallal, S., Sreeshylam, P., & Sridhar, S. (2010). Experimental studies on fiber optic sensors embedded in concrete. *Measurement*, 43.
- Lau, K. T. (2003). Fibre-optic sensors and smart composites for concrete applications. *Magazine of Concrete Research* 55(1)
- Leung, C. K. Y., Wan, K. T., Inaudi, D., et al. (2015). Review: Optical fiber sensors for civil engineering applications. *Materials and Structures*, 48(4), 871–906.
- Martin, R. P., Bazin, C., & Toutlemonde, F. (2012). Alkali aggregate reaction and delayed ettringite formation: common features and differences. 14th International conference on alkali aggregate reaction, ICAAR14.
- Meggitt, B. T. (2010). Fiber Optics in Sensor Instrumentation—Chapter 17 in Instrumentation Reference Book (Fourth Edition).
- Michie, C. (2000). Optical Fiber sensors for advanced composite materials. *Comprehensive Composite Materials*, Vol. 5.
- Noel, M., Sanchez, L., & Tawil, D. (2017). Structural Implications of Internal Swelling Reactions in Concrete: Review & Research Needs Article in Magazine of Concrete Research.
- Pan, J. W., Feng, Y. T., Wang, J. T., Sun, Q. C., Zhang, C. H., & Owen, D. R. J. (2012). Modeling of alkali-silica reaction in concrete: A review. *Frontiers of Structural and Civil Engineering*, 6(1), 1–18.
- Pei, H., Li, Z., Zhang, B., & Ma, H. (2014). Multipoint measurement of early age shrinkage in low w/c ratio mortars by using fiber Bragg gratings. *Materials Letters*, 131.
- Pignatelli, R., Comi, C., & Monteiro, P. J. M. (2013). A coupled mechanical and chemical damage model for concrete affected by alkali-silica reaction. *Cement and Concrete Research*, 53, 196–210.
- Ramakrishnan, M., Rajan, G., Semenova, Y., & Farrell, G. (). Overview of Fiber optic sensor technologies for strain/temperature sensing applications in composite materials. *Sensors*, 16(1).
- Rocha, R. P. O., Jarek, A., Divino, P. L., De Melo, A. V., De Carvalho, A. L., Medeiros, B. L., & De Lacerda, L. A. (2013). *Installation of fiber optic sensors for AAR expansion monitoring in PETI DAM, ICOLD-2013 International Symposium*. Seattle.
- Sakiyama, F. I. H., Lehmann, F. A., & Garrecht, H. (2019). Structural health monitoring of concrete structures using fibre optic based sensors: A review. *Magazine of Concrete Research*, 1–45.
- Sakiyama, F. I. H., Lehmann, F. A., & Garrecht, H. (2019). Structural health monitoring of concrete structures using fibre optic based sensors: A review. *Magazine of Concrete Research*.
- Selier, A., Grimal, E., Multon, S., & Boudarot, E. (2017). Swelling Concrete in Dams and Hydraulic Structures, Civil Engineering and Geomechanics Series, DSC.
- Surahayo, A. (2019). Concrete. In: Concrete Construction. Springer, Cham.
- Surahayo, A. (2019). Physical Properties of Concrete. In: Concrete Construction. Springer, Cham.
- Sieñko, R., Zych, M., Bednarski, Ł., & Howiacki, T. (2018). Strain and crack analysis within concrete members using distributed fibre optic sensors. Structural Health Monitoring.
- Sims, I., & Poole, A. B. (2017). Alkali-Aggregate Reaction in Concrete: A World Review. CRC Press.

- Taheri, S. (2019). A review on five key sensors for monitoring of concrete structures. *Construction and Building Materials*, 204.
- Tseng, K. K. (2002). Health monitoring of concrete structures subjected to environmental attacks. *Smart Structures and Materials: Smart Systems for Bridges, Structures, and Highways*.
- Thomas, M. D. A., Fournier, B., & Folliard, K. J. (2013). Alkali-Aggregate Reactivity (AAR) Facts Book Office of Pavement Technology Federal Highway Administration.
- Uva, G., Porco, F., Fiore, A., & Porco, G. (2014). Structural monitoring using fiber optic sensors of a pre-stressed concrete viaduct during construction phases. *Case Studies in Nondestructive Testing and Evaluation*, vol. 2.
- Yehia, S., Landolsi, T., Hassan, M., & Hallal, M. (2014). Monitoring of strain induced by heat of hydration, cyclic and dynamic loads in concrete structures using fiber-optics sensors. *Measurement*, vol. 52.
- Yu, Z., Jian, M., Hu, S., & Xiaodong, S. (2016). Delayed Ettringite Formation in Fly Ash Concrete under Moist Curing Conditions 5th International Conference on Durability of Concrete Structures—Shenzhen University, Shenzhen, Guangdong Province, P.R.China.

Evaluation of Lime Solution in Kneading Water for the Preparation of Roughcast and Plaster Coating



A. M. Santos, A. J. Costa e Silva, J. M. Freitas Mota, J. M. P. Q. Delgado, F. A. N. Silva, and A. C. Azevedo

Abstract Comprehension of the mechanical fixation behaviour of coatings is crucial for a better understanding of the bonding systems, especially at the interface between the mortar and the base. Physical adherence is related, among other things, to the contents of the materials used in the roughcast and plaster, due to the necessary colloidal water penetration into the pores of the substrate, providing mechanical locking of hydrated calcium sulfoaluminate and calcium silicate crystals, according to the principle of active pores. This study proposes to evaluate the influence of the use of a lime solution as a substitution for the kneading water in the preparation of roughcast and plaster, with blends of 0% (reference), 5%, 10%, and 15% in relation to the amount of water used. The experiment included preparing masonry panels $220 \times 180 \text{ cm}^2$, prepared with concrete blocks and ceramic bricks. Direct tensile bond strength tests were performed, and the results, with a 95% confidence level, showed significant differences for levels from 10% lime blend in the roughcast, in both base types, reaching increments of up to 39% in relation to the reference sample, a behaviour not identified in the plaster samples.

A. M. Santos · J. M. F. Mota

Federal Institute of Education Sciences and Technology of Pernambuco (IFPE), Recife 50740-545, Brazil

e-mail: andresantos@recife.ifpe.edu.br

A. J. Costa e Silva · F. A. N. Silva

Department of Civil Engineering, Catholic University of Pernambuco, Recife, PE 50050-900, Brazil

e-mail: angelo.silva@unicap.br

F. A. N. Silva

e-mail: fernando.nogueira@unicap.br

J. M. P. Q. Delgado (✉) · A. C. Azevedo

Departamento de Engenharia Civil, CONSTRUCT-LFC, Universidade Do Porto, Rua Dr. Roberto Frias, s/n, 4200-465 Porto, Portugal

e-mail: jdelgado@fe.up.pt

A. C. Azevedo

e-mail: antonio.costaazevedo@fe.up.pt

© The Author(s), under exclusive license to Springer Nature Switzerland AG 2022

J. M. P. Q. Delgado (ed.), *Building Rehabilitation and Sustainable Construction*,

Building Pathology and Rehabilitation 23,

https://doi.org/10.1007/978-3-030-95487-1_4

Keywords Adherence · Mortar · Hydrated lime · Spatterdash

1 Introduction

A primary step for a satisfactory behaviour of mortar coating systems is the preparation of the base, with the objective of ensuring adequate tensile strength of the system. The use of roughcast is one of the most used techniques in this sense, since it standardizes the characteristics of the base, increases the contact area and, mainly, increases the roughness of the surface.

To further increase the adhesion in this interface, it is common to damend the substrate and, in some cases, the transport of the calcium element to the pores of the base by spraying lime solution before the application of the roughcast or the ambush, as described in several studies (Costa e Silva et al., 2018; Mota et al., 2009; Scartezini and Carasek, 2003; Chase, 1985).

Silva (2004) points out that the water/binder ratio is a determining factor in the behaviour of roughcast adhesion, since the amount of adequate (controlled) snoozing water favors the reduction of porosity at the interface. Moreover, this relationship should also be seen as a requirement of technological control of mortar and all materials whose matrix is cementitious, to the extent that the higher the coefficient of sorptivity (function of porosity), the greater the pergrowth and the possibility of moving deleterious agents, thereby mitigating the durability.

Several authors, as Silva (2004), Barbosa et al. (2006) and Apolônio et al. (2015), identified that the water/cement ratio is inversely proportional to the tensile strength. However, mineral additions elevate this property and promote the form of adequate rupture, that is, in the block (see Mota et al., 2011).

Carasek (1996) reports that, on porly bases, the adhesion resistance is inverse to moisture content and directly proportional to cement content. However, the pore system is directly responsible for capillary suction, having as an important vector for analysis, the substrate moisture (suction). Therefore, the context of the mechanical adhesion process is defined by the mean and variable rays of the capillaries of the mortar; which must be higher than those of the base.

It is well known that in mortar coatings, adhesion to substrates depends on factors related to physical, chemical, mechanical characteristics, details related to application, environmental conditions, among other factors (Rudit, 2009).

The mortar coating system [base preparation layer (roughcast) and finishing layer (plaster or plaster)] fixed on substrates has initial support directly influenced by the rheological properties of the mortar, considering that the release still occurs in the milling state. This condition influences the surface tension of the substrate surface at the time of contact, a tension that will result in the joining forces that must be strong and stable enough to ensure that this formed interface is not the weak link of the union of materials (Paes, 2004 and Zanelato, 2015).

The main objective of this study is to verify the influence of the use of lime solution in place of the water of the amassing of the roughcast and the plaster, in contents of

0, 5, 10 and 15% (in relation to the amount of water used of the lime) on the adhesion resistance to concrete block bases and ceramic brick.

1.1 Theory

Evaluating the adhesion itself, especially the interface of the preparation mortar (roughcast) with the base, there is a predominantly mechanical process. This process occurs, essentially, by transferring water in the colloidal state of the mortar to the substrate through suction. Thus enabling the entry of part of the cement-paste into the pores of the masonry in the dissipation stage of hydroxides, silicates and aluminates, in such a way that it promotes mechanical anchorage due to the locking after tightening of these crystals arising more abundantly in the state of precipitation until hardening (Carasek, 1996; Mota, 2015).

Another aspect that affects adhesion is the porosity of the substrate. Work presented by Torres et al. (2018) evidences the strong influence of substrate porosity on adhesion, based on an experimental study developed with different types of bases and mortars. High absorption substrates can result in insufficient water for the complete hydration of cement near the interface area between the substrate and the roughcast, which weakens this region (approximately 20 μm). On the other hand, substrates with low absorption can generate water accumulation in the interface zone, increasing porosity due to the wall effect that leads to high water/cement ratio (Apolônio et al., 2015; Carasek, 1996), reducing its mechanical support capacity. Figure 1 shows the mechanism of adhesion of mortars in ceramic blocks.

As observed in the figures presented, the mixed mortars of cement and hydrated lime (proportions, in volume, of 1:3 and 1:0.25:3 (cement:lime:sand), for the images on the left and right side, respectively) have greater capacity of adhesion extension at the microscopic level. It is observed that, at the interface, its structure is denser and continuous, as well as decreasing micro cracks in this region. Therefore,



Fig. 1 Aspect of the interface region between mortar with different proportions of cement and lime, and base in ceramic brick (Carasek, 1996)

mixed cement and lime mortars can be considered ideal because they provide the complementary qualities of the two materials (Carasek et al., 2001).

Figure 1 also shows the importance of the workability of the mortar in the adhesion with the base, since it is determinant to provide the greatest extent of anchorage possible between the layers. Stolz et al. (2016) identified even more significant influence of the rheological behaviour of the mixture than of the roughness of concrete substrates in the adhesion of mixed cement mortars and hydrated lime, in some situations.

In this sense, the lime present in the mortar plays an important role in the adhesion, because it improves workability, water retention, adhesion extension, initial adhesion, in the fresh state, and, in the hardened state, provides greater resistance to surface abrasion, compression, traction, deformability and potential adhesion resistance (Mota, 2006).

In fact, the use of lime for the manufacture of mortars, even as the main binder, refers to buildings executed since before the widespread use of Portland cement. For the laying of blue-storey at the end of the nineteenth century, hydrated lime pastes were used, with the ability to support mechanical support and durability proven to be adequate, judging by their conservation in these historic buildings to this day (Botas et al., 2017).

In the interaction of mortar with substrate, there is the theory of active pores, from which the water flow between the mortar and the substrate can be understood as the interaction of two pore systems (Detriché et al., 1985 and Dupin et al., 1988), with a sense of this flow from the pores of greater to the smallest diameter.

It is known that the pore system of the ceramic substrate, for example, presents with approximately constant rays over time. In turn, the mortar in the fresh state presents itself with a system of pores of variable rays over time, which decrease with the hydration of the agglomerations of the mortar. When the mortar is released into the porous substrate of initially empty capillaries, it is observed that the mean rays of the mortar are higher than those of the capillaries of the substrate, thus providing the flow of water in the direction of the mortar to the substrate. In the suction there is a mechanical tightening of the solid particles of the mortar, in view of the depression of the capillaries, concomitantly with an acceleration of crystallization resulting from the hydration of the dissolved products of the binder, resulting in anchorage (Dupin et al., 1988).

Mortar pores vary in diameter 0.001 μm to approximately 5 μm . Therefore, the pores of the substrate that exceed the maximum value of 5 μm will be understood as dead pores, not active, since they do not have adequate capillary strength. The average radius of the pores of the mortars can be increased by changing the proportions of binders and aggregate, the latter increasing the granulometric distribution (increasing the fineness modulus), thus aiming at increasing the suction capacity of the substrate (Winslow & Liu, 1990).

Based on these concepts, we can see the important influence of porosity and water avidity from the base on the adhesion of mortar coatings. Comparing the concrete blocks with the ceramic bricks it is possible to note that not only the total absorption of water is important, but mainly the absorptivity, or the speed that water

can penetrate the base, measured from the initial water absorption test. In this case, the measurement identifies the amount of water absorbed during 1 min of contact, reproducing more faithfully the flow that occurs between the paste present in the mortar and the base.

Concrete blocks, in general, although they may present lower total water absorption, usually present higher initial absorption levels, which strongly contributes to mechanical adhesion. In the case of ceramic bricks, porosity is very dependent on the manufacturing characteristics, notably its sintering temperature. Article presented by Azevedo et al. (2018) evidence this influence, correlating the adhesion of mortar coatings with temperature, with an increase of up to 50% in their behaviour when cooking goes from 750 to 950 °C.

However, in addition to the microanchorage that governs in the adhesion, the important macroanchorage is evidenced by the roughness and geometry imposed on the surfaces. In the microstructure, the cement hydration products responsible for the bond between substrate and mortar are ettringite and C-S-H crystals (Polito et al., 2009), and in the macrostructure roughness can influence the regulation of shear resistance. Figure 2 shows the relationship of ettringite crystals with the interface.

However, Silva and Libório (2003) studied the adhesion mechanism in ceramic bricks and concluded that the extensive interlaced fibrous network of C-S-H growing on the masonry surface is the main responsible for mechanical adhesion. Although adhesion is necessary in all layers of the mortar coating system, roughcast is the only one that has adhesion as its main function, since it anchors the posterior layer, regulating porosity and uniformizing absorption (Mota, 2015 and Santos et al., 2019).

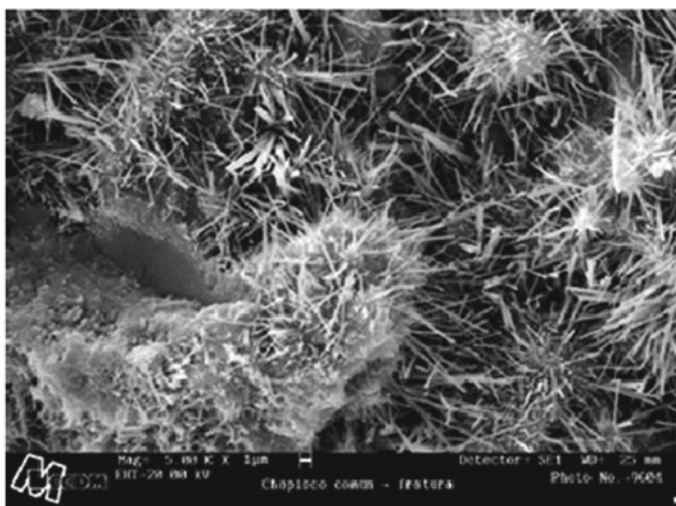


Fig. 2 Ettringite crystals at the interface of the common roughcast/concrete (Silva and Libório, 2003)

It is observed that the roughcast is a fluid mortar, composed of trace in volume of 1:3 to 1:4, cement and medium or coarse sand, and this compound, after released on the surface, must go through a curing period of three days before receiving the coating, with a maximum thickness of 0.5 cm (Yazigi, 2004). In turn, the behaviour of mortars is a function of the base (cleaning and porosity), the model of the service execution process (labour) and the anchorage layer (Thomaz, 2001).

Environmental conditions (room temperature, ventilation, humidity, etc.) during roughcast execution can also influence its behaviour, which can be attenuated from the performance of wet curing. Moura (2007) studied the curing in mortar coatings applied to concrete substrates and states that in all combinations (three types of roughcast mortar and coating), the effect of heat resulted in the fall of adhesion resistance of the samples.

Regarding the use of lime solution, Voss (1933) observed, from petrographic and crystallographic analyses, that at the interface between mortar and ceramic blocks is a layer of calcium called “adhesion layer” (microanchorage with predominance of ethringitis).

In the same vein, Chase (1985) showed that calcium settlement in ceramic base forms a denser crystalline structure in the interfaces of mortars with ceramic substrates, thus justifying a greater resistance of mechanical adhesion.

Several researchers, as Scartezini and Carasek (2003), Mota et al. (2009) and Costa e Silva et al. (2018), verified the beneficial effect of lime solution on ceramic and concrete block masonry on the adhesion of mortar coatings. Another researcher who conducted a similar study was Angelim (2005), who concluded that the coating applied on lime solution presented superior tensile adhesion resistance than that applied on roughcast, however it was not verified with industrialized mortars.

2 Materials and Methods

The experimental study discussed in this work was designed to verify the adhesion resistance of mortar coatings on two specific substrates, one ceramic and the other concrete, simulating coatings and substrates commonly found in residential construction, where numerous adhesion problems have been observed between the coating and the substrate. Thus, laboratory experiments were used to determine if the conditions of the mortar coating found in situ would also appear in tests in a controlled environment.

To evaluate the effect of kneading water blended with hydrated lime (percentages of 0 (reference), 5, 10, and 15%) in the preparation of roughcast and plaster, the experiment began with the construction of masonry panels $220 \times 180 \text{ cm}^2$ using ceramic and concrete blocks, both with sealing properties, rendered with mortar in 3 different situations, as follows:

- (a) Situation 1—evaluation of the influence of the lime solution used to substitute kneading water for plaster applied to conventional roughcast, mixed only with water;
- (b) Situation 2—evaluation of the influence of the lime solution used to substitute the kneading water of roughcast applied under conventional plaster, mixed only with water;
- (c) Situation 3—evaluation of the influence of the lime solution used to substitute the kneading water of roughcast, without applying plaster.

It is noteworthy that situations (a) and (b) are justified by seeking to verify the adherence of the complete coating construction system (with the addition of lime blends only in the roughcast, or only in industrialized coating mortar, in relation to the cement), and situation (c) is justified because it is the technological contribution to pure adhesion at the interface of the prepared mortar base (roughcast) at the wall with a ceramic block base, predominant in current building sites in the country.

2.1 Materials

The masonry was made of ceramic blocks and concrete blocks, with subsequent preparation of the base (roughcast) and an industrialized mortar coating application. The objective was to verify the tensile bond strength. The materials used for this purpose were:

- Portland cement: CP II Z—32;
- Hydrated lime: CH-I;
- Small aggregate: natural quartz origin with maximum characteristic diameter of 4.8 mm, fineness modulus 2.28.
- Industrialized mortar: for coating on roughcast, widely used in the Region, being purchased locally. It is well-known that the specification of this material for this coating endeavoured to establish characteristics as homogeneous as possible for this layer;
- Kneading water: drinkable and supplied by the local supply company.

For the classification of the different blocks, tests were applied to determine the Initial Water Absorption Index (WAI), as recommended by the ASTM C67 (2009) standard. For this test, the humidity is previously removed in an oven for 48 h at a temperature of 100 to 110 °C and then cooled for 4 h at room temperature, at which point the dry mass is determined. Subsequently, the blocks are immersed in a water layer of approximately three (3) mm for 1 min. After that, all excess water is removed from the surface in contact, then the wet mass is determined, as Fig. 3 shows, which determines the initial absorption process of the ceramic blocks. The equation gives the calculation of the initial water absorption index of the block:

$$\text{WAI} = (P_i - P_a) / A \quad (1)$$



Fig. 3 Initial water absorption test (WAI)

where WAI is the initial water absorption index ($\text{kg}/\text{m}^2\text{min}$); P_i is the mass (kg) of the unit after immersion for 1 min; P_a is the mass (kg) of the kiln-dried unit for 24 h and A is the area (m^2) of the unit's face in contact with water.

According to Gonçalves and Bauer (2005), there is no consensus regarding the relationship between the WAI and the adhesion. Some of the criticisms made to this determination process are that the time involved in the test performance is relatively short for constituting a water transport mechanism since the capillary forces continue to act for a more extended period. Likewise, he mentions that the referred to process occurs in “free” water and not in “restricted” water, of which fresh mortar is comprised.

The fact that this absorption of free water (WAI determination) is not impeded by various forces acting on mortar is also noted. These forces are capillary forces, physical adsorption by the mortar components, and, at a later stage, the chemical bond of the water due to the evolution in the hydration of the binder (cement). In reality, substrate and mortar must be considered two independent pore systems as the interaction between these systems determines water flow.

Compression strength tests were performed to characterize the block's mechanical properties in the same position in which these elements were used to elevate the panels, with perforations positioned uniformly, in the case of the ceramic blocks. Before applying the tests, capping was performed with cement pastes in order to level the surfaces horizontal load reception (see Fig. 4). In both cases, a calibrated hydraulic press was used, with a nominal capacity of 30 tonnes, in addition to the positioning of 2-inch-thick metal skirt allowing for uniform load transfer on all surfaces of the test samples, as determined by NBR 15,270–1 (2017) and NBR 12,118 (2013).

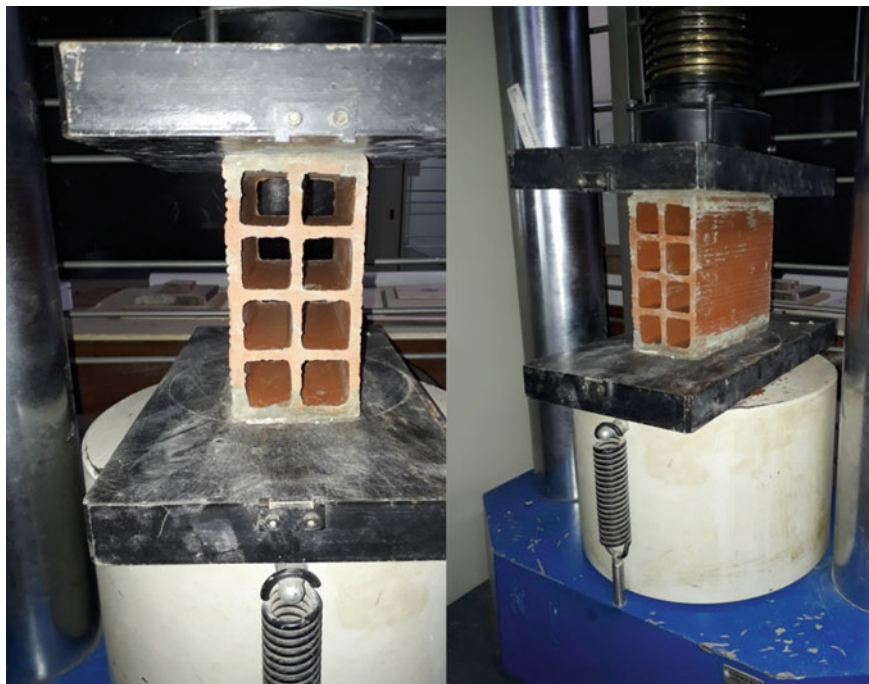


Fig. 4 Mechanical characterization tests of ceramic blocks

2.2 Sample Preparation

In this study, three wall panels were constructed, with dimensions of $220 \times 180 \text{ cm}^2$, one of concrete block and two of ceramic blocks, one of which was located outside the laboratory, simulating field conditions (ceramic block), and the other two were placed inside. The three study panels were erected on the same day and covered with the same materials. The following sample preparation details are given for better understanding according to the three test conditions devised for this study.

2.2.1 Situations 1 and 2: Roughcast and Plaster Prepared with a Lime Solution

As previously mentioned, for these conditions, masonry panels were constructed with ceramic and concrete blocks, both with sealing characteristics, followed by the application of roughcast and plaster, with an average thickness of 5 mm and 20 mm, respectively. Figure 5 shows the walls built inside the laboratory for adhesion testing purposes.

The amount of kneading water was derived from the minimum amount necessary to produce plasticity identified as suitable for a 5 mm thick roughcast. It is a known



Fig. 5 Wall of ceramic blocks with plaster being applied

fact that in roughcast, a reduced water-cement ratio mitigates porosity at the interface between the paste and the substrate, just as the use of lime increases the extent of adhesion (Carasek, 1996; Mota, 2006 and Silva, 2004).

In all cases, the base (roughcast) was prepared 24 h after erecting the walls. Curing was executed by spraying water on the roughcast for three consecutive days following its application. The same stonemason carried out all activities to avoid a distinction of operational effects on the test results.

Samples were created with the addition of lime to the conventional roughcast for block masonry, ceramic (Samples CB-1 to CB-8), and concrete (Samples CB-9 to CB-16), in proportions of 0 (reference), 5, 10, and 15% in proportion to the water used in the mixture.

The roughcast ratio was 1:3:0.8 (cement, sand, water-cement ratio), and the ratio for construction of the masonry walls was 1:6:1.5 (cement, lime, sand, and water-cement ratio). The minimum amount of water necessary to produce suitable workability was used for a thickness of 5 mm of roughcast. It is a known fact that in roughcast, a reduced water-cement ratio mitigates porosity at the paste/substrate interface, just as lime increases the extent of adhesion (Carasek, 1996) (Table 1).

In all cases, the base (roughcast) was prepared 24 h after constructing the walls. Water curing was executed three days after the application of the roughcast. Following this period of curing the roughcast, the industrialized mortar coating was applied manually to the two panels, using the amount of water established by the product

Table 1 Description of the ceramic blocks analysed

Sample	Percentages of lime addition to the plaster (%)	Percentages of lime addition to the roughcast (%)
CB-1	0	0
CB-2	5	0
CB-3	10	0
CB-4	15	0
CB-5	0	0
CB-6	0	5
CB-7	0	10
CB-8	0	15

supplier, each with an average thickness of 20 mm. All activities were carried out by the same stonemason to avoid a distinction of operational effects on the test results, as shown in the following figure.

In Fig. 6 the roughcast application processes on the ceramic and concrete block walls, where curing in the figures can be verified. Figure 7 shows the samples, i.e., the concrete walls with a lime solution and plaster application (Table 2).

After 28 days, tests were executed to determine the tensile bond strength (18 points per sample) by a specific, experienced, and trained professional following the procedures described in NBR 13,528 (2019) for current regulations.

The selection of testing points was established, in Fig. 8, by way of horizontal and vertical markings on the masonry. To prevent the defined points from being torn

**Fig. 6** Concrete and ceramic block walls with roughcast containing lime



Fig. 7 Concrete block base with a lime solution and plaster application

Table 2 Description of the concrete blocks analysed

Sample	Percentages of lime addition to the plaster (%)	Percentages of lime addition to the roughcast (%)
9	0	0
10	5	0
11	10	0
12	15	0
13	0	0
14	0	5
15	0	10
16	0	15

off, these were positioned at the joints, thus ensuring that the pull-out tests be carried out exclusively on the base, without compromising the results.

The tests were executed on 50 mm diameter circular test units, with the adherometer installed on metal dolly glued with high-adhesion epoxy adhesive. The test was performed with a force transducer, pull-off testing equipment, brand ALFA INSTRUMENTOS (indicator for test machines 3105C), serial number 10F0E6, precision class III, manufactured 04/2014, and associated electronic instrumentation, brand ALFA INSTRUMENTOS, five-digit nominal range, and 1 point, adhering to the procedures defined in standard NBR 13,528 (2019).

Due care was taken with the joints of both masonry bases to avoid any influence on the test. Highly adhesive epoxy (Sikadur 31—Sika) was used. Metal dollies were glued to the test unit of each coating with quick-drying plastic glue. This glue provides



Fig. 8 View of the ceramic block panel during the application of plaster mortar

greater force than the coating can withstand, guaranteeing the dolly's adhesion to the coating for bonding the circular dolly for the tensile strength test of the coatings, cutting the mortar with a cutting disc (cup saw).

Following the rupture, the load recorded by the apparatus, the rupture shape, and the diameter of the test unit were registered in two locations to calculate the area. As the device already provided the load data (Kgf_r) for 50 mm test bodies, a conversion was necessary to obtain the test's real breaking stress point (Figs. 9 and 10).

Figure 11 presents, in an illustrative way, the variables used in the two study situations carried out in the investigation. In both cases, industrialized plaster mortar, as indicated by the supplier to be specific for coating in external environments, was used to ensure homogeneity.

To the plaster and the roughcast mix, the water for the mortar was prepared with the different amounts of lime established in this investigation. For example, in the



Fig. 9 Gluing the adhesion plates and Adhesion test

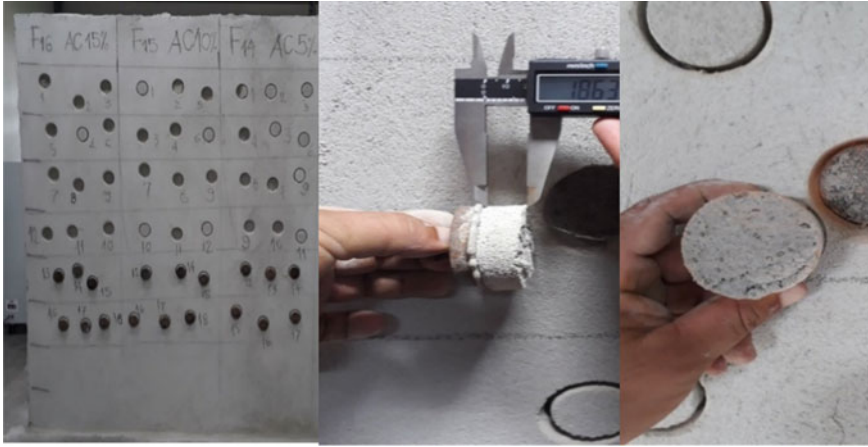


Fig. 10 Example of the wall and concrete block tested, checking the pull out thickness and form of ruptures

5% blend, 50 g of hydrated lime was used for each 1000 ml of water, while 100 g and 150 g were used for the 10 and 15% blend, respectively.

The amount of lime solution used in the mixtures was determined by adding 8.2 L of water for each 10 kg as a reference, in the case of roughcast samples, and 16 L of water for each 100 kg of industrialized mortar, for the plaster families. These quantities were established to present a suitable consistency for application on the walls.

The application of this mortar was performed manually, followed by wet curing for three consecutive days. The same stonemason carried out all activities to avoid a distinction of operational effects on the test results.

2.2.2 Situation 3: Roughcast with Lime Solution - Without Plaster

The roughcast used was prepared in a proportion, in volume, of 1:3:0.8 (cement Portland CPHZ-32, coarse sand, water-cement ratio), exclusively on the ceramic sealing blocks, with blends of lime added to the kneading water of 0, 5, 10, and 15%. Eighteen months after the panels' preparation, tensile bond strength tests were performed directly on the roughcast according to procedures described in NBR 13,528 (2019).

The option for the prolonged cure time to perform this test was designed to analyse the influence of bad weather on the wall, since the panel, in this case, was outside the laboratory for the entire period.

The tests were performed on 50 mm diameter circular test bodies, with the adherometer installed on metal dollies glued with high-adhesion epoxy adhesive. The detail relevant to obtaining an adequate surface (smooth and regular) for gluing the metallic dolly onto the roughcast was the installation of a 50 mm diameter PVC

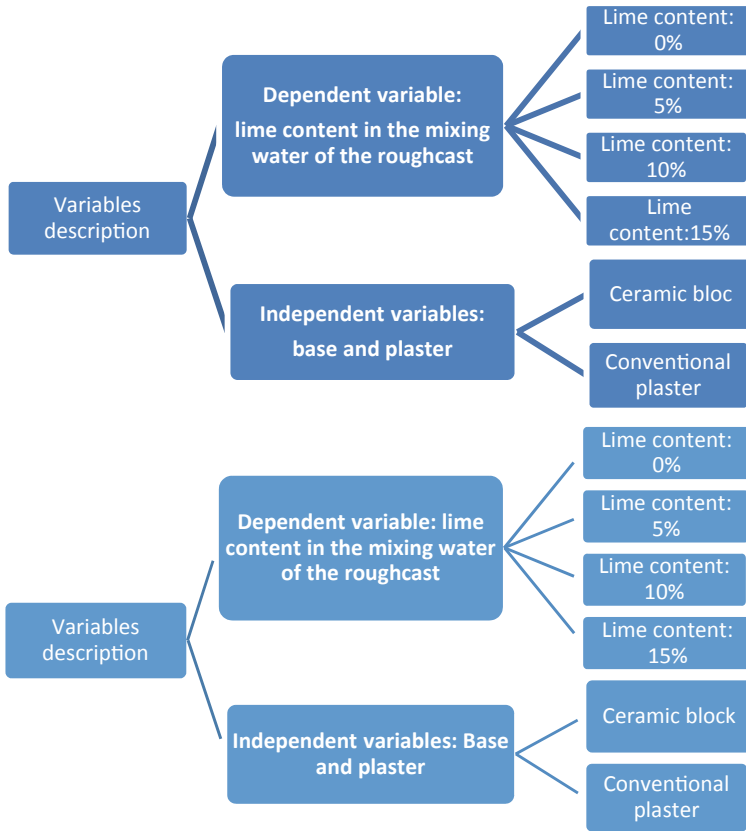


Fig. 11 Flowchart of the experiment (Situations 1 and 2)

mounting skirt, secured with silicone, in such a way that after 24 h, it was filled with epoxy for subsequent bonding of metallic dollies, also using epoxy. Under these conditions, the test could be performed by evaluating the tensile bond strength exclusively of the roughcast itself at the base's interface.

Just as in the previously described condition, the metallic pieces were positioned only on the ceramic blocks' surface, and the statistical analysis was performed based on the analysis of variance (ANOVA).

3 Results and Discussion

For a more accurate evaluation of this study, the values obtained during the characterization of the materials used (blocks and mortars) will be presented initially, followed

by the results of the adhesion tests in reference to the analysis of the influence of the addition of lime in the roughcast and plaster samples.

3.1 Material Characterization Tests

Portland cement CP II Z-32 was used to prepare the various mortar samples, and the physical and chemical characteristics of the cement used are presented in Table 3. Likewise, the hydrated lime used throughout the work was of the CHI type, calcium, and its main characteristics are described in Table 4. Finally, fine natural quartz sand aggregate was used and this material is characterized as described in Table 5 and Fig. 12.

The characterization of the ceramic and concrete blocks used in the study is shown in Table 6, which identifies the results' average values according to NBR15270-1 (2017). In each case, 19 samples were tested, 13 for compressive strength, and the others for geometric characterization and determination of physical indices (absorption and WAI). In concrete blocks, the test procedures adhere to the requirements presented in NBR 12,118 (2013).

Table 3 Characteristics of the cement (CP II Z-32)

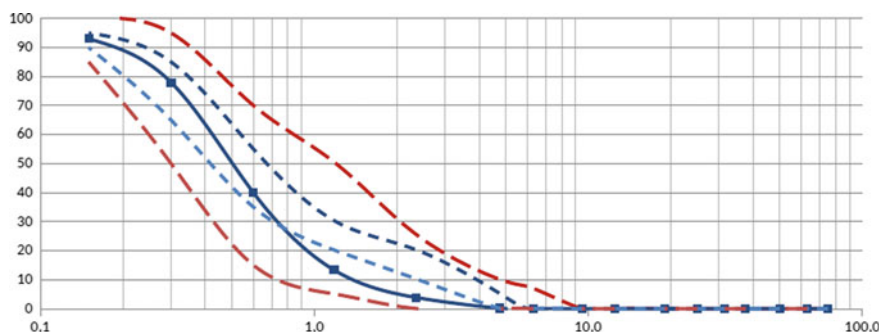
Physical characterization	Apparent density (g/cm^3)		1.2 g/cm^3
	Specific mass (g/cm^3)		3.09 g/cm^3
	Compressive strength	28 days (MPa)	39.5
Chemical characterization (%)	Potential composition of Clinkle	C ₃ S	20–70
		C ₂ S	10–60
		C ₃ A	1–15
		C ₄ AF	5–15
	CaO / free lime		0–2
	MgO / SO ₃		0–6

Table 4 Characteristics of hydrated lime

Mineral	Limestone
CO ₂	≤ 2.21
Ca(OH) ₂	≥ 92.5%
SO ₃	≤ 0.05
Mg(OH)	≤ 5.0%
SiO ₂	≤ 1.3%
Relative Humidity	≤ 2.0%
Apparent Density	0.56 g/cm^3

Table 5 Characteristics of the fine aggregate

Description	Results
Unit mass	1.3 g/cm ³
Fineness module	2.28
Maximum diameter	2.36 mm
Powder content (%)	2.38%

**Fig. 12** Granulometric curve of the fine aggregate used**Table 6** Characteristics of the blocks used

Base	Dimensionss (cm)	Water absorption (%)	Compressive strength (MPa)	WAI—Initial Rate of Absorption (g/200ccm ² /min)
Ceramic block	9 × 19x19	14.6	2.8	12.1
Concrete block	9 × 19x39	6.4	4.0	16.9

In the roughcast case, its hardening properties were evaluated for each of the families with the corresponding percentages of lime added to the roughcast water mixture. Figure 12 describe the performance of the tests according to the NBR 13,279 (2015) standard. In this case, the mechanical aspects of the mortar were evaluated in the hardened state (Figs. 13 and 14).

Figure 15 show the growing resistance behaviour in the two aspects of the tests developed, i.e., in the flexural strength and the compression of the mortar bars made with the roughcast mix and their respective lime additions to the families studied.

3.2 Adhesion Resistance Tests

To facilitate understanding the results, the presentation and discussion of these tests will be separated according to the study conditions previously described.



Fig. 13 Ceramic and concrete blocks used



Fig. 14 Tensile test in flexion and compression test on mortar bars

3.2.1 Situation 1 - the Influence of the Lime Solution in Water Used for Plaster Mortar

Tables 7 and 8 show the results of tensile bond strength of families 5 to 8 (panel composed of ceramic blocks) and 13 to 16 (panel composed of concrete blocks) where the plaster application contained a lime solution, respectively 0, 5, 10 and 15%, with no lime in the preparation of the roughcast.

The results obtained in this situation are shown in Fig. 16, which indicates the average value found in 18 samples tested for each sample analysed.

From the experimental results presented above, it is clear that the contribution of the lime solution to the plaster mortar was not significant, which could be proven

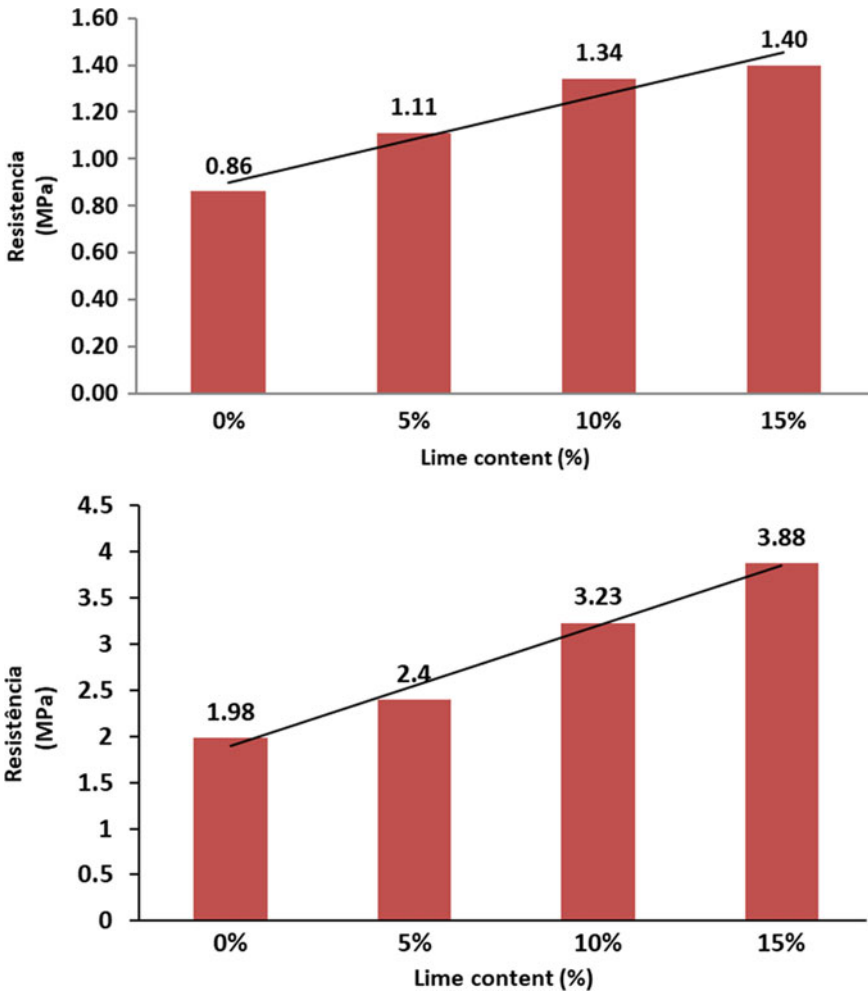


Fig. 15 a Tensile strength in mortar prisms and b resistance to roughcast compression

from the variance analysis (ANOVA) performed with a 95% confidence interval, in which a significant difference between samples was not observed (see Table 8).

It is essential to highlight that, in these cases, the predominant rupture was of the cohesive type, most in the body of the plaster mortar itself, which hinders a more effective analysis of the possible contribution to adherence at the interface between layers.

Table 7 Average adhesion strength values obtained from plaster with a lime solution in the roughcast base without lime in the ceramic blocks

Sample	Medium resistance (Mpa)	Coefficient of variation (%)
CB-1	0.21	41
CB-2	0.25	29
CB-3	0.27	22
CB-4	0.23	36
CB-5	0.21	41
CB-6	0.23	28
CB-7	0.19	49
CB-8	0.25	34
CB-9	0.34	33
CB-10	0.38	42
CB-11	0.41	33
CB-12	0.49	33
CB-13	0.31	42
CB-14	0.29	43
CB-15	0.31	44
CB-16	0.33	39

Table 8 Variance analysis (influence of the lime solution in plaster), with a significance level of 95%

Influence	F _{calculated}	F _{critic}	Significant difference
Concrete block			
Reference (0%) × 5%	0.13	4.13	No
Reference (0%) × 10%	0.005	4.13	No
Reference (0%) × 15%	0.3	4.13	No
Ceramic block			
Reference (0%) × 5%	1.25	4.13	No
Reference (0%) × 10%	0.44	4.13	No
Reference (0%) × 15%	3.82	4.13	No

3.2.2 Situation 2 - the Influence of the Lime Solution in Water Used in Roughcast Mortar

Present the results of tensile bond strength for CB-1 thru CB-4 (panels composed of ceramic blocks) and CB-9 thru CB-12 (panels composed of concrete blocks) where

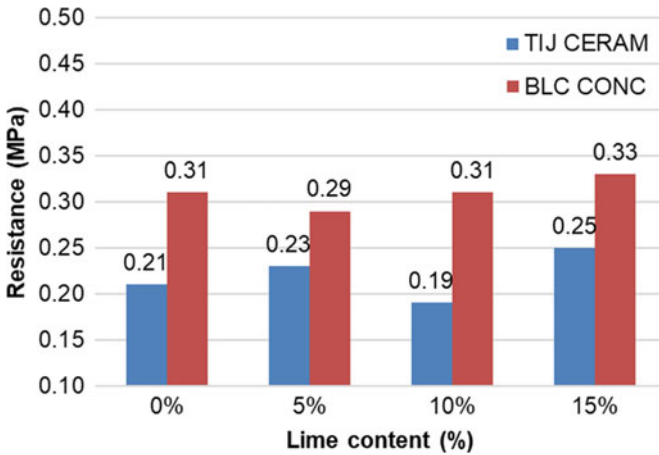


Fig. 16 Influence of lime solution used in the water for plaster mortar

the roughcast application contained a lime solution, respectively 0, 5, 10 and 15%, with no lime in the preparation of the plaster mortar.

Contrary to what was observed in the plaster application, a significant influence of the lime solution on the adhesion was identified in the case of roughcast, especially for the blends of 15% in concrete blocks and 10% for ceramic bricks (see Table 9).

Compared to the reference (0% lime content), gains of 12%, 21%, and up to 44% were observed for the blend of 15% lime in the mixture used for concrete blocks, and 19, 29, and 10% for ceramic bricks. These results point to a more marked influence in the case of concrete blocks, which may be due to their naturally greater roughness and initial suction, characteristics that make the base more sensitive to changes in

Table 9 Variance analysis (influence of lime solution on roughcast), with a 95% significance level

Influence	F _{calculated}	F _{critic}	Significant difference
Concrete block			
Reference (0%) × 5%	0.86	4.13	No
Reference (0%) × 10%	2.9	4.13	No
Reference (0%) × 15%	11.1	4.13	Yes
Ceramic block			
Reference (0%) × 5%	3.21	4.13	No
Reference (0%) × 10%	6.8	4.13	Yes
Reference (0%) × 15%	0.94	4.13	No

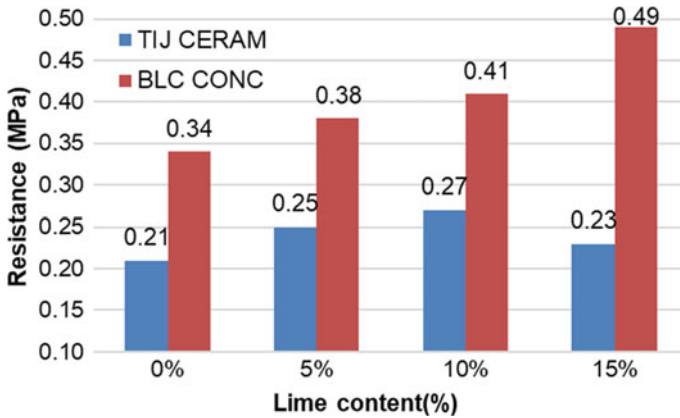


Fig. 17 The influence of the lime solution used in the water for roughcast mortar

the contact surface with the mortar, caused by micro anchoring due to the mechanical locking of crystals produced in cement hydration (C-S-H and, fundamentally, ettringite) in their pores (active pore principle) (Fig. 17).

It is also interesting to note a slight decline in the values achieved in the samples containing 15% lime in the case of ceramic bricks, which may indicate an optimum potential blend for this type of application for this type of base.

The results obtained in both situations, in addition to indicating the greater importance of adding lime to the roughcast layer, also pointed out more significant adhesions in masonry with the concrete block than ceramic brick. This finding can be justified considering that the last element's smoother and denser surface provides more significant difficulties for micro-anchoring and macro-anchoring.

3.2.3 Situation 3: Roughcast Applied to the Base of the Ceramic Blocks - Without Plaster

The results of the tests are shown in Fig. 18, indicating the average values and the respective variation coefficients obtained in the 12 samples tested for each sample studied. From this data, a tendency. In the increase of adhesion between the roughcast and the base can be seen in direct proportion to the increase of lime content in the roughcast water, with potential gains of 17%, 27%, and up to 39% in relation to traditional roughcast without lime. These results corroborate the expected behaviour for this interface found in similar studies using a lime solution as an alternative to achieve improvement in the interface with ceramic blocks, something that is also confirmed by the variance analysis obtained (see Table 10).

It is essential to point out that the same values were found even with low levels of water suction in these blocks, which suggests that further in-depth studies are necessary to verify the potential of gain found from this type of technique.

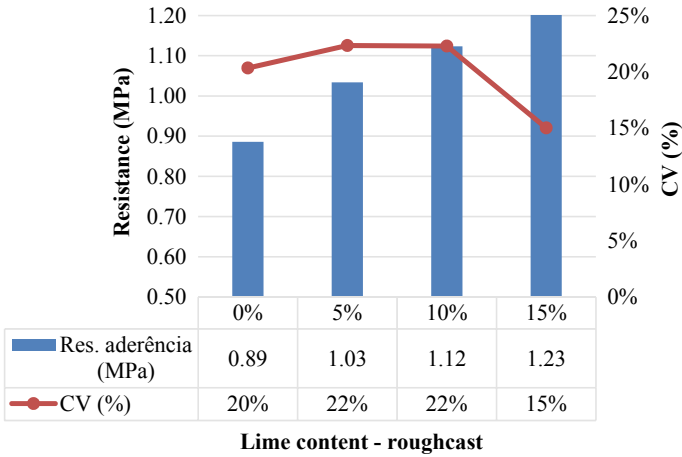


Fig. 18 Indicative graph of tensile bond strength tests

Table 10 Variance analysis (influence of the lime solution on roughcast without plaster), with a 95% significance level

Influence	F _{calculated}	F _{critic}	Significant difference
Reference (0%) × 5%	3.06	4.3	No
Reference (0%) × 10%	7.10	4.3	Yes
Reference (0%) × 15%	21.3	4.3	Yes

4 Conclusions

Based on the discussion of this text as well as on the results obtained from experimentation, it is possible to present some highly relevant considerations of the influence of lime solution as a substitution for kneading water in mortar, as follows:

- In the samples in which the experiments were carried out with the lime solution as a substitute for the kneading water in plaster, no influence was identified for any of the levels used in the research, either for the bases with concrete blocks or for those with ceramic bricks;
- On the other hand, the lime solution mixed into the tested roughcast with subsequent application of the industrialized mortar showed significant influence (with a 95% confidence level according to the variance analysis) for 10% lime content, in the case of concrete blocks, and 15%, for ceramic bricks, with gains of 44 and 29%, respectively, compared to the reference samples;
- In this case, the type of rupture observed in some samples of the plaster mortar applied (cohesive rupture) denotes that the actual bond strength between the interface and the base could be equal or even higher. Thus, it is necessary to act not only

upon the accuracy of the interface connections but also on the support capacity of the entire coating system;

- The highest adherence values were obtained for roughcast applied on concrete block bases compared to ceramic bricks, which must be due to the increased initial water absorption. This increased absorption favors the flow of the paste present in the mortar into the substrate pores, increasing the local population network of the ettringite and C-S-H crystals (micro-anchorage - active pores principle);
- The proportionally more accentuated improvement observed in concrete blocks, compared to ceramic bricks, can also be credited to its greater surface roughness, which makes this material more sensitive to the penetration and accumulation of the lime solution between its interstices;
- In samples with pure roughcast, in this case, applied exclusively on ceramic brick bases, without plaster, there was also an increase in adherence when used with the incorporated lime solution. Significant influence was identified, with a 95% confidence level, for the 10 and 15% lime levels in relation to the reference samples, with gains of up to 39% adherence;
- In this case, the adequacy of the test method adapted from NBR 13,528 (2019) exclusively for evaluating the adherence of the roughcast to the base stands out, as perceived from the predominant rupture observed in the interface between the roughcast and the base. The average tensile bond strength of the coating where the preparation of the substrate was done with traditional roughcast, reinforces the need and importance of this fact in applying mortar coatings.
- The lime solution incorporated into the roughcast kneading water proved to be efficient, while further studies are recommended.

It can be concluded, from this study, that the preparation of the base is of fundamental importance for the tensile bond strength and that, therefore, the addition of lime solution to the roughcast is an economically viable and satisfactory alternative to obtain positive results in environments where the bonding strength is highly compulsory. However, it is necessary to emphasize the need to develop new research to establish a more extensive range of information about the roughcast with lime solution, especially with the analysis of more substrate options and different variables.

The analytics performed indicate that the study's main conclusion reveals that the substitution of traditional kneading water for the lime solution in the preparation of the roughcast, with blends of 10 and 15%, presented promising results regarding the adherence gain in comparison with the reference samples executed conventionally.

It should be noted that the proposed solution is very low-cost (estimated at R \$ 0.08 / m²) and easy to implement at the building site, given the natural availability of lime and the simple change in the mortar preparation procedure. Additionally, there is also a better rheological behaviour of mortars mixed with a lime solution, which favours the adhesion incrementation with the base.

Finally, for ongoing research projects, some experiment options can be suggested, for example:

- Evaluate the application of roughcast and roughcast system plus plaster directly on structural concrete.

- Adapt the adhesion test procedure to identify the adhesion in this interface region so that the cut performed penetrates through to the interface between the roughcast and the plaster.
- Apply the coating directly to the studied substrates—ceramic block and concrete block—to evaluate the influence of lime on this layer’s adhesion autonomously.
- Add other lime additive blends, including mineral additives (pozzolans) in the roughcast, to assess other possible adherence benefits.

References

- American Society for Testing and Materials. (2009). ASTM C67: Standard Test Methods for Sampling and Testing Brick and Structural Clay Tile. ASTM International, West Conshohocken, PA.
- Angelim, R. R. (2005). Efficiency of substrate preparation of ceramic blocks with lime solution in the adhesion resistance of mortar coatings. In: VI Brazilian Symposium on Mortar Technology, Florianópolis: UFSC, ANTAC, Brazil.
- Apolônio, P. H., Mota, J. M. F., Barbosa, F., Costa E Silva, A. J., Silva, G. A., & Oliveira, R. A. (2015). Comparative analysis of roughcast adhesion resistance with different water/ligand ratios and addition of methcaulin. In: Brazilian Symposium on Mortar Technology, XI, Porto Alegre, UFRGS, ANTAC, Brazil
- Azevedo, A. R. G., França, B. R., Alexandre, J., Marvila, M. T., Zanelato, E. B., & Xavier, G. C. (2018). Influence of sintering temperature of a ceramic substrate in mortar adhesion for civil construction. *Journal of Building Engineering*, 19, 342–348.
- Barbosa, F. R., Mota, J. M. F., & Carneiro, A. M. P. (2006). Influence of the addition of metemolim on the properties in the hardened state: capillarity and mechanical resistance of inorganic mortars for the recovery of historical monuments. In: National Meeting of Environment Technology Built, XI, Florianópolis-SC, UFSC, ANTAC, Brazil.
- Botas, S., Rosário, M., & Velosa, A. (2017). Air lime mortars for conservation of historic tiles: Bond strength of new mortars to old tiles. *Construction and Building Materials*, 145, 426–434.
- Brazilian Association of Technical Standards. (2019). NBR 13528: Render made of inorganic mortars applied on walls—Determination of bond tensile bond strength. Rio de Janeiro, Brazil.
- Brazilian Association of Technical Standards. (2005). NBR 13279: Mortars applied on walls and ceilings—Determination of the flexural and the compressive strength in the hardened stage. Rio de Janeiro, Brazil.
- Brazilian Association of Technical Standards. (2017). NBR 15270–1: Ceramic components—Clay blocks and bricks for masonry Part 1: Requirements. Rio de Janeiro, Brazil
- Brazilian Association of Technical Standards. (2013). NBR 12118: Hollow concrete blocks for concrete masonry—Test methods. Rio de Janeiro, Brazil.
- Carasek, H. (1996). Portland cement-based mortar adhesion to porous substrates—evaluation of intervening factors and contribution to the study of the binding mechanism. PhD Thesis, Universidade de São Paulo, São Paulo, Brazil.
- Carasek, H., Cascudo, O., Scartezini, L. M. (2001). Importance of materials in the adhesion of mortar coatings. In: Brazilian Symposium on Mortar Technology, IV, Brasília, UnB, ANTAC, Brazil.
- Chase, G. W. (1985). The effect of pretreatments of clay brick on brick-mortar bond strength. In: 3rd North American Masonry Conference, Arlington, USA.
- Costa E Silva, A. J., Azevedo, A. A. C., Souza, M. T. G. (2018). Influence of base preparation on adhesion of mortar coatings on ceramic bricks. In: 7th Euro-American Congress On Construction

- Pathology, Rehabilitation Technology And Heritage Management—REHABEND 2018, Cáceres, Spain.
- Detriché, C. H., Gallias, J. L., Grandet, J., & Maso, J. C. (1985). Influence des paramètres de mise en oeuvre et de composition sur le comportement des mortiers d'enduit. *Materials and Structures*, 18(3), 193–200.
- Dupin, I., Détriché, C. H., & Maso, J. C. (1988). Accrochage Direct d'un Enduit Sur un Isolant Par Une Liaison de Type Mécanique Dans le Cadre d'un Procédé d'Isolation Par l'Extérieur. *Materials and Structures*, 21(5), 370–378.
- Gonçalves, S. R., & Bauer, E. Case study of variation of tensile adhesion resistance on a wall. In: VI Brazilian Symposium on Mortar Technology, pp. 562–567. Florianópolis: SBTA, Brazil.
- Mota, J. M. F. (2006). Influence of coating mortar on axial compressive strength in resistant masonry prisms of ceramic blocks. MSc Thesis, Universidade Federal de Pernambuco, Recife, Brazil.
- Mota, J. M. F. (2015). Reinforcement of Resistant masonry with Reinforced Mortar and Addition of Metakaolin. PhD Thesis, UFPE—Universidade Federal de Pernambuco, Recife, Brazil.
- Mota, J. M. F., Carasek, H., Costa E. Silva, A. J., Barbosa, F. R., Feitosa, A., & Santos, W. (2011). Inorganic mortars with the addition of metakaolin. In: Brazilian Symposium on Mortar Technology, IX, Belo Horizonte, UFMG, ANTAC, Brazil.
- Mota, J. M. F., Costa E. Silva, A. J., Carasek, H., & Barbosa, F. R. (2009). Work analysis of the adhesion resistance of mortar coatings with the preparation of the substrate with lime and roughcast solution. In: X Congreso Latinoamericano de Patología Y XII Congreso de Calidad en la Construcción, CONPAT 2009, Valparaíso-Chile.
- Moura, C. B. (2007). Adhesion of external mortar coatings on concrete substrates: influence of temperature conditions and ventilation to cure roughcast. MSc Thesis, Universidade Federal do Rio Grande do Sul, Porto Alegre, Brazil.
- Paes, I. N. L. (2004). Evaluation of Water Transport in Mortar Coatings in the Initial Moments after Application. PhD Thesis, Universidade de Brasília, Brasília-DF, Brazil.
- Polito, G., Carvalho Júnior, A. N., & Brandão, P. R. G. (2009). Microstructural characterization of mixed mortar interface/ceramic block. In: Brazilian Symposium on Mortar Technology, VIII, Curitiba, UFPR, ANTAC, Brazil.
- Rudit, F. R. (2009). Contribution to the study of adhesion of mortar coating and roughcasts in concrete substrate. MSc Thesis, Universidade Federal do Rio Grande do Sul, Porto Alegre, Brazil.
- Santos, A. M., Costa E. Silva, A. J., & Mota, J. M. F. (2019). Influence of lime on lime adhesion for coating. In: Brazilian Symposium on Mortar Technology. XIII, Goiânia, UFG, ANTAC, Brazil.
- Scartezini, L. M., & Carasek, H. (2003). Factors that influence the tensile strength of mortar coatings. In: Brazilian Symposium on Mortar Technology, V, São Paulo, EPUSP, ANTAC, Brazil.
- Silva, V. (2004). Adhesion of roughcasts in structural concrete—Improvement of the microstructure of the interface zone by adding silica from rice husk. PhD Thesis, Universidade de São Paulo, São Paulo, Brazil.
- Silva, V. S., & Liborio, J. B. L. (2003). Evaluation of the effect of silica extracted from rice husk on the adhesion of mortars and roughcasts. In: Brazilian Symposium on Mortar Technology, V, São Paulo, EPUSP, ANTAC, Brazil.
- Stolz, C. M., Masuero, A. B., Pagnussat, D. T., & Kirchleim, A. P. (2016). Influence of substrate texture on the tensile and shear bond strength of rendering mortars. *Construction and Building Materials*, 128, 298–307.
- Thomaz, E. (2001). Technology, management and quality in construction. São Paulo: Editora Pini, São Paulo, Brazil.
- Torres, I., Veiga, M. R., & Freitas, V. P. (2018). Influence of substrate characteristics on behavior of applied mortar. *Journal of Materials in Civil Engineering*, 30(10), 04018254.
- Voss, W. C. (1933). Permeability of brick masonry walls: An hypothesis proceedings of the American Society for Testing Materials, Philadelphia, USA.
- Winslow, D., & Liu, D. (1990). The pore structure of paste in concert. *Cement and Concrete Research*, 20(2), 227–235.
- Yazigi, W. A. (2004). Building technique, 6ª Edition, São Paulo: Editora Pini, São Paulo, Brazil.

Zanelato, E. B. (2015). Roughcast influence on tensile bond strength of mortar coatings in ceramic blocks. MSc Thesis, Universidade Estadual do Norte Fluminense Darcy Ribeiro, Campos dos Goytacazes, Brazil.

Technological Performance of Cellulose Fibre Reinforced Cement-Based Mortars



E. C. L. Rezende, A. J. Costa e Silva, J. M. P. Q. Delgado, and A. C. Azevedo

Abstract This work presents the study of the effect of the incorporation of cellulose fibres in mortars, as waste recycling alternatives in the productive chain of construction, in favor of sustainability policy. Building construction is an area of great potential to absorb waste in its productive chain, producing alternative materials and thus reducing the environmental impact with the reuse of by-products or waste from other industries and its own chain. In the search for innovation, the use of vegetable fibres and particularly cellulose fibres in cementitious composites have been studied throughout the world and in mortars, such fibre-matrix interaction allows to enhance certain properties inherent to the material. Thus, this research was aimed to evaluate the effect of fibre in the deformability of the mortars, focusing on mechanical behavior from comparing mortars with fibre and mortar without fibre, these called reference mortar. To obtain the composites were formulated experimental dosages of mixed mortar cement and lime in a ratio of 1:1:6 by weight with the addition of fibre at 5 and 10% of the total mix weight, and a water/agglomerates rate fixed at 0.60. The analysis between the mortars was made in the fresh state with tests for measuring the consistency and the weight density and in the hardened state with tests of tensile strength when bending and compression strength tests. The results showed that the greater the fibre content added smaller are the tensile and compression strengths, however antagonistically, the higher the fibre content the higher is the value of tenacity and deformability of the composite clearly characterized at the load versus deformation curve. Thus, even supporting lower load bearing, the use of

E. C. L. Rezende · A. J. C. Silva
Civil Engineering Department, Universidade Católica de Pernambuco, Recife, Brazil
e-mail: emanuelalobo@hotmail.com

A. J. C. Silva
e-mail: angelo.silva@unicap.br

J. M. P. Q. Delgado (✉) · A. C. Azevedo
Departamento de Engenharia Civil, CONSTRUCT-LFC, Universidade Do Porto, Rua Dr. Roberto Frias, s/n, 4200-465 Porto, Portugal
e-mail: jdelgado@fe.up.pt

A. C. Azevedo
e-mail: antonio.costaazevedo@fe.up.pt

the cellulose fibres provides a greater bearing capacity to deformations required for the mortar, particularly in post crack stage, absorbing more energy before rupture.

Keywords Cement · Cellulose fibres · Stiffness · Toughness

1 Introduction

The environmental issue and the concept of sustainability have been widely discussed in the world and solutions have been sought that minimizes aggression so far, either by reducing the exploitation of natural resources or by reducing waste and waste in production chains. Building construction, despite being a branch of technological activity considered as a villain as a major consumer of resources and waste generator, presents itself as a sector with great potential for the use of solid waste in its own production chain, especially in the area of construction materials.

“Restrictions on the use of environmentally inappropriate materials and the growing need to use waste have led industry to seek new alternatives to the products offered on the market. A clear example of this trend is the restriction on the use of asbestos fibres [...]” (Macedo et al., 2012).

The use of plant fibres and alternative cements - both from waste - is considered a good option in the search for alternative fibre cements (Silva, 2002). Increasingly, the reinforcements of mortars in building construction (reinforced composites) with the addition of natural and synthetic fibres are studied. Since 1970, different fibres have been researched as possible substitutes for asbestos fibre for cementitious matrix reinforcement (Motta and Agopyan, 2007).

The wide variety of these fibres and their peculiarities regarding their physical and mechanical properties represent a universe of possibilities, characteristics, advantages and disadvantages, being necessary the characterization and study to evaluate their behaviour integrated to the matrices and thus the feasibility of application as reinforcement to mortars.

These studies are paramount, because even synthetic ones that have a greater expressiveness of use, present significant variations even when they are of the same type, but from different manufacturers, as showed Motta and Agopyan (2007).

The same is the case with plant fibres, depending on the characteristics of the plant, soil and environment. In Brazil, as an example of these natural fibres, we have coconut bagasse, sugarcane, cellulose pulp tailings of eucalyptus, sisal, bamboo, pine and others. Because it is a natural material and exists in abundance, the use of plant fibres has often been motivated by the fact that it is a renewable, biodegradable material, due to its availability at low cost, including often presented as waste.

In this work, the approach focuses on the incorporation into mortars of cellulose fibres from white paper residues, as an alternative. In building construction, the use of cellulosic pulps in the reinforcement of materials based on cementitious matrices has acquired increasing importance worldwide, especially in developed countries (Savastano Jr., 2000).

Apart from the tailings of cellulosic pulp, the white paper residue represents about 25% of the content of Brazilian household waste, as Neves (2003) reports, and if it is possible to recycle it, it would reduce the environmental impact and pollution generated mainly by burning, the form most used by the population. The practice of recycling is well established in the world and in the country, and the use of cellulosic mortar has been an alternative for the reuse of this waste as added by Neves (2003).

Thus, the study of the effect of these residues of cellulose fibres on the deformability of mortars will experimentally enable an evaluation of the mechanical behavior, strength and tenacity of these reinforced composites, evaluating whether there is potential to use white paper fibres in mortars efficiently as an alternative to sustainable construction policy.

1.1 Objectives

The general objective of this work is to evaluate the technical potential of the use of cellulose fibres from white paper in the composition of alternative mortars. The specific objectives of this work are:

- To form a theoretical basis on the theme related to research;
- Compare the properties in the fresh and hardened state of mortar with 2 contents of fibre incorporated with reference mortar without fibres;
- Study the difference of resistances between the mortars with fibres and the reference mortar without fibres; - check whether the mortars with fibres have a better response to the deformations imposed by mechanical tests;
- Check how the mortar behaves with cellulose fibres for tenacity;
- Evaluate whether the production of composites reinforced with cellulose fibres is feasible from a sustainable point of view for building construction, based on the results of the experimental work.

1.2 Fibrous Materials as Reinforcement

According to the definition of the Aurelio dictionary, fibres are slender filaments that, arranged in bundles, constitute certain animal, plant or mineral substances. Figueiredo (2001) defines fibres as discontinuous elements, the length of which is much longer than the larger dimension of the cross-section, for its study of fibre-reinforced concrete.

Silva (2002) classifies the fibres as organic and inorganic according to their composition, and subdivides the organic fibres into natural and artificial. He points out that there is still disagreement among some authors regarding the classification and types of fibre, especially with regard to cellulose fibres, which, even having natural origin, undergo pre-treatment before their use, as in the case of papers.

There is a wide variety of natural and artificial fibres with potential use for reinforcement of composites for the construction industry. For this work, the emphasis will be given to plant fibres, whose classification is organic fibre, even if there is conflict as to their origin, because it is understood as coming from natural resources.

Building construction employs fragile matrices: pastes, mortars and concrete. These matrices, mostly derived from mineral binders, rupture without plastic deformation and, although resistant to compression efforts, do not support large tensile requests and dynamic loads. To compensate for this deficiency, other materials, such as steel, are used as reinforcement sums of cement-based materials. Reinforced concrete can be described as the classic example (Silva, 2002).

The addition of fibres in rigid materials causes part of the force acting on the body to be transferred to it [...]. This decreases the level of tension on the most requested parts of the body, reducing the impairment caused by possible microstructural defects and increasing the mechanical strength of the material (Peret et al., 2003).

Many researchers advocate the use of fibres in mortars because they benefit the post-cracking behavior of the composite (Silva and Barros, 2007). The fibres then, functioning as a bridge of tension transfer, contribute to the increase of resistant capacity, increased deformation capacity and the tenacity of the composite, giving the mortar an almost dubious fracture, as the researchers explain.

The use of fibres as reinforcement of fragile matrices appears as a technical alternative in the elaboration of constructive elements, whether in coverings, as in sealing elements, and in coatings and laying mortars, because the minimization of composite retraction is one of the great advantages offered by the mixture.

Since 1970, different fibres have been researched as possible substitutes for asbestos fibre reinforcement of cementitious matrices. However, even with good properties none of them brings together all the advantages of asbestos, such as good dispersion of large volume of fibres, excellent adhesion fibre-matrix in the hardened state, outside the optimal mechanical properties, such as the high modulus of elasticity and high strength, as explains by Motta and Agopyan (2007). However, due to the ills caused in health by the inhalation of asbestos fibres, its use has been banned in many countries, including Brazil, and so research has been intensified.

1.2.1 Vegetable Fibres

Natural fibres exist in abundance and have their use motivated by being renewable, biodegradable, due to their availability at low cost, often as waste, enabling the production of composites also economically viable. (Motta and Agopyan, 2007).

Plant fibres are fibres of low modulus of elasticity and high tensile strength. Its use as reinforcement provides cementitious matrices with greater resistance to impact, caused by greater energy absorption, the possibility of working in the post-fissured stage and an increase in the capacity of thermoacoustic insulation. (Agopyan and Savastano Jr., 1997; Silva, 2002).

The reinforcement of building materials with vegetable fibres is known for millennia, such is the case of the use of vegetable fibres as reinforcement of gypsum

since the Renaissance. (Savastano, 2000). The use of straws, grasses and roots to reinforce raw bricks is very old and has the function of giving greater stability to the brick, reducing the problems of shrinkage by drying (Savastano, 1986). Savastano evaluated the use of plant fibres in building construction, specifically in cementitious matrices in research esof 1986 to 2000.

According to Motta and Agopyan (2007), to increase the strength and stiffness of composites, the reinforcement fibres should have a modulus of elasticity greater than the matrix. This is a condition difficult to be achieved by both synthetic fibres and plant fibres, but the addition of fibres have other advantages such as increased deformation capacity, increased impact resistance and crack control, and properties are often more important than increased resistance, depending on the need for the application of the composite.

Despite presenting many advantages and efficiency as reinforcement in the field of construction, plant fibres still have little use on an industrial scale, probably due to still cultural obstacles, misinformation of the availability of fibres for the construction market and the possible costs of adaptations of the production system. Another factor that inhibits a greater exploitation of plant fibres is the use of synthetic fibres, also called artificial fibres, which emerged to replace vegetables overcoming them in the issues of durability, low water absorption and the possibility of better quality control (Motta and Agopyan, 2007).

Motta and Agopyan (2007), in his study of characterization of short fibres used in building construction, conclude that the variables of cost, sustainability, compatibility and durability in the matrix underpin the decision-making regarding the choice of the type of fibre used. Also, the authors showed that the cost of synthetic fibres, in this case polypropylene and PVA have undoubtedly much higher cost than the natural fibres studied, such as sisal and coconut fibres, while these, the vegetables, suffer superior degradation in the medium. Thus, they reinforce that the characterization allows more accurate analyses of the properties of the material to be used, including the feasibility of use.

In an extensive work on the use of plant fibres as reinforcement of fragile matrices, Agopyan (1991) relates 19 potential fibres for building construction. The authors presented their availability in Brazil, highlighting their physical characteristics, mechanical properties, cost and durability in the natural environment, in addition to other aspects, and then selects some more appropriate comparing their properties with asbestos and polypropylene fibres, as described in Table 1.

Savastano Jr (2000) conducts a research of residues of plant fibres in Brazil with information obtained in-field from the main Brazilian centers producing and/or processors of eight different types of vegetable fibre. The work collect data from about 20 companies, and thus classifies the residues and agricultural by-products, among which are the cellulose tailings from the production of paper in the kraft and bleaching processes, and summarizes these data as shown in Table 2.

Thus, composites reinforced with plant fibres depend on the application and expected performance of the interaction that can occur between the matrix and the fibre, taking into account that the fibres present variability in their properties, which is why several studies have been done on the different potential fibres worldwide.

Table 1 Physical and mechanical characteristics of plant fibres, asbestos and polypropylene

Properties	Density (kg/m ³)	Maximum absorption (%)	Elongation at break (%)	Tensile strength (Mpa)	Elasticity modulus (GPa)
Coconut	1177	93.8	23.9 to 51.4	95 to 118	2.8
Sisal	1370	110.0	4.9 to 5.4	347 to 378	15.2
Mauve	1409	182.2	5.2	160	17.4
Pulp for press paper	1200 to 1500	400	nd	300 to 500	10 to 40
Bamboo	1158	145	3.2	73 to 505	5.1 to 24.6
Jute	nd	214	3.7 to 6.5	230	nd
Piçava	1054	34.4 to 108	6	143	5.6
Banana	1031	407	2.7	384	20 to 51
Chrysotile asbestos	2200 to 2600	-	2	560 to 750	164
Common polypropylene	913	-	22.3 to 26.0	250	2.0

1.2.2 Cellulose Fibres

As defined by Silva (2002) fibre is the set of individual filaments, formed by fibrils and joined by non-crystalline organic chemical species (lignin and hemicellulose). These fibrils are formed by cellulose molecules, oriented at various angles, resulting in several layers that thus make up the macro-fibre.

As it has greater crystallinity and a high degree of polymerization, cellulose commonly presents greater stability in the aspect of degradation, of chemical, mechanical or thermal order when compared to the co-formation non-cellulosic components of plant fibres. For this reason, the durability and tensile strength presented by individual cellulose fibres will be nobly higher than those presented by their macro-fibres.

Cellulose is a white substance, insoluble in water, with high tensile strength, composed of carbon, hydrogen and oxygen. In cellulose, fibres are present sugar, starch, carbohydrate and lignin, which is an organic acid that surrounds the fibre (Neves, 2003).

Cellulose fibres usually present in the form of pulps or leaves, used for various purposes, especially the production of various types of paper. (Coutts, 1986 and Silva, 2002).

In Brazil the production of cellulose fibres, specifically in the commercial form of leaves, is practically found in all regions, as they are produced from various types of plant species, whether fibrous plants (such as sisal and bamboo) or woods (such as eucalyptus, pine), in accordance with local availability.

Paper is a tangle of cellulose fibres obtained from the pasty mass composed of fibres and water dwell son on a thin canvas. While the water flows through the fabric,

Table 2 Some residues from the processing of plant fibres

Fibre	Product	Residues				
		Denomination	Use for other purposes	Market value (US\$/t)	Quantity (t/year)	Relationship Residue/Main Prod. (%)
Sisal	Green fibre before drying	Green bushing (already separated from bagasse)	Potential use for pulp production	Null	30,000	300
	Benefited fibre	Scrap / bushing	Reinforcement of gypsum, production of yarn and cellulose	90 - 125	10,000	6
	Wires and ropes	White bushing (untreated)	Pulp production (total use)	180	25	1,5
	Rugs	Yarn flap (hot dyeing)	Pulp production	Null	54	6
Coconut	Long and medium fibres	Short fibres (1–3 cm)	Partial: filters, blankets, carpets and agricultural substrate	270	3000	40
	Long fibres	Short fibre	Partial	900	36	23
Cotton	Yarns for weaving	Micro-fibres: 85% cotton. and 15% polyester	Filling for mattresses and pillows	90	270	15
Eucalyptus pulp	Paper production	Reject	Lower quality paper	15	17,000	0,5
Mauve	Clean raw fibre	Fibre type 4	Weaving and spinning, with low yield	340	1180	20

the fibres that are deposited there, after pressing and drying, constitute the paper. Pastes or pulps can be obtained by simply mechanical dispersion of cellulose in water or through chemical processes [...]. The pastes can still be bleached by the action of chlorine or hypochlorite (Neves, 2003).

According to Neves (2003), papermaking has gone through a wide variety of raw materials, from the use of shrubby vegetables to the papyrus, through flax, grass straw, cotton fibres and reaching the definitive raw material, wood. However, the design of the original paper making process has continued to be the same since the second century.

The pulp and paper industry is very representative in Brazil, with the sector present in 16 states, consisting of 220 companies that generate 107,000 direct jobs according

to 1996 data from *Revista Celulose e Papel*, researched by Neves (2003). Also in this survey, Brazil appears as the 7th and 11th world producer of pulp and paper, respectively, supplying the domestic market and also the external market.

As waste, paper and cellulose fibre are treated as class II A residue—not inert—as per NBR 10,004 (2004), due to its biodegradability properties. The use of cellulosic pulps in the reinforcement of materials based on cementitious matrices has acquired increasing importance worldwide, especially in developed countries (Savastano Jr., 2000).

Some authors call cellulosic mortar the composite consisting of cement matrix and sand reinforced with cellulose fibres from paper recycling. Thus, the use of cellulose fibre in cementitious composites adds the benefits of reinforcing properties (since it is a fragile matrix that receives a reinforcement of organic fibre with low modulus of elasticity) to the issues of reuse in the form of waste (reducing the tailings released in the environment), favouring a sustainable practice in building construction worldwide.

2 Experimental Campaign

The work was developed following seven steps: fibre preparation, material selection, mortar production, fresh state testing, moulding of specimens, wet curing by immersion for seven days and tests in the hardened state.

The properties of consistency and density of the mortar in its fresh state and later, in its hardened state, were evaluated the mechanical behaviour and the tenacity from the samples produced in the laboratory.

This work study and evaluate the influence of the addition of paper fibres with different compositions, 5 and 10%, in relation to the reference trace without fibre addition (0%), as detailed in Table 3.

For the experimental dosage, the unit trace by weight of the agglomerate plus aggregate was the same for the three mixtures, in case 1:3, and the added water was 375 ml, which corresponds to a constant water/binder ratio of 0.60. For each stroke,

Table 3 Experimental dosing plan

Mix	Trace (c:l:s:f) ¹	Matrix ²	Fibre content (%) ³			a/agl ⁴	Mass matrix (g)
			0	5	10		
F1	1:1:6:0	1:3	x			0.60	312: 312: 1872: 375: 0
F2	1:1:6:0.4	1:3		x		0.60 ⁵	312: 312: 1872: 375: 125
F3	1:1:6:0.8	1:3			x		312: 312: 1872: 375: 250

¹Cement:lime:sand:fibre

²Ratio of binder and sand, unit mass.

³Percentage of the amount of fibres in relation to the total mass of solids (binder + sand).

⁴a/agl: considered water/binder ratio.

⁵The water added to the mixture from the added fibre that was moist was not considered.

two specimens were moulded in the dimensions of 50 mm in diameter \times 100 mm in length, according to NBR 7215 (1997) and three specimens of prismatic format in dimensions of 40 mm thickness \times 40 mm in height \times 160 mm in length, according to NBR 13,279 (2005).

2.1 Materials

The raw materials used in this work were the agglomerations of Portland cement and hydrated lime, in addition to sand, public water and white paper cellulose fibres. Portland cement type II (CP II-E32) was used to prepare the mortar, in accordance with NBR 11,578 (2005). The composite cement had blast furnace granulated slag additions, i.e., it is characterized as an intermediate composition between ordinary Portland cement and Portland cement with additions (blast furnace and pozzolanic). This cement combines good results and fast drying with low hydration heat and increased endurance, and it is recommended for structures that require moderately slow heat detachment or may be attacked by sulphates (see Table 4).

Hydrated lime CH-I (see Table 5) was used as aerial binder, according to NBR 7175 (2003). The hydrated lime is composed of a mixture of calcium hydroxide and magnesium hydroxide and a mixture of calcium hydroxide, magnesium hydroxide and magnesium oxide, as described by NBR 7175 (2003). The natural fine aggregate used was quartz sand, resulting of the sieving of the cleaned medium sand acquired from a local river. The sand was previously screened and homogenised for a correct application in mortar.

Table 4 Components and chemical requirement of CP II – E 32 (%), according NBR 11,578 (2005)

Insoluble waste	Magnesium Oxide MgO	Sulphur trioxide SO ₃	Carbon dioxide CO ₂	Clinkered + calcium sulphates	Granulated blast oven slag	Carbonate material
≤ 2.5	≤ 6.5	≤ 4.0	≤ 5.0	94–56	6–34	0–10

Table 5 Physical and chemical requirement of hydrated lime CH – I (%)

Physical requirement				Chemical requirement		
Fineness retained -sieve 0.600 mm	Fineness retained -sieve 0.075 mm	Water retention	Plasticity	Carbon dioxide CO ₂	Anhydrite calcium oxide and magnesium CaO + MgO	Total oxides on the basis of non-volatile CaO _t + MgO _t
$\leq 0.5\%$	$\leq 10\%$	≥ 75	≥ 110	≤ 5 (factory) ≤ 7 (warehouse)	≤ 10	≥ 90

Fig. 1 Cellulose fibre used in the experiment



The cellulose fibres used in the production of cellulosic mortar came from white paper residues used in offices, also known as sulphite paper (see Fig. 1). The collected material was, initially, cut into strips, and submerged in water during 12 h, for saturation. Subsequently, it was crushed with water (in a proportion of 100 g of paper to 750 ml of water), using a liquefier, model RI2101, at a frequency of 50/60 Hz, equivalent to 3000 to 3600 rpm, for 10 min. This high-rotation stirring procedure caused the paper fibres disintegration into the water. Then, the excess water was removed through the use of a simple sieve, squeezing the fibre to leave it only wet. This process is completely mechanical (cutting, saturation and crushing), and no chemical product was added for fibre processing, as shown in Fig. 2.

2.2 Mortar Mix Preparation

The mortar constituent materials were added in a 1:1:6 ratio (cement:lime:sand) and the cellulose fibres were added in the following proportions: 0% (reference), 5% and 10% over cement mass (see Fig. 3).

For the preparation, a mechanical mortar mixer, model I3010 of *Contenco Indústria e Comércio Ltda.*, with a capacity of approximately 5L, equipped with a metal shovel that rotates around itself and in planetary motion around the axis of the tank, movements directed in opposite directions, with speeds of 62 ± 5 rpm (low) or 125 ± 10 rpm (high). The production process of the experimental mortar followed the same order of placement of the materials and mixing time for the three traits used, in order to maintain a standardization of the technique and avoid possible intermediate external factors in the test result. The procedure adopted for mixing followed the following steps:

- Initially cement, lime and all water were added to the mixer tub. The mixture was performed for a time of 30 s at low speed (62 ± 5 rpm);
- Then the sand and the fibre were added to the formed paste and the mixture was carried out for a time of 30 s;
- The mortar was left to rest for 60 s;

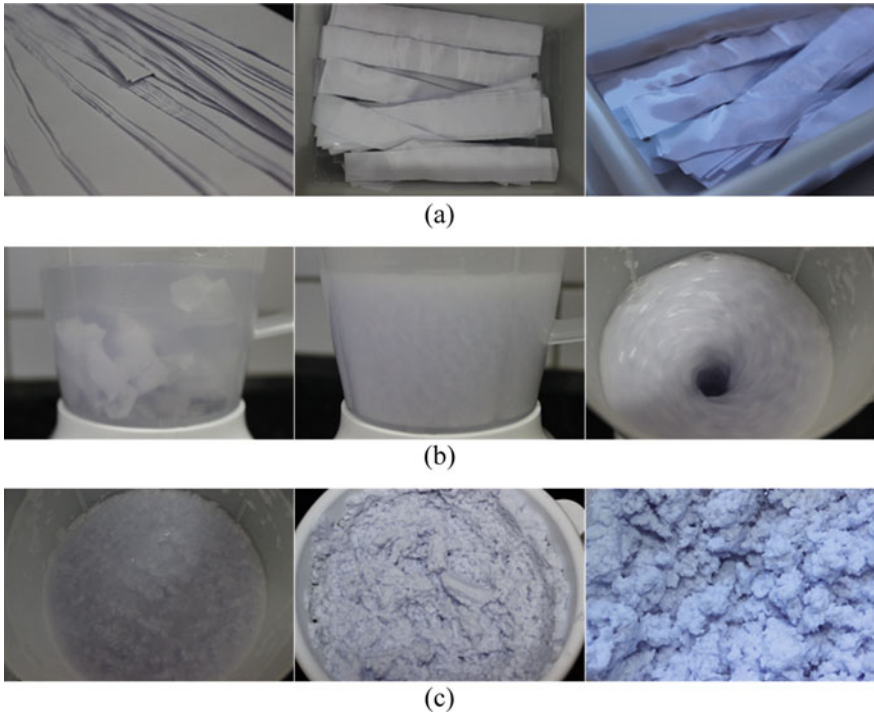


Fig. 2 a Fibre processing - cutting step of paper into strips and saturation; b Fibre processing—snotted and grind with water for 5 min and c Fibre processing - removal of excess water



Fig. 3 Separate materials for the preparation of mortars—Mixtures F1, F2, F3

- Finished the mixture at high speed (125 ± 10 rpm) for 60 s in order to favour the complete homogenization of the mortar.

The technique explained above was used for the experimental tests of mix 2 (5% fibre) and mix 3 (10% fibre). For the mix 1 (reference mortar with 0% fibres) the sand was added without the fibre, but the same order of the procedure adopted followed and the same execution time of the phases (2×30 s at low speed, 60 s of rest and 60 s at high speed) followed.

After the mixture, the test was performed to determine the consistence index—flow table according to NBR 13,276 (2005) and the five specimens of each mixture

were moulded, two cylindrical and three prismatic. Still in the fresh state was weighed the empty cylindrical test body and the same test body filled with the dense mortar, in order to determine the mass density of each mixture of the matrix studied.

The mixing and production of the two cylindrical specimens (50 mm × 100 mm), for each mixture, were performed according to NBR 7215 (1997), and the three prismatic specimens (40 mm × 40 mm × 160 mm) were performed according to NBR 13,276 (2016). The initial cure of the specimens was made in the laboratory at room temperature during 48 h, after this period the specimens were removed from the forms, identified and submerged in water during more 12 h, before the mechanical characterization tests.

2.3 Experimental Methods—Fresh State

In the fresh state, the flow behaviour (a workability indicator) of the prepared cellulose fibre mortar specimens was determined, by a flow table test, in accordance with standard NBR 13,276 (2016). This test was carried out for the three mixtures studied, in order to evaluate the variation of mortar consistency index with different percentages of cellulose fibre additions, which affects the mortar mixture plasticity. Densities of the three-mortar mixture studied were determined in accordance with NBR 13,278 (2005).

2.3.1 Consistence Index—Flow Table Test

According to NBR 13,276 (2005) for the consistence index determination test, a table called a consistency table and a conical trunk mould placed in the center of this table are used, shown in Fig. 4. Initially, a release was passed on the table and the rehearsal began. The conical trunk mould was glued to the center of the table and filled with 3 successive layers of mortar compressed with 15, 10 and 5 blows of the



Fig. 4 Mortar scattering—Diameter measurement

system respectively. The mould was razed and removed. Then 30 blows were applied to the table, one blow every second, totalling 30 s, and with each blow the mortar was settling/spreading on the table. The consistence index was given by the average of three measurements of the diameter formed by the scattering of the mortar.

This test was carried out for the three mixtures studied, in order to evaluate the variation of mortar consistency with the different fibre additions, directly affecting its plasticity.

2.3.2 Density

The mass density consists of filling a container with a volume equal to 400 ml and known mass, a procedure described in NBR 13,278 (2005). For this work, the procedure was adapted and the cylindrical test body mould of 50 mm in diameter × 100 mm in length was used, whose calculated volume was 196.35 ml (196.35 cm³). The test body was weighed empty and then weighed after moulding, as exemplified in Fig. 5. The mass density found was the ratio between mass and volume, and the mass was considered the difference of the filled set and the empty mould, according to the following mathematical expression:

$$\rho = \frac{m}{V} \tag{1}$$

where ρ is the mass density (g/cm³), m is the difference between the mass of the assembly and the mass of the empty mould (g) and V is the mould volume (cm³).



Fig. 5 Weighing process for calculating mass density

Table 6 Classification of mortars for mass density

Mortar	Density (g/cm ³)	Principal aggregates used	Application
Light	< 1.4	Vermiculite, perlite, expanded clay	Thermal and acoustic insulation
Normal	≥ 1.4 - ≤ 2.3	River sand (quartz) and crushed limestone	
Heavy	> 2.3	Berita (barry sulfate)	Radiation protection

Table 6 shows the classification of mortars for mass density according to Carasek (2010). The results of this essay are seen in the next chapter of this work.

For each mortar produced, that is, for each trace adopted (F1, F2 and F3), two cylindrical specimens (CPs) of 50 × 100 mm and three prismatic CPs of 40 × 40 × 160 mm were moulded. Before moulding, the moulds of the specimens received internally a thin layer of demoulder (mineral oil of low viscosity) to facilitate demoulding after the initial curing period, to prevent the mortar from being adhered to the mould, as shown in Figs. 6 and 7.

The mortar was placed in the specimens in successive layers and was compacted with metal pylon blows. For cylindrical plants, the recommendation of NBR 7215 (1996) was followed, with mortar placement in four successive layers, thickened with 30 blows per layer. Prismatic specimens were moulded in two layers, receiving 30 blows for densification and compaction, according to NBR 13,279 (2005). After filling and thickening, the specimens had their surfaces razed and regularized with metal spatula.



Fig. 6 Specimens prepared for moulding



Fig. 7 Molding of specimens

The initial cure of the specimens was made in the laboratory at room temperature for 48 h and after this period were removed from the forms, identified and submerged in water up to 12 h before the time of mechanical characterization tests (Fig. 8).

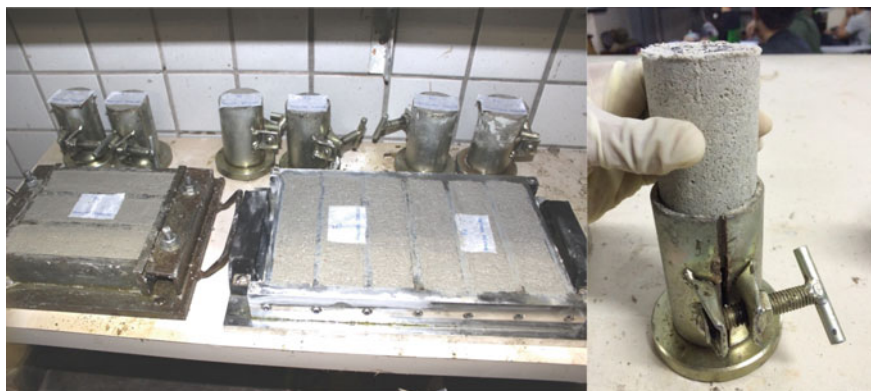


Fig. 8 Moulded and moulded specimens after 48 h

2.4 Experimental Methods – Hardened State

Regarding the hardness state, after a curing period of 7 days, the mechanical resistance was determined (compression and flexural strength test), in order to evaluate the tenacity and deformations observed, by using a pressure press (EMIC, model DL60000) with a test speed of 50 ± 10 N/s for flexion and 500 ± 50 N/s for compression.

2.4.1 Tensile Strength in Bending

The tensile strength test in three-point flexion was performed according to the recommendations of NBR 13,279 (2005). For this test, the prismatic specimens were used and before positioning them in the press, the shaft and markings of 50 mm were demarcated for each side, in order to ensure the centrality of the load on the specimen, shown in Fig. 9a.

The equipment used was a universal Emic test machine, model DL60000, with a load cell Trd 28 of 500 Kgf (~5000 N), as shown in Fig. 9b, where a point load was applied and centered on the test body until rupture.

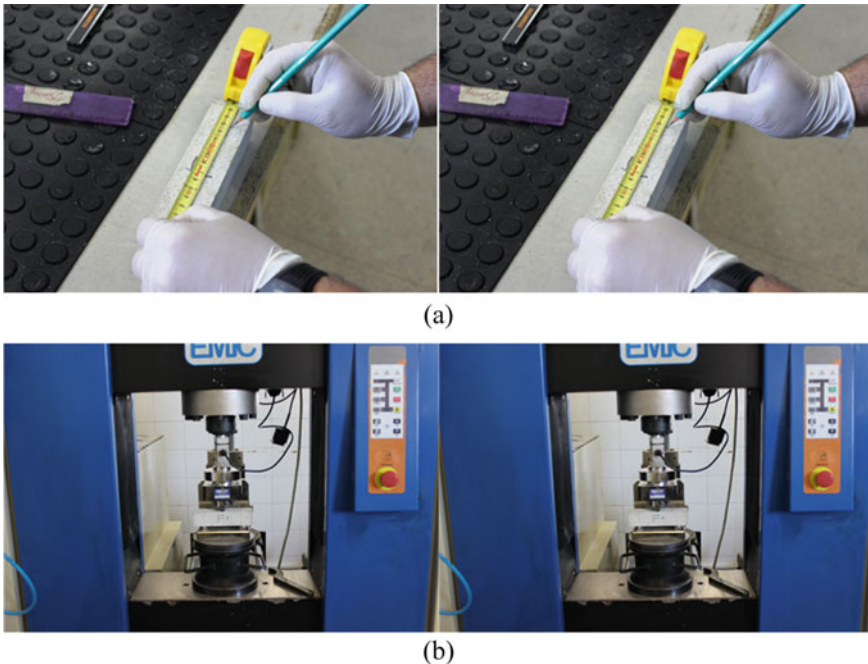


Fig. 9 a Marking axes in prismatic test body; b Universal test machine with load cell and support device for bending traction test

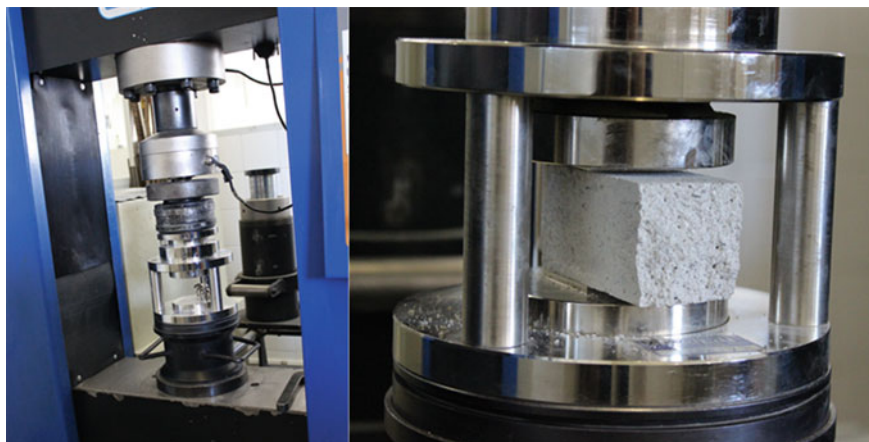


Fig. 10 Universal test machine with axial compression test—PRISMATIC CP

2.4.2 Axial Compressive Strength in Prismatic Test Body

The axial compressive strength test was performed according to the recommendations of NBR 13,279 (2005). The halves of the specimens used in the bending test were used, i.e., samples of $40 \times 40 \times 80$ mm approximately.

The same press described in the previous test, EMIC DL60000, was used, but with another support device and load cell Trd 24 of 10tf (~100KN), and with a force increment of 500 ± 50 N/s as determined by the standard until rupture. The press and support devices used in this test are shown in Fig. 10.

2.4.3 Axial Compressive Strength in Cylindrical Test Body

The cylindrical test of compression resistance was performed in accordance with the recommendations of NBR 7215 (1996). Before being tested, the specimens received on the top and base faces a capping with a mixture of 90% sulphur and 10% hot metakaolin, at a maximum thickness of 2 mm, as shown in Fig. 11a. This capping layer, slightly larger than the top of the specimen, has the function of ensuring that the tops of the specimens are parallel, smooth and intact, reducing friction between the specimen and the plates of the press. Alternatively, the deviations of the axis of the specimen in relation to the direction of application of the load imposed by the press, which would cause eccentricity by the non-uniform loading applied, negatively influencing the final resistance evaluated.

The same press of the anterior axial compress strength test, EMIC DL60000, was used, including with the same load cell Trd 24 of 10tf (~100KN), with a force increment of 500 ± 50 N/s until rupture. The specific support device for this test is shown in Fig. 11b.

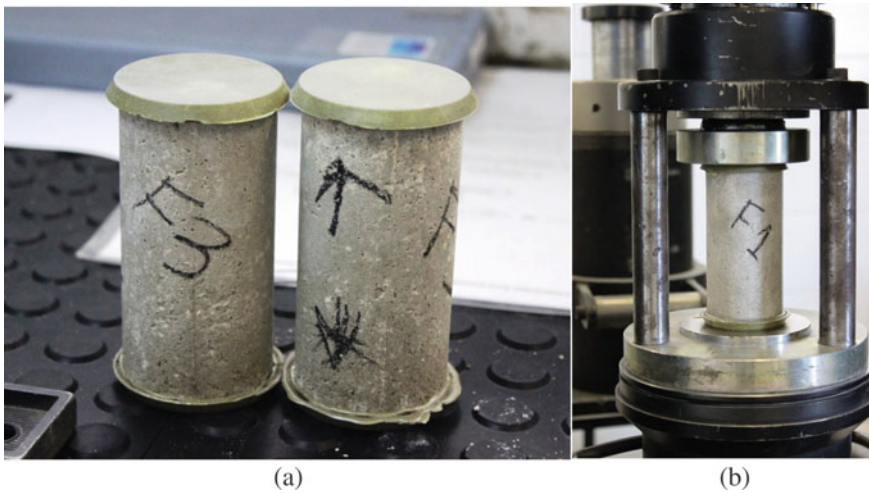


Fig. 11 **a** Capped cylindrical specimens; **b** Equipment support device for compression test of cylindrical CP's 5 × 10 cm

3 Results and Discussion

Firstly, for the fresh state, the consistency of the mixture and the mass density were evaluated, which directly influence the workability of the mortar. Regarding consistency, it was observed that the higher the fibre content added to the mixture, the mortar tended to become firmer, i.e., from plastic to dry, as shown in Fig. 12, clearly visualized in a comparison of the abatement of the three traces as shown in Fig. 13. The experimental test data are presented in Table 7.

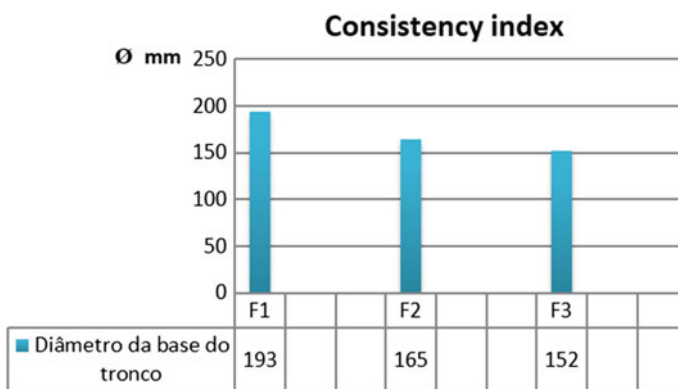


Fig. 12 Consistence index of the different experiments

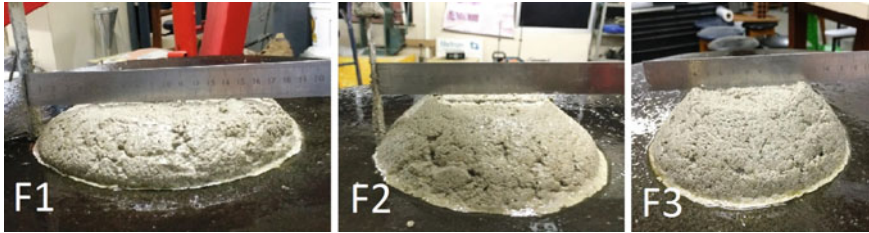


Fig. 13 Abatement of the conical trunk test body of the 3 mixtures studied—flow table

Table 7 Flow table test data

Mixture	Diameter of trunk base	
	(mm)	Average (mm)
F1	190	193
	195	
	195	
F2	165	165
	160	
	170	
F3	155	152
	150	
	150	

In relation to mass density, results were obtained within the normal density classification, but with the addition of fibre the mortar tends to become light, a function of the low apparent density of the paper (in the form of cellulose fibre) incorporated into the mixture. Table 8 and Fig. 14 show the results of the densities found for the experimental mortars of this study.

Table 8 Mass densities of the themortars analysed

Mix	Volume Mould (cm ³)	Weight CP		Weight Mortar (g)	Density, ρ	
		Empty CP (g)	Filled CP (g)		(g/cm ³)	Average (kg/m ³)
F1	196.35	912.1	1321.3	409.2	2.08	2088.9
		917.4	1328.5	411.1	2.09	
F2	196.35	905.3	1296.9	391.6	1.99	2000.8
		909.5	1303.6	394.1	2.01	
F3	196.35	910.7	1292.1	381.4	1.94	1940.2
		916.3	1296.8	380.5	1.94	

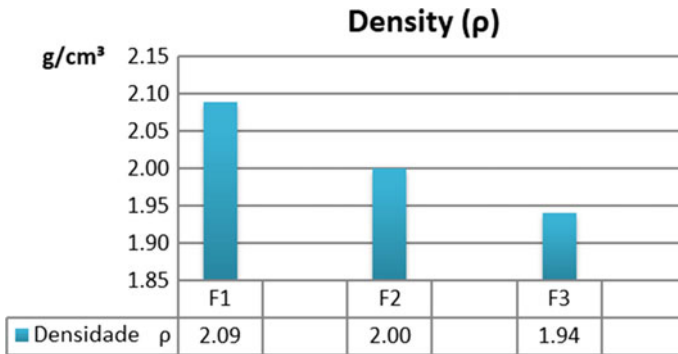


Fig. 14 Mass Density of the experimental tests

In the hardened state, the tensile strength and compressive strength tests allowed the mortar behaviour to be evaluated for mechanical strength capacity and deformation and toughness. Figure 15 shows a comparison of the average results of axial compression tests. Although the geometry and position of the moulds in the tests are different, the values maintain the tendency to fall proportionally to the fibre content incorporated into the matrix.

Figure 16 shows individual graphs with the average results of the mechanical strength capacity of the fibre mortars for each of the tests in the hardened state (tensile strength in flexion, axial compressive strength in prismatic CP and cylindrical CP).

The order of magnitude of the result of the reference grout compressive strength test (without fibre addition) is around 5 MPa. Analysing the mean values of this experiment, it is observed that the addition of cellulose fibres in mortars favours the drop in compressive strength, as expected (the difference between the strength of the reference mortar and those with fibre is between 6 to 31% F2-F1, and 30 to 53% F3-F1).

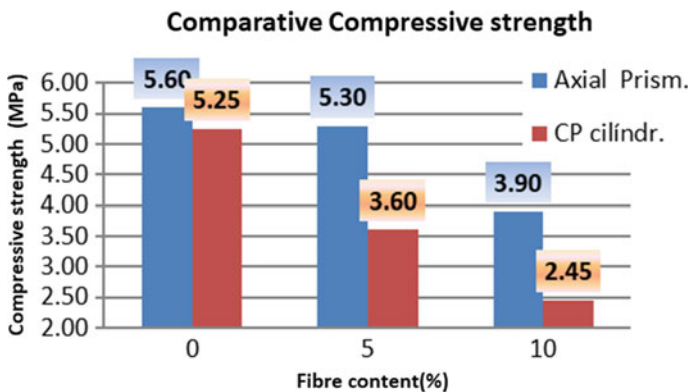


Fig. 15 Comparison of the compression test results

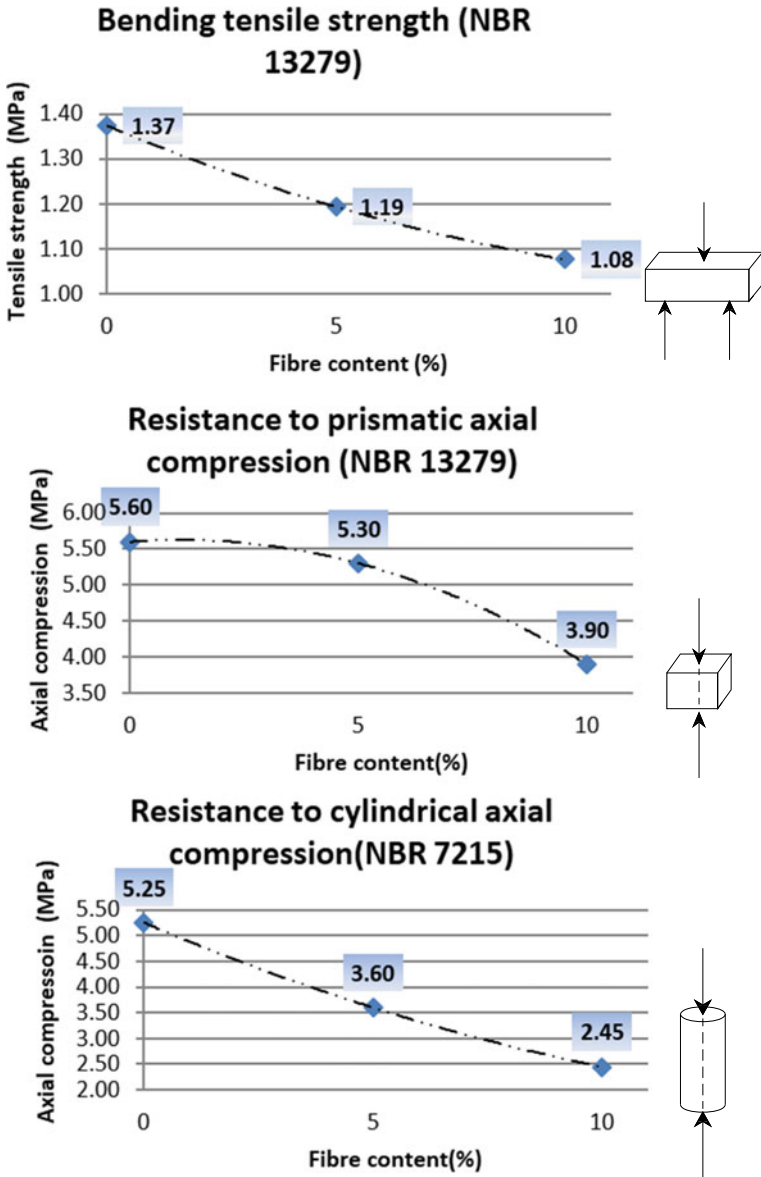


Fig. 16 Average tensile strength results in bending and compressive strength

The mean tensile strength value in flexion for the reference mortar was in the order of 1.37 MPa. In relation to bending tensile stresses, resistance drops were also observed between the reference mortar and cellulosic mortars (difference of the reference F1 mixture and mixtures F2 and F3 around 13 to 21%).

The hypothesis for this reduction is associated with the amount of water in the mixture, since the added fibre was moist, carrying, for sure, more water to the matrix. The water/binder ratio is the main parameter associated with the porosity of the mortar and directly affects its mechanical strength. With the increase of water incorporated into the mixture, since the water/binder ratio was not corrected, the mortar tended to be empty when evaporating this water. Based on this, it is evident in the experiment a greater fall in resistance the higher the fibre content added, a function of the addition of water in the composite.

Another hypothesis concerns the air content incorporated by the addition of the fibre, or the low resistance to compression efforts of the fibre itself, or the incompatibility of the fibre in alkaline medium, but these variables were not the subject of study in this work. It is essentially concluded that the reduction of resistance occurs due to the increase in the water content of the mixture, as well as the presence of the fibre itself. However, in the bending test it was possible to verify that the cellulose fibre added to the mortar allowed a change in the post-cracked behaviour, as shown in Fig. 17.

It is observed by Fig. 17, which submitted to the maximum load, the reference mortar presented sudden rupture (typical of fragile fracture), while in mortars with the addition of fibres, after the first crack, the composite continues to deform until it reaches the rupture.

For the reference mortar, the rupture results illustrated in this graph show that when there is the first crack, the collapse occurs. For mortars with fibres, after the first crack there is a change in behaviour and direction of the curve, typical of the fibre's action. At this point, the energy is transmitted to the fibre that integrated into

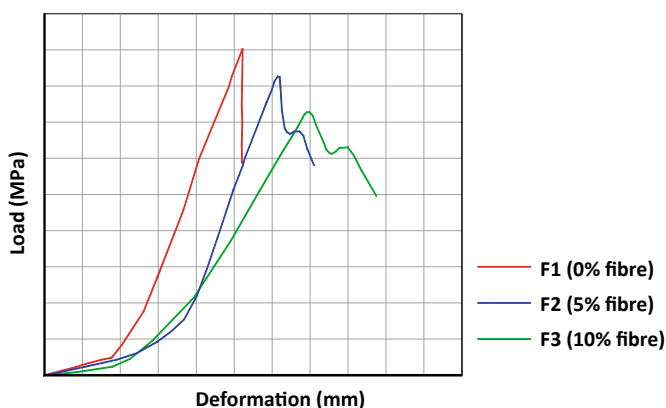


Fig. 17 Load graph versus deformation

the matrix absorbs more energy allowing the material to deform before breaking. Thus, the added fibres allow a survival to the mortar, even presenting the first crack at a lower maximum load.

This is clearly evidenced in the graph through the area under the load versus deformation curve, whose calculated value is the tenacity of the material. This tenacity is the mechanical energy supported/absorbed by the material to the point of fracture. In the matrix-fibre composite, the stresses are transferred to the fibres and they postpone the deforming fracture. The results found are shown in Table 9 and in Fig. 18.

As a tendency of smoothing of the curves is presented, for the calculation of the mortars tenacity the limit areas where the test was interrupted were considered (in this case the area under the curve below the point where the test was interrupted was considered as this being the fracture point for each stroke – see Fig. 17).

Thus, despite the presence of fibres reducing the compressive and tensile strength in the bending in proportion to the fibre content employed, they allow to achieve positive properties in the post-crack phase of the mortars, as they continue to support

Table 9 Tenacity results

Mix	Fibre content (%)	Sample	Tenacity	
			Tenacity	Average tenacity
F1	0	CP1	0.18	0.18
		CP2	0.20	
		CP3	0.16	
F2	5	CP1	0.24	0.21
		CP2	0.15	
		CP3	0.23	
F3	10	CP1	0.31	0.32
		CP2	0.33	
		CP3	0.33	

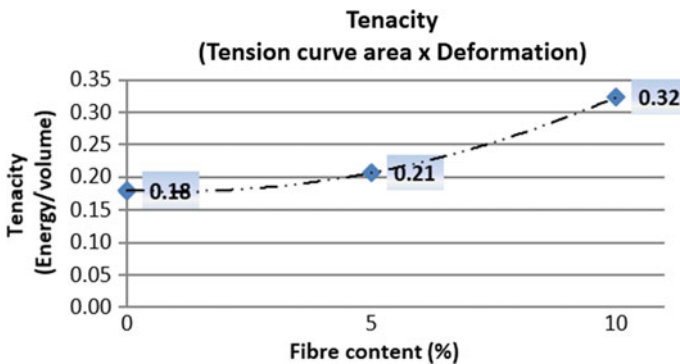


Fig. 18 Tenacity values of the experiments

loading before rupture, even after the cracking begins. Thus, even supporting lower maximum load, the mortar achieves greater deformation and tenacity, distancing itself from a fragile fracture material due to the matrix-fibre interaction.

4 Conclusions

This work showed that the addition of cellulose fibres has potential for use in mortars as it favours certain properties, if not qualities necessary in mortars such as the ability to absorb deformations. It was observed that although the presence of cellulose fibres reduces compressive and tensile strength proportionally to the incorporated fibre content (because the results were lower than the reference mortar), they provided better results in the post-fissure state, promoting more deformation and significantly improving the tenacity.

More, it is observed that the fibres allow delaying the survival of mortars, because after reaching the maximum strength of the matrix (in the case of the reference mortar), the fibre begins to act causing a deformation and tenacity directly proportional to the fibre content employed. In this way, the fibre incorporated into the cement matrix allows you a less fragile fracture.

In this work, the durability of the matrix with the addition of cellulose fibre was not evaluated. Although other studies comment that cellulose fibre does not behave satisfactorily in the alkaline medium, because the long-term tendency would be for the fibre to disintegrate, the results of this experimental study indicate a potential use for the addition of these fibres in cementitious composites due to the deformability and tenacity provided. That is, it is considered necessary a deepening of the research in order to evaluate these variables and even the impact of the loss of mechanical resistance for the practice of mortars in constructions, including studying the retraction and adhesion properties provided by the incorporation of fibre to the matrix.

Regarding the applicability, there was little difficulty in the process of air expulsion in the density of the mass probably due to the incorporation of the fibre, however, for the curbing of the specimens, this difficulty was not obtained.

Finally, it is concluded that the effect of the addition of cellulose fibres in mortars, derived from white paper residue, as an alternative of technical innovation is very promising, besides allowing sustainable destination and use of this type of residue regarding aspects of deformability and tenacity.

References

- Agopyan, V., & John, V. M. (2011). *The challenge of sustainability in building construction*, Vol. 5. Sao Paulo: Blucher.
- Agopyan, V. *Fibre-reinforced materials for construction in developing countries: the use of plant fibres*. MSc Thesis, Universidade de São Paulo, São Paulo, Brazil, 1991.

- Araujo, M. A. A. (2008). Modern sustainable construction. Institute for the Development of Ecological Housing. www.idhea.com.br/pdf/moderna.pdf.
- Brazilian Association of Technical Standards (ABNT). (2003). NBR 7175. Hydrated lime for mortars—Requirements. Rio de Janeiro, Brazil.
- Brazilian Association of Technical Standards (ABNT). NBR 7215. (1996). Portland cement—Determination of compressive strength of cylindrical test specimens. Rio de Janeiro, Brazil.
- Brazilian Association of Technical Standards (ABNT). (2004). NBR 10004. Solid waste - Classification Rio de Janeiro, Brazil.
- Brazilian Association of Technical Standards (ABNT). (2005). NBR 11578. Portland composite cement—Specification. Rio de Janeiro, Brazil.
- Brazilian Association of Technical Standards (ABNT). (2005). NBR 13276. Mortars applied on walls and ceilings - Determination of the consistence index. Rio de Janeiro, Brazil.
- Brazilian Association of Technical Standards (ABNT). NBR 13278. (2005). Mortars applied on walls and ceilings - Determination of the specific gravity and the air entrained content in the fresh stage. Rio de Janeiro, Brazil.
- Brazilian Association of Technical Standards (ABNT). NBR 13279. (2005). Mortars applied on walls and ceilings - Determination of the flexural and the compressive strength in the hardened stage. Rio de Janeiro, Brazil.
- Brazilian Association of Technical Standards (ABNT). (2009). NBR ISO 14040. Environmental management—Life cycle assessment - Principles and framework. Rio de Janeiro, Brazil.
- Brazilian Association of Technical Standards (ABNT). (2009). NBR 14044. Environmental management - Life cycle assessment—Requirements and guidelines. Rio de Janeiro, Brazil.
- Brazilian Association of Technical Standards (ABNT). (2008). NBR ISO 15392. Sustainability in buildings and civil engineering works—General principles. Rio de Janeiro, Brazil.
- Brazilian Association of Technical Standards (ABNT). (2007). NBR ISO 21930. Sustainability in buildings and civil engineering works—Core rules for environmental product declarations of construction products and services. Rio de Janeiro, Brazil.
- Carasek, H. (2010). Argamassas. In: G. C. Isaia (Ed.), Civil Construction materials and principles of science and materials engineering, vol. 2, 2nd ed., São Paulo: IBRACON, Brazil.
- Carvalho, P. E. F. (2014). Study of the properties and performance of laying mortars with kraft paper fibres. MSc. Thesis, Federal University of Goiás. Goiânia, Brazil.
- Coutts, M. P. (1986). Components of tree stability in Sitka spruce on peaty gley soil. *Forestry*, 59, 173–197.
- Figueiredo, A. D. (2011). Concrete reinforced with fibres. MSc. Thesis, Polytechnic School of the University of São Paulo. Sao Paulo, Brazil.
- Lucas, D., & Benatti, C. T. (2008). Use of industrial waste for the production of cementitious and clayey artifacts used in civil construction. *Revista em Agronegócios e Meio Ambiente*, 1(3), 405–418. <http://periodicos.unicesumar.edu.br/index.php/rama/article/view/850/663>.
- Macedo, A. N., Souza, A. A. C., & Pompeu Neto, B. B. (2012). Wood cement plates with waste from the timber industry of the Amazon Region. *Ambiente Construído, Porto Alegre*, 12(2), 131–150.
- Mano, E. B. (2000). Polymers as engineering materials. 2nd edition, São Paulo: Edgar Blucher, Brazil.
- Motta, L. A. C., & Agopyan, V. (2007). Characterization of short fibres used in civil construction. Technical Bulletin. Polytechnic School of the University of São Paulo. São Paulo: EPUSP, Brazil.
- Motta, S. R. F., & Aguiar, M. T. P. (2009). Sustainability and building project processes. *Gestão & Tecnologia de Projetos*, 4(1), 84–119. <http://www.iau.usp.br/gestaodeprojetos/index.php/gestao-deprojetos/article/view/79>.
- National Environment Council—CONAMA. (2002). Resolution No. 307 of 5 July 2002. It provides for guidelines, criteria and procedures for the management of construction waste. <http://www.mma.gov.br/port/conama/legiabre.cfm?codlegi=307>.
- National Environment Council—CONAMA. Resolution No. 348 of August 16, 2004. Amends CONAMA Resolution No. 307 of 5 July 2002, including asbestos in the hazardous waste class. <http://www.mma.gov.br/port/conama/legiabre.cfm?codlegi=449>.

- Neves, C. M. M. (2003). Housing components of cellulosic mortar and polyurethane foam. In: J. C. Rocha & V. M. John (Eds.), Use of waste in housing construction. Collection HABITARE, vol. 4, pp. 176–217, Porto Alegre: ANTAC, Brazil.
- Peret, C. M., Salomão, R., Zambon, A. M., & Pandolfelli, V. C. (2003). Mechanical reinforcement by polymeric fibres and their effects on drying refractory concretes. Federal University of São Carlos, São Paulo. *Cerâmica* 49, pp. 257–261, São Carlos. Available at <http://www.scielo.br/pdf/%0D/ce/v49n312/a1149312.pdf>.
- Rocha, J. C., & Cheriaf, M. (2003). Use of waste in construction. In: J. C. Rocha & V. M. John (Eds.), Use of waste in housing construction. Collection HABITARE, vol. 4, pp. 72–93, Porto Alegre: ANTAC, Brazil.
- Sattler, M. A. (2002). Sustainable buildings and communities. Department of Civil Engineering/NORIE, Federal University of Rio Grande do Sul. Porto Alegre, RS, Brazil. Available at <http://www.usp.br/nutau/CD/sattler.pdf>.
- Savastano Jr., H. (1986). Vegetable fibres for construction—Coconut fibre. Technical Bulletin. Polytechnic School of the University of São Paulo. São Paulo.
- Savastano Jr., H. (2000). Cement-based materials reinforced with plant fibre: waste recycling for low cost construction. Thesis (Free teaching). Polytechnic School of the University of São Paulo. São Paulo, Brazil.
- Silva, A. C. (2002). Study of the durability of composites reinforced with cellulose fibres. MSc Thesis, Polytechnic School of the University of São Paulo. São Paulo, Brazil.
- Silva, R. P., & Barros, M. M. S. B. (2007). Mortar with the addition of polypropylene fibres; study of rheological and mechanical behaviour. Technical Bulletin. Polytechnic School of the University of São Paulo. São Paulo: EPUSP.

Use of Construction Waste to Replace Conventional Aggregate in Reinforced Concrete Production



F. A. N. Silva, M. T. A. Silva, F. A. F. Lopes, J. M. P. Q. Delgado,
and A. C. Azevedo

Abstract The work aims to study the influence of using construction and demolition waste (CDW) in replacing coarse and fine aggregate in the production of concrete and its impact on hardened concrete properties. To compare and analysis its behavior a moderate compressive strength concrete was used as a benchmark. Compressive and splitting tests were performed using 120 cylindrical concrete specimens with 150 mm diameter and 300 mm length. Additionally, reference and RAC concrete beams were prepared and tested under four points loaded scheme to investigate the mechanical response on both maximum load capacity, displacements and also evaluate the flexural strengths of the beams tested. Results obtained showed to be a good solution for an adequate destination to the CDW from the construction industry and the full recycled fine aggregate replacement exhibited better performance in all tests performed proving, this way, great potentialities to be used as fine aggregate in concrete production.

Keywords Sustainable construction · Concrete with recycled aggregate · Construction waste

F. A. N. Silva · M. T. A. Silva
Civil Engineering Department, Universidade Católica de Pernambuco, Recife, Brazil

F. A. F. Lopes
Central de Tratamento de Resíduos de Petrolina S.A, Recife, Brazil

J. M. P. Q. Delgado (✉) · A. C. Azevedo
Departamento de Engenharia Civil, Universidade Do Porto, CONSTRUCT-LFC, Rua Dr. Roberto Frias, s/n, 4200-465 Porto, Portugal
e-mail: jdelgado@fe.up.pt

A. C. Azevedo
e-mail: antonio.costaaezevedo@fe.up.pt

1 Introduction

Urban development around the world, combined with inefficient management of public and private spaces plays an important role in the generation of construction and demolition waste (CDW). In the same direction, the increase in the use of concrete and the consumption of natural resources to produce its raws material a process that demands large amounts of energy can lead to the depletion of natural aggregates (Ozbakkaloglu et al., 2018; Kisku et al., 2017; Torgal and Jalil 2011). CDW is usually discarded in nature through an inadequate process, sometimes polluting natural resources, and this fact is already an aspect that has been causing major problems for metropolises worldwide.

Global demand for construction aggregates is forecast to rise by about 2.5% per year to approximately 48 billion metric tons in 2023. This demand can be explained by several facts, among which stand out the continued strong growth in global construction activity, the rebound in global cement demand to build necessary infrastructure in several underdeveloped countries around the world (Hafez et al., 2020). This scenario points to the need to develop research to find technically and financially sustainable alternatives for the use of CDW. When one observes that the use of CDW is very incipient in most continents on the planet, representing less than 5% of worldwide aggregate demand (Cho & Yeo, 2004; Dhir & Paine, 2010), it becomes clear the great potential of this emerging market.

Recycled Aggregate Concrete (RAC), produced with partial or total replacement of natural aggregates by recycled aggregates in the concrete mix, has been shown to provide significant environmental benefits and economic benefits (Bravo et al., 2015; Song & Liang, 2011). However, RAC has to be seen as a secondary material with quality inferior to usual aggregates used to produce despite its countless environmental advantages (Makul, 2020).

Compressive strength obtained through standard tests to access concrete properties is considered as an important indicator of normal aggregates concretes quality and can also be used to get an approximate value for other properties, i.e., young's modulus, flexural and tensile strengths, when specific tests are not available.

Most existing research on RAC have shown that the relationships between compressive strength and other mechanical factors and properties related to the durability vary with the rate of substitution of the recycled aggregate (Dilbas et al., 2016; Ozbakkaloglu et al., 2018; Poon et al., 2007; Thomas et al., 2014).

In general, the use of CDW is focused mainly on the issues regarding the technical development of the material with insights on the environmental impacts of the process. However, the emphasis on market viability is a commitment to the effectiveness of research, since the social benefits of a research process will only be fully realized if the new product produced generates jobs, reduces the volume of landfills, consumes waste in instead of natural resources and avoid contamination of the environment or compromise the health of the population (Duan et al., 2013).

In resume, the evaluation of the use of CDW in the construction sector has been stimulated in several parts of the world and many studies have been developed to

increase knowledge about the behavior of these residues for the production of new materials. The discussion about this issue is the main goal of this paper, focusing on the evaluation of RAC structural performance.

2 Material and Method

In this work, CDW was used to produce both fine and coarse aggregated to be used as cement replacements in reinforced concrete beams. CDW used came from a civil construction recycling plant and its composition contains materials from several origins like excavation residues, demolition of simple and reinforced concrete elements, the residue of ceramic masonry materials—bricks and tiles- and also mortar cement-based bricks and mortars. Before processing the CDW, an initial manual separation was carried out to remove materials such as wood, plastic, and plaster. The material is, then, taken to a CDW recycling plant where it begins its processing that can be summarized as it follows: (a) feeding & pre-screening, (b) aggregate scrubbing, (b) contaminant removal, (c) metals and others undesirable materials removal, (d) sand washing, (e) aggregate sizing, (f) primary stage water treatment and (g) deposited in bags according to their granulometry. Figures 1 shows a general view of the CDW recycling plant.



(a) Material transport and washing



(b) Final stage of the process



(c) Fine aggregate obtained



(d) Coarse aggregate obtained

Fig. 1 Overview of a CDW recycling plant

2.1 Physical Characterization Tests

Table 1 shows the results of physical characterization and Fig. 2 exhibits the size distribution profile for usual aggregate and both, fine and coarse aggregates, obtained from the processing of the CDW investigated.

Fine and coarse recycled aggregate presented a nominal maximum size of 4.8 and 25 mm, respectively. As the natural and CDW coarse aggregates are obtained through an industrialized process, the granulometric size distribution behavior shown

Table 1 Physical properties of aggregates used

Test	Fine aggregate		Coarse aggregate	
	Usual	CDW	Usual	CDW
Specific gravity (g/cm ³)	2.65	2.50	2.54	2.32
Water absorption rate (%)	-	-	0.30	3.51
Fineness modulus (-)	2.07	1.90	-	6.97

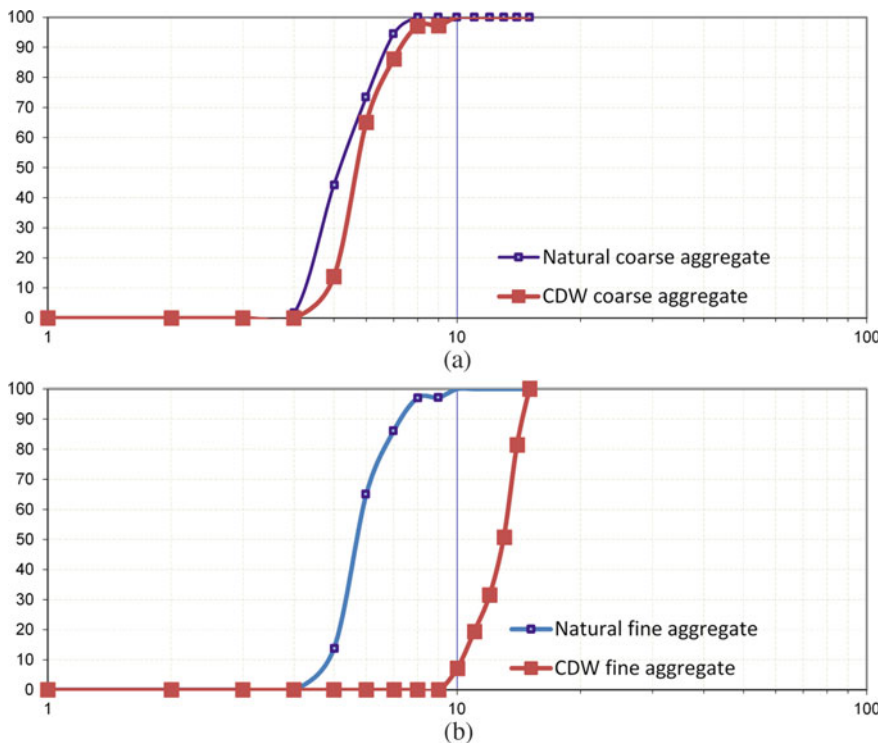


Fig. 2 Aggregate size distribution: **a** Natural and CDW coarse aggregates; **b** Natural and CDW fine aggregates

in Fig. 2 is justified—quite a similar curve. The same does not happen, however, with the natural small aggregates because it is available in nature and the one obtained with CDW goes through an industrial improvement process and, this way, it is very difficult to get both curve close.

2.2 Concrete Mixtures and Mechanical Characterization Tests

To produce the concretes with fine and coarse aggregates from CDW, the following methodology was adopted:

- RAC with fine aggregates from CDW
 - Use of Ordinary Portland Cement PC-II-F;
 - Use of natural quartz coarse aggregate with a maximum size of 25 mm;
 - Replacement of natural sand by 50% and 100% in weight of fine recycled aggregate
- RAC with coarse aggregates from CDW
 - Use of Ordinary Portland Cement PC-II-F;
 - Use of natural fine aggregate with a maximum size of 4.8 mm;
 - Replacement of natural quartz coarse aggregate by 50% and 100% in weight of coarse recycled aggregate

Tables 2 and 3 exhibits the concrete mixture prepared using fine and coarse aggregate from CDW, respectively.

To prepare RAC mixtures, coarse aggregates were saturated before its use. This process was done by placing the aggregates submerged in water for 15 (fifteen) minutes. This period was determined by making several measurements of a pre-determined mass of the aggregate at different time intervals in which it remained submerged. When his weight no longer increased from a previous measurement to the next measurement, it was assumed that his ability to absorb water had reached

Table 2 RAC with fine aggregate from CDW

Ref	w/c	C (kg)	FA (kg)	CA (Kg)	W (kg)	FRA (kg)
1:1.58:2.99 (RCM)	0.50	5.40	8.54	16.14	2.70	-
1:0.79:0.79:2.99 (RAC50)	0.50	5.79	4.57	17.31	2.90	4.57
1:0:1.58:2.99 (RAC100)	0.50	5.79	-	17.31	2.90	9.14

RCM = Reference Concrete Mixture, RAC50 = Concrete with 50% of FRA, RAC100 = Concrete with 100% of FRA, C = Cement, FA = Fine Aggregate, CA = Coarse Aggregate, W = Water, FRA = Fine Recycled Aggregate.

Table 3 RAC with fine coarse aggregate from CDW

Ref	w/c	C (kg)	FA (kg)	CA (Kg)	W (kg)	CRA (kg)
1:1.58:2.99 (RCM)	0.50	5.40	8.54	16.14	2.70	-
1:1.58:1.49:1.49 (RAC50)	0.50	5.79	9.14	8.66	2.90	8.66
1:1.58:0:2.99 (RAC100)	0.50	5.79	9.14	-	2.90	17.31

RCM = Reference Concrete Mixture, RAC50 = Concrete with 50% of FRA, RAC100 = Concrete with 100% of FRA, C = Cement, FA = Fine aggregate, CA = Coarse aggregate, W = Water, CRA = Coarse Recycled Aggregate

its limit (Brito et al., 2011). This procedure is necessary to avoid that the coarse aggregate, due to its high absorption rate, absorbs part of the water used in the preparation of the concrete.

To access concrete's mechanical properties, destructive tests were performed—compression and tension tests—as well as non-destructive ones—ultrasonic pulse and sclerometry tests. Compressive and tensile strengths were obtained through tests in one hundred and twenty concrete cylindrical specimens (100 mm in diameter and 200 mm in height). In total, 120 cylindrical concrete specimens were prepared to be 60 for each test performed—compression and tension tests. From each test performed, 15 cylindrical specimens were used to get for both coarse and fine RAC for each amount of replacements studied—50 and 100%. The number of 15 concrete cylindrical specimens used for each of the conditions analyzed was determined based on the need to have a 95% confidence level in the results obtained. Concrete cylindrical specimens were all prepared by NBR 5738 (2018).

The compressive strength of concrete was determined by axial compression tests of cylindrical specimens, according to the requirements set by the NBR 5739 (2018) using a servo-hydraulic press EMIC DL-20000 with 200 kN load capacity. Tensile strength tests were performed using the Brazilian Method according to NBR 7222 (2011) using the same servo-hydraulic press.

Ultrasound tests were performed on all specimens according to NBR 8802 (2019). One day before starting the ultrasonic wave speed tests, all specimens were removed from the chamber to surface drying. PUNDIT equipment with a 500 kHz longitudinal transducer frequency was used and placed so that the wave reading was directly transmitted—the most efficient way of transmitting the ultrasonic wave in continuous media (Ozbakkaloglu et al., 2018).

Rebound hammer tests were made according to NBR 7584 (2012) and the equipment used provides correlation curves between the rebound value and concrete strength.



Fig. 3 Four-point beams tests

2.3 Concrete Beams Models

Figure 3 shows the type of bending test performed on beams made with conventional concrete and RAC from CDW for both fine and coarse recycled aggregate. The bending test consists of the application of a monotonic load on a simply supported beam until it reaches a failure or until it reaches a pre-established deformation state. This test is well known as the four-point flexural test which is an indirect way to estimate the tensile strength of beams and its more adequate than the three-point test because it produces a pure bending state over a significant area of the specimen. In this aspect, 4-point bending is quite similar the tension/compression test.

Three 2.20 m concrete beams with a square cross-section with a side of 20 cm were prepared, one made with the reference concrete and the other two beams made with concrete with full replacement of both types of recycled aggregates studied. All beams were designed to avoid the sudden non-ductile shear failure and a balanced condition was imposed to perform longitudinal reinforcement calculation and detailing. This study aims to investigate the mechanical response of RACs on both maximum load capacity, displacements, and also evaluate the flexural strengths of the beams tested.

Vertical displacements at mid-span were measured using high precision linear variable differential transformer—LVDT—located as indicated in Fig. 3c.

3 Results and Discussion

3.1 Ultrasonic Pulse Velocity (UPV) Tests

Table 4 summarizes the results of ultrasonic pulse velocity tests performed in all concrete cylindrical specimens. Average UPV values indicated in this table were obtained for a sample of 15 results for each concrete studied and the coefficient of

Table 4 Ultrasonic pulse velocity test results

Concrete	UPV		
	Average (m/s)	St. Dev. (m/s)	CV (%)
RCM	4.56	0.17	6.25
RAC-F50	4.54	0.09	2.20
RAC-F100	4.17	0.11	2.90
RAC-G50	3.98	0.09	2.25
RAC-G100	3.20	0.14	4.31

RCM = Reference Concrete Mixture, RAC-G50 = Concrete with 50% of CRA, RAC-G100 = Concrete with 100% of GRA, RAC-F50 = Concrete with 50% of FRA, RAC-F100 = Concrete with 100% of FRA C = Cement, FA = Fine aggregate, CV = Coefficient of variation

Table 5 Mechanical test results

Concrete	Average f_c (MPa)	Average f_{st} (MPa)
RCM	27.0 ± 1.23	2.90 ± 0.23
RAC-F50	24.0 ± 1.42	3.30 ± 0.27
RAC-F100	28.0 ± 1.36	3.51 ± 0.24
RAC-G50	21.49 ± 2.00	2.94 ± 0.35
RAC-G100	17.49 ± 0.99	2.30 ± 0.32

variation associated was very low. Taking into account that the higher the coefficient of variation, the greater the level of dispersion around the mean, the results obtained indicated that concrete quality was excellent for all concrete mixtures studied.

Additionally, it can be observed that for the RACs, except those produced with 50% of fine aggregate replacement, exhibited slow UPV when compared with the reference concrete mixture. This behavior can be explained by the higher density than concrete made with natural aggregates present comparing with those produced with recycled coarse aggregates, thus generating higher speeds. The concretes made with coarse recycled aggregates exhibited the lowest values of ultrasonic wave speeds and it is even decreasing with the increase of the replacement. This happens due to the lower density of the recycled aggregates, thus interfering in the propagation speed of the ultrasonic waves. For RAC-G100 it was observed a decrease close to 30% in UPV, the same behavior observed by other researchers that reported a decrease of about 5% in UPV with 50% replacement of fine aggregate from CDW (Saha et al., 2020; Cantero et al., 2020; Singh et al. 2018).

Table 6 Flexural tests of the experimental results

Specimen	Maximum load (kN)	Maximum displacement (mm)
RCM-Beam	94.25	12.95
RAC-F100 Beam	81.68	12.25
RAC-G100 Beam	52.10	12.10

3.2 Compression and Tension Split Strength Tests

Compressive strength test results are indicated in Table 5. It is possible to observe from this table that, among the studied RACs, the one that presented the best performance in terms of compressive strength was that produced with 100% recycled fine aggregate. Oppositely, the RACs produced with recycled coarse aggregates did not show the same behavior and, when the compressive strength of concrete made with 100% recycled coarse aggregate is compared with the reference concrete, a decreasing about 35% was observed. This can be explained based on the RAC microstructure. RAC has an additional interfacial transition zone (ITZ) between the aggregate and the old mortar attached (i.e., old ITZ) to the surface of recycled concrete aggregates. ITZ is generally regarded as the weak link in concrete. Therefore, the presence of an additional ITZ in RAC leads to a lower value of compressive strength (Xie et al., 2018). Moreover, because of the porous nature of the old mortar attached to the surface of recycled concrete aggregates, the ITZ between the old and new mortar (new ITZ) with low compressive strength, and it forms another weak link in the concrete, which in turn results in a lower f_{cm} (Medina et al., 2015).

According to previous reviews on RAC and natural aggregate concrete (NAC), the splitting tensile (f_{st}) strength of RAC is generally lower than those of NAC with the same concrete mix (Behera et al., 2014; Safiuddin et al., 2013; Xiao et al., 2006). Other researchers reported that RAC with full replacement of coarse aggregate by CDW presented a decrease in tensile strength close to 23% (Mefteh et al., 2013; Thomas et al., 2013; Wu et al., 2001).

3.3 Four-Point Beam Tests

Failure profile for all beams tested is shown in Fig. 4. The examination of this figure identifies the difference in behavior at failure, with the concrete compressed block of the RAC-G100 beam failed in compression before the most expressive cracking process in the tensioned region of the beam has manifested itself, situation diametrically opposite to what was observed with the reference beam. This happened due to the low compressive strength of the coarse recycled aggregate used when compared to natural coarse aggregate, which significantly interfered in the modification of the beam failure profile.

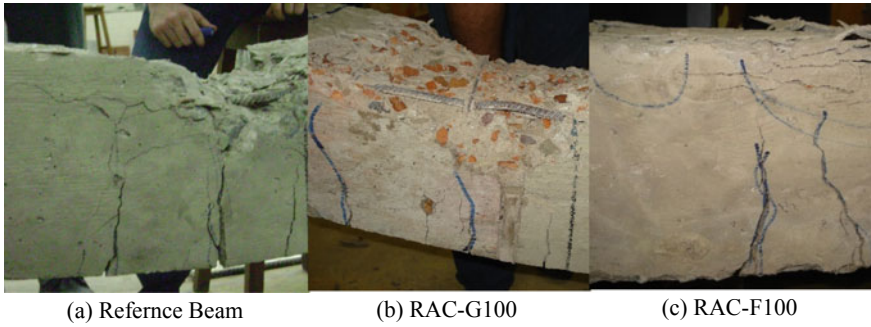


Fig. 4 Overview at failure of beams tested

For the beam made with RAC with fine aggregate, there is little difference in behavior at the moment of failure when compared to the reference beam. The cracks in the tensioned part and the crushing of the concrete in the compressed part presented a similar profile. It has been seen previously that from compressive strength, concrete with 100% recycled fine aggregate presented an excellent performance when compared to concrete with conventional fine aggregate.

Figure 5 shows a graph which typifies the dependence of the force F on the vertical displacement δ . This graph overall characterizes the experimental data obtained from the tests performed. Three different behaviors can be observed in this figure and the beam produced with RAC-G100 is the one that presented the greatest discrepancy when compared to the RCM beam. This shows that the beam made with RAC-G100 proved to be less efficient to the flexural behavior, an aspect that validates the other experimental results performed.

The shape of the load mod-span displacement showed in Fig. 5 indicates, also, a linear behavior until de failure, except for the first stage of the RCM beam which

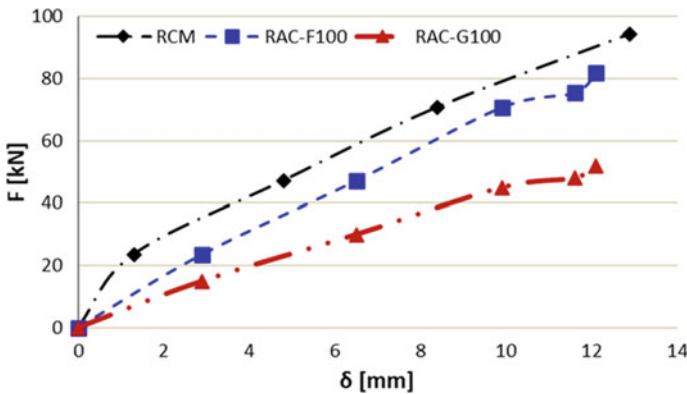


Fig. 5 Force (F) versus displacement (δ) Curves

presented a slight change in the slope of the F vs. δ curve, an aspect that indicates the beginning the begin of beam cracking process. The same behavior was not observed for RAC's beam which means that those beams presented a very brittle behavior.

The maximum load and displacement are reported in Tabel 6, separately for each beam tested. It can be seen that the load capacity was decreased with the amount of recycled aggregate being the less one obtained with the full coarse aggregate replacement which presented a failure load close 55% of the RCM beam in spite small differences in displacements values have been observed. It means that the overall behavior of beams with recycled aggregates was not very affected because the reinforcement controls the flexural performance of RC beams (Younis et al., 2020). Moreover, the cracking profile during the tests showed to be dependent on the type of RAC used (Fahmy & Idriss, 2019).

4 Conclusions

The following conclusions can be drawn from the results of tests performed:

- RAC showed to be a good solution for an adequate destination to the CDW from the construction industry;
- Tests performed to evaluate RAC properties did not show significant differences when compared with moderate NAC values;
- The use of replacement of fine aggregate for those obtained from CDW presented a better behavior when compared with coarse aggregates from CDW;
- In flexural behavior, coarse aggregates replacement generated an important decrease in beam capacity, an aspect that recommends its uses in small lengths flexural elements;
- For the same load level, the beam made with 100% fine aggregate of RCD presented greater vertical displacements than those made with 100% conventional aggregate, an aspect that characterizes a lower rigidity of the beam made with recycled aggregate.
- Full recycled fine aggregate replacement exhibited better performance in all tests performed proving, this way, great potentialities to be used as fine aggregate in concrete production;
- It was observed that the concrete with 50% addition and 100% substitution of recycled aggregate from construction and demolition residues has characteristics similar to the reference concrete, being able to achieve higher compressive strength, but with higher consumption of cement and water than reference concrete.

References

- Behera, M., Bhattacharyya, S. K., Minocha, A. K., Deoliya, R., & Maiti, S. (2014). Recycled aggregate from C&D waste & its use in concrete—A breakthrough towards sustainability in construction sector: A review. *Construction and Building Materials*, *68*, 501–516.
- Bravo, M., Brito, J., Pontes, J., & Evangelista, L. (2015). Mechanical performance of concrete made with aggregates from construction and demolition waste recycling plants. *Journal of Cleaner Production*, *99*, 59–74.
- Brito, J., Bizinotto, M. B., & Ferreira, L. (2011). Influence of the pre-saturation of recycled coarse concrete aggregates on concrete properties. *Magazine of Concrete Research*, *63*(8), 617–627.
- Cantero, B., Bravo, M., Brito, J., Bosque, I.S., & Medina, C. (2020). Mechanical behaviour of structural concrete with ground recycled concrete cement and mixed recycled aggregate. *Journal of Cleaner Production*, *275*, 122913.
- Cho, Y.-H., & Yeo, S.-H. (2004). Application of recycled waste aggregate to lean concrete subbase in highway pavement. *Canadian Journal of Civil Engineering*, *31*(6), 1101–1108.
- Dhir, R., & Paine, K. (2010). Value added sustainable use of recycled and secondary aggregates in concrete. *Indian Concrete Journal*, *84*, 7–26.
- Dilbas, H., Çakir, Ö., & Şimsek, M. (2016). Recycled aggregate concretes (RACs) for structural use: An evaluation on elasticity modulus and energy capacities. *International Journal of Civil Engineering*, *15*(2), 247–261.
- Duan, Z. H., Kou, S. C., & Poon, C. S. (2013). Prediction of compressive strength of recycled aggregate concrete using artificial neural networks. *Construction and Building Materials*, *40*, 1200–1206.
- Fahmy, M. F. M., & Idriss, L. K. (2019). Flexural behavior of large scale semi-precast reinforced concrete T-beams made of natural and recycled aggregate concrete. *Engineering Structures*, *198*, 109525.
- Hafez, H., Kurda, R., Al-Hadad, B., Mustafa, R., & Ali, B. (2020). A critical review on the influence of fine recycled aggregates on technical performance, environmental impact and cost of concrete. *Applied Sciences*, *10*(3), 1018.
- Kisku, N., Joshi, H., Ansari, M., Pandra, S. K., Nayak, S., & Dutta, C. (2017). A critical review and assessment for usage of recycled aggregate as sustainable construction material. *Construction and Building Materials*, *131*, 721–740.
- Makul, N. (2020). Cost-benefit analysis of the production of ready-mixed high-performance concrete made with recycled concrete aggregate: A case study in Thailand. *Heliyon*, *6*, e04135.
- Medina, C., Zhu, W., Howind, T., Rojas, M. I. S., & Frías, M. (2015). Influence of interfacial transition zone on engineering properties of the concrete manufactured with recycled ceramic aggregate. *Journal of Civil Engineering and Management*, *21*(1), 83–93.
- Mefteh, H., Kebaïli, O., Oucief, H., Berredjem, L., & Arabi, N. (2013). Influence of moisture conditioning of recycled aggregates on the properties of fresh and hardened concrete. *Journal of Cleaner Production*, *54*, 282–288.
- NBR 5738. (2018). Concrete—Procedure for molding and curing concrete test specimens. Brazilian Association of Technical Standards, ABNT, Rio de Janeiro, Brazil.
- NBR 5739. (2018). Concrete—Compression test of cylindrical specimens. Brazilian Association of Technical Standards, ABNT, Rio de Janeiro, Brazil.
- NBR 7222. (2011). Concrete and mortar—Determination of the tension strength by diametrical compression of cylindrical test specimens. Brazilian Association of Technical Standards, ABNT, Rio de Janeiro, Brazil.
- NBR 7584. (2012). Hardened concrete—Evaluation of surface hardness by reflecting esclerometer—Test method. Brazilian Association of Technical Standards, ABNT, Rio de Janeiro, Brazil.
- NBR 8802. (2019). Hardened concrete - Determination of ultrasonic wave transmission velocity. Brazilian Association of Technical Standards, ABNT, Rio de Janeiro, Brazil.

- Ozbakkaloglu, T., Gholampour, A., & Xies, T. (2018). Mechanical and durability properties of recycled aggregate concrete: Effect of recycled aggregate properties and content. *Journal of Materials in Civil Engineering*, 30(2), 04017275.
- Poon, C. S., Kou, S. C., & Lam, L. (2007). Influence of recycled aggregate on slump and bleeding of fresh concrete. *Materials and Structures*, 40(9), 981–988.
- Safiuddin, M., Alengaram, U. J., Rahman, M. M., Salam, M. A., & Jumaat, M. Z. (2013). Use of recycled concrete aggregate in concrete: A review. *Journal of Civil Engineering and Management*, 19(6), 796–810.
- Saha, A. K., Majhi, S., Sarker, P.K., Mukherjee, A., Siddika, A., Aslani, F. and Zhuge, Y. (2020). Non-destructive prediction of strength of concrete made by lightweight recycled aggregates and nickel slag. *Journal of Building Engineering*, 33, 101614.
- Singh, N., & Singh, S. P. (2018). Evaluating the performance of self-compacting concretes made with recycled coarse and fine aggregates using non-destructive testing techniques. *Construction and Building Materials*, 181, 73–84.
- Song, L., & Liang, D. (2011). Lean construction implementation and its implication on sustainability: A contractor's case study. *Canadian Journal of Civil Engineering*, 38(3), 350–359.
- Thomas, C., Sosa, I., Setién, J., Polanco, J. A., & Cimentada, A. I. (2014). Evaluation of the fatigue behavior of recycled aggregate concrete. *Journal of Cleaner Production*, 65, 397–405.
- Thomas, C., Setien, J., Polanco, J. A., Alaejos, P., & Sanchez, J. M. (2013). Durability of recycled concrete aggregate. *Construction and Building Materials*, 40, 1054–1065.
- Torgal, F. P., & Jalali, S. (2011). Construction and demolition (C&D) wastes. Eco-efficient construction and building materials. Springer, London, UK.
- Xiao, J. Z., Li, J. B., & Zhang, C. (2006). On relationships between the mechanical properties of recycled aggregate concrete: An overview. *Materials and Structures*, 39(6), 655–664.
- Xie, T., Gholampour, A., & Ozbakkaloglu, T. (2018). Toward the development of sustainable concretes with recycled concrete aggregates: Comprehensive review of studies on mechanical properties. *Journal of Materials in Civil Engineering*, 30(9), 04018211.
- Wu, K. R., Chen, B., Yao, W., & Zhang, D. (2001). Effect of coarse aggregate type on mechanical properties of high-performance concrete. *Cement and Concrete Research*, 31(10), 1421–1425.
- Younis, A., Ebead, U., Suraneni, P., & Nanni, A. 2020. Short-term flexural performance of seawater-mixed recycled-aggregate GFRP-reinforced concrete beams. *Composite Structures*, 236, 111860.

Thermal Performance of Dwellings: Comparative Study Between Simulation Methods with NBR 15,575 (2013) and NBR 15,575 (2021)



M. M. Barbosa, P. E. Silva de Oliveira, A. J. Costa e Silva,
J. M. P. Q. Delgado, and A. C. Azevedo

Abstract Depending on the constructive, geographical, and geometric characteristics, the thermal performance of buildings is parameterized by regulatory technical standards that aim to promote appropriate thermal comfort conditions for users. The knowledge of the ways to mitigate radiation, the biggest source of thermal gains in buildings, is essential to enable better thermal energetic levels and, above all, reduce the consumed thermal load. This work aims to carry out a comparative analysis between the computational simulation methods recommended by NBR 15,575 (2013) and NBR 15,575 (2021). For this purpose, two buildings were selected: one housing of social interest and another with a high-end standard level. From this, computational models for thermoenergetic simulation were carried out using the Energy-Plus software. The results obtained in the social interest housing simulations indicated compliance with the minimum level, but there was no compliance with the criteria of the intermediate and superior levels given the two normative methods analyzed. In the simulations carried out in the high-end building, compliance with the minimum level was achieved only with the use of shading devices in the frames, and, like social housing, it did not meet the intermediate and higher levels. When observing the simulations, in spite of being different, the service profile between the two methods was maintained. The house of social interest, whose construction systems are similar to the normative reference model, predisposes to meeting the minimum level, whereas buildings with large areas of transparent elements tend to have greater difficulties in meeting the thermal performance requirement. This work also shows the normative advances given by NBR 15,575 (2021) through the insertion

M. M. Barbosa · P. E. S. de Oliveira · A. J. C. Silva
Departamento de Engenharia Civil, Universidade Católica de Pernambuco, Recife, Brazil
e-mail: angelo.silva@unicap.br

J. M. P. Q. Delgado (✉) · A. C. Azevedo
Departamento de Engenharia Civil, CONSTRUCT-LFC, Universidade Do Porto, Rua Dr. Roberto
Frias, s/n, 4200-465 Porto, Portugal
e-mail: jdelgado@fe.up.pt

A. C. Azevedo
e-mail: antonio.costaazevedo@fe.up.pt

of parameters that incorporate energy efficiency and the concept of annual analysis of buildings.

Keywords Thermal performance · NBR 15,575 (2013, 2021) · Numerical simulation · Energy-plus

1 Introduction

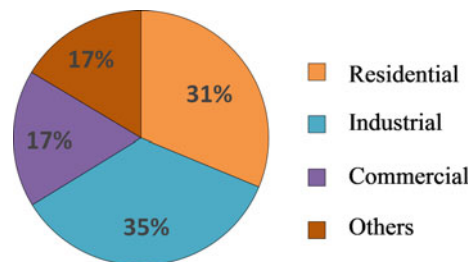
Thermal performance could be defined as thermal parameters established by regulatory standards that a building must meet. The adequate thermal performance implies better conditions of comfort in the use of the building, as well as the reduction of the housing energy consumption. It is valid to state that thermal performance is not equal to thermal comfort, since thermal comfort refers to the physical and mental state that represents the satisfaction of the individual with the thermal environment in which it is inserted (ASHRAE, 2017a; Lamberts et al., 2014; Sorgato et al., 2013).

The thermal performance of a building depends on numerous variables from which they undergo the site of housing (topography and climatic conditions) and characteristics of the building (number of floors, dimensions of the environments, as well as the building height, the orientation of the facades, among others). In terms of thermal performance, Brazil, with continental dimensions and a great climatic variability, is a challenging country for designers and consultants to ensure good conditions of comfort in buildings. Thus, knowledge in the materials used and configuration of the building in the climate in which it is inserted is fundamental to ensure better thermal energetic conditions (Ioannou & Itard, 2015; Novais et al., 2014; Silva & Ghisi, 2014).

In 2020, Brazil presented an energy consumption of 474.22 Twh, of which the residential sector represented a share corresponding to 31% related to total consumption (see Fig. 1).

According to Jardim (2011), the housing adequacy, during use, to thermal comfort represents about 84% of energy consumption and highlights the importance of rationalizing the building envelope in order to promote better levels of thermos-energetic efficiency. The studies presented by Almeida (2014), Fajkus (2013) and Yoshino et al (2017) confirmed the influence of the thermos-energetic properties of the envelope

Fig. 1 Distribution of electricity consumption by sector, in 2020 (EPE, 2020)



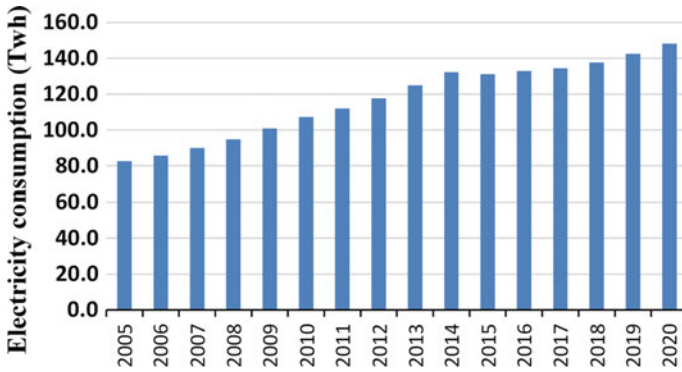


Fig. 2 Electricity consumption of the residential sector (2005–2020), EPE (2020)

on the energy balance of the system and the impact on the energy consumption of buildings.

According to EPE statistics, the growth of energy consumption in the Brazilian residential sector between 2005 and 2020 presented an increase of 79.4% compared to the initial value (see Fig. 2). Based on the technical note 030/2018, EPE states that the acquisition of air conditioners, with a growth of 9% per year, in residential buildings was crucial in the increase of 61% of Brazilian electricity in the residential sector between 2005 and 2017. These data demonstrate the relevance of air conditioning systems in the need of Brazilians to obtain comfort and reinforce their impact on the Brazilian electrical system, which, in turn, implies greater generation and distribution needs to meet energy demands, especially at peak times.

According to Dornelles (2008), the largest source of thermal gains in buildings comes from the incidence of solar radiation and states that the most sustainable means to mitigate heat gains in buildings is given by controlling the effects of solar radiation that reaches constructive envelope. Therefore, the investment in efficient techniques that mitigate thermal exchanges in a building can therefore enable better comfort conditions with reduced energy consumption. In terms of energy, Lamberts et al (2014) states that one building is more efficient than another when it provides the same environmental conditions with lower energy consumption.

In resume, the main research, of this work, is a comparative analysis of the computational simulation methods used in the thermal performance requirement by NBR 15,575 (2013) and the new methods proposed in Amendment 1 of NBR 15,575 (2013), new standard NBR 15,575 (2021). More in detail:

- Study the heat transmission processes of the building envelope;
- Perform computational simulations to obtain internal temperatures in each long-stay enclosure analyzed;
- Perform computational simulations to obtain annual energy consumption of buildings, due to the needs of cooling the bedrooms;
- Analyze the temperature and energy consumption numerical results obtained.

2 Literature Review

External vertical sealing systems, floor systems, roofing systems and windows constitute the building envelope. These systems and elements have the function of isolating the internal environment from external climatic conditions, acting as a barrier to air passage (infiltration and ventilation), heat (thermal energy) and relative humidity. Therefore, being aware of the physical processes that are part of the building envelope becomes essential to investigate the behavior of the building as a function of meteorological changes, the location, besides having competence to define the necessary parameters of the materials that will compose the project since its conception and, consequently, more efficient decision-making.

There are several types of energies such as kinetic, electrical, magnetic, mechanical, nuclear, potential, chemical and thermal energy, whose sum represents the total energy of a system. Among the existing forms of energy, those that relate to the molecular structure of a system and the degree of molecular activity are named microscopic energy. The sum of all microscopic energies results in the internal energy of the system (Çengel and Ghajar, 2012).

Regarding internal energy, which is configured in two ways: kinetic internal energy and potential internal energy, this work is limited to the study of internal energy associated with the kinetic energy of molecules, called sensitive energy or sensitive heat, that is, when thermal energetic transfers do not involve alteration in the physical state of matter. In this context, heat, or thermal energy, is conceptually understood as energy associated with the random movement of atoms and molecules whose average velocity and degree of activity are proportional to the temperature increase.

The general concept for defining specific heat is the energy needed to increase the temperature by a degree of a given unit of mass of the substance. There are two specific heat types: heat specific to constant pressure and specific heat to constant volume; the values for the two specific types of heat are equivalent when it comes to incompressible substances, when the density does not change due to temperature or pressure variation. The specific heat of incompressible substances depends only on a variable, temperature, and therefore the mathematical expression that measures the physical concept of variation of internal energy (sensitive heat) of solids or liquids, is represented by Eq. (1),

$$Q = m c \Delta T \quad (1)$$

where Q is the heat flow (J), m is the mass (kg); c is the specific heat ($\text{kg/J} \cdot \text{K}$) and ΔT is the temperature gradient (K).

Understanding heat transfer mechanisms is crucial to achieving better conditions of comfort and thermal performance, as well as energy efficiency. Specht et al. (2010) state that “*The design of energy-efficient buildings requires knowledge about the transfer of heat from the external environment to the interior of the buildings, in order to create solutions that associate different materials and layer dimensions with the desired conditions of thermal comfort. The production of this knowledge through*

the construction of prototypes, besides being costly, presents difficulties with regard to the variation of the materials and dimensions of the layers”.

It is also worth mentioning that, in NBR 15,575 (2013), it is contemplated the analysis of the thermal properties of the building envelope systems in the simplified method of evaluating the thermal performance of buildings, the calculation procedure is expressed in NBR 15,220 (2005) and is based on the determination of thermal transmittance and thermal capacity (seen Sect. 2.1.1 Conduction).

2.1 Heat Transfer Mechanisms

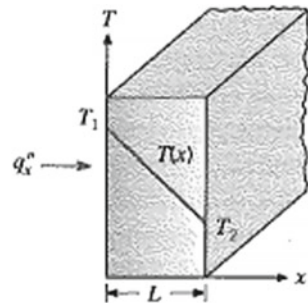
Heat transfer could be defined as thermal energy in transit by the action of a temperature gradient in space. In general, when there is a temperature gradient in a medium or between media, i.e. solid(s) or fluid(s), there will be heat transmission. There are three forms of heat transmission: we call it conduction, the heat transfer that occurs through a stationary medium; convection as the transfer of heat between a surface and a moving fluid and, finally, the thermal radiation that is the energy emitted by matter, which is at a non-zero temperature, through electromagnetic waves (Incropera and Dewitt, 2008).

2.1.1 Conduction

The heat conduction process (see Fig. 3) respects the second law of thermodynamics, which states that the meaning of heat transfer should be in the direction of lower temperature. The heat conduction rate (q') by one medium is proportional to geometry and temperature difference, and inversely proportional to thickness. The governing equation of the heat conduction rate, the Fourier law of thermal conduction, under steady-state conditions, is defined by:

$$q = -\lambda \cdot A \cdot \frac{\Delta T}{L} \tag{2}$$

Fig. 3 Heat conduction sketch (Incropera and Dewitt, 2008)



where q is the heat conduction rate (W); λ is the thermal conductivity (W/m · K); A is the area perpendicular to the direction of heat transfer (m²); ΔT is the temperature difference, obtained by subtracting the cold temperature from the hot temperature and L is the thickness, parallel to the heat transfer direction (m).

Note: The negative sign of the equation ensures that the heat transfer in the positive direction of L is a positive value.

From Eq. (2), the heat flux density (q'') is given by the ratio of the rate of heat conduction by the area, thus:

$$q'' = \frac{q}{A} \therefore q'' = \lambda \cdot \frac{\Delta T}{L} \quad (3)$$

Thermal Resistance of Conduction

In general, thermal resistance is a property associated with the difficulty of passing heat through a medium, taking into account the difference in temperature, thermal energy, cross-sectional area to the transfer direction and thickness. There is a range of ways to treat thermal resistance in engineering, the three most used are:

- **Absolute thermal resistance (R_t)**

This parameter defines the strength of a system whose geometric characteristics of area and thickness are known. For the absolute thermal resistance, only one temperature difference between surfaces is enough to determine the heat transferred from a system. The expression representing by R_t is derived from Eq. (2),

$$q = \frac{\Delta T}{R_t} \quad (4)$$

with the absolute thermal resistance (R_t) given by,

$$R_t = \frac{L}{\lambda \cdot A} \quad (5)$$

where R_t is the absolute thermal resistance (K/W).

- **Thermal resistance as R-value (R)**

This parameter is a constant of the material and indicates the difficulty of changing the temperature of the material, every linear meter, by inserting a unit of energy. Material thickness and a temperature difference are necessary to establish the transferred heat. The units representing the specific thermal resistance are mK/W.

- **Thermal resistance as R-value (R)**

The R value is known as the thermal insulation factor, it is directly proportional to the insulation, that is, the higher the R-value, the better the resistance of the material against the passage of heat in its environment. Expresses the thermal resistance of the unit area of a system. The unit representing this type of thermal resistance is $\text{m}^2 \cdot \text{K}/\text{W}$. For the determination of transferred heat, an area and temperature difference is required. The physical model that defines R is:

$$\mathbf{R} = \frac{\mathbf{L}}{\lambda} \quad (6)$$

Therefore, the heat flux density is expressed as:

$$\mathbf{q}'' = \frac{\Delta \mathbf{T}}{\mathbf{R}} \quad (7)$$

In composite systems, it is common to use an analogy to Newton's law of cooling as a way of treating the system's heat transfer. In this mode, a U coefficient is adopted which means *global heat transfer coefficient*, or thermal transmittance, and expresses the rate of heat flux that crosses the unit area of a component when there is a thermal gradient of 1 K between its faces. Thermal transmittance obeys the following expression:

$$\mathbf{U} = \frac{\mathbf{q}''}{\Delta \mathbf{T}} \quad (8)$$

where U is the thermal transmittance coefficient ($\text{W}/\text{m}^2 \cdot \text{K}$). Correlating Eq. (7) with Eq. (8), the thermal transmittance of a component can be understood as the inverse of the sum of the thermal resistances of each element that integrates the component, demonstrated by,

$$\mathbf{U} = \frac{1}{\sum \mathbf{R}} \quad (9)$$

Electrical Analogy

There is an important analogy made from the heat conduction rate equation with the electric current flow equation.

$$\mathbf{I} = \frac{\Delta \mathbf{V}}{\mathbf{R}_e} \quad (10)$$

$$\mathbf{q} = \frac{\Delta \mathbf{T}}{\mathbf{R}_t} \quad (11)$$

Just as electrical resistance is associated with conducting electricity, thermal resistance is associated with conducting heat. This relationship is very favorable when you have different materials that make up a medium, as you can use the rule of summing the resistance of electrical circuits for thermal circuits and determine an equivalent resistance of the thermal circuit, being associated in series and/or parallel.



$$R_{eq} = \sum_{i=1}^n R_i \quad (12)$$

$$\frac{1}{R_{eq}} = \sum_{i=1}^n \frac{1}{R_i} \quad (13)$$

Thermal Diffusivity

In transient heat conduction analyses, a property that measures the speed of heat propagation in a medium is called thermal diffusivity and it is linked to the thermal conductivity and thermal capacity of the material. This, in turn, concerns the heat storage capacity of a material, as well as specific heat, but it differs from specific heat in that it refers to the heat storage capacity per volume unit, whereas specific heat refers to the heat storage capacity per unit of mass.

The diffusivity of a given material is the result of the fraction between its thermal conductivity and its thermal capacity. Thermal capacity is the result of the product between density and specific heat of a material,

$$\kappa = \frac{\lambda}{\rho c} \quad (14)$$

where κ is the thermal diffusivity (m^2/s); λ is the thermal conductivity ($W/m \cdot K$); ρc is the thermal capacity ($J/m^3 \cdot K$); ρ is the density (Kg/m^3) and c is the specific heat ($kg/J \cdot K$). Should be noted that it is common to find in some literatures and standards, especially when it comes to constructive systems, the thermal capacity as a result of the product between the density, thickness and specific heat of the corresponding material. In this particularity, the thermal capacity expresses the heat storage efficiency of a material per unit area, which must be perpendicular to the heat transfer direction, in $J/m^2 \cdot K$.

Brazilian Convention for the Calculation of Thermal Capacity and Thermal Resistance

In Brazilian civil construction, the calculation of thermal capacity and thermal resistance of building component and element systems are recommended by the NBR 15,220 (2005) standard.

2.1.2 Convection

The convection heat transfer mode involves the transfer of heat between a moving fluid, gas or liquid and a surface of which there is a temperature gradient. Convection takes place through two mechanisms: energy transfer by random molecular motion and by global, or macroscopic, fluid motion (advection). It is noteworthy that in the absence of mass movement of a fluid, heat transfer between the solid surface and the adjacent fluid takes place through a conduction process.

A model for understanding the conduction process is to consider a hot surface which must be cooled by cold air on its face. The consequence of the interaction between the heated surface of the surface and the fluid is the emergence of a region whose velocity varies from zero (in contact with the upper surface, higher, $y = 0$) to a finite value (v_∞); there will also be a region where the surface temperature will vary from T_s , at $y = 0$, to T_∞ , fluid temperature. In this way, we say that surface heat is cooled by convection, caused by the combined effect of conduction within the air caused by random movement of air molecules and by mass movement or macroscopic movement of the air that replaces the heated surface air with a cooler air. It is important to note that when the fluid velocity reaches the finite value (v_∞), this region is known as the hydrodynamic or velocity boundary layer and it is at this same level that we will also have the thermal boundary layer, with the fluid reaching temperature T_∞).

The classification of conduction heat transfer varies according to the nature of the fluid flow and can be forced, mixed or natural. We claim that convection is said to be forced when fluid is forced to flow over the surface by external means such as a fan, pump, or atmospheric winds. In the case of natural convection, fluid flow is caused by fluctuating forces induced by density differences, due to fluid temperature variation. In mixed convection, both forced and natural convection processes occur simultaneously.

Regardless of the nature of the fluid flow, the rate of heat transfer by convection respects Newton's law of cooling, expressed as

$$\mathbf{q} = \mathbf{h} \cdot \mathbf{A}_s \cdot (T_s - T_\infty) \quad (15)$$

where h is the convection heat coefficient ($\text{W}/\text{m}^2 \cdot \text{K}$); A_s is the area of the surface on which convection heat transfer is taking place (m^2); T_s is the surface temperature ($^\circ\text{C}$ or K) and T_∞ is the fluid temperature far enough from the surface. ($^\circ\text{C}$ or K).

Should be noted that the value of the convection heat coefficient h is experimentally determined and depends on all boundary layer variables that influence convection, such as surface geometry, nature of fluid movement, fluid properties and mass velocity of the fluid.

There are some important considerations to note about Newton's law of cooling. First, when the surface temperature is greater than the fluid temperature, it follows that heat is being transmitted from the surface to the fluid. Second, when the fluid temperature is greater than the surface temperature, it follows that heat is being transmitted from the fluid to the surface. From these two considerations, one can arrange the convection heat transfer rate equation according to the two scenarios mentioned so that the transfer rate results in a positive value.

Finally, the expression that represents the thermal convection resistance is obtained from a reorganization of Newton's law of cooling, given by

$$\mathbf{q} = \frac{(\mathbf{T}_s - \mathbf{T}_\infty)}{\mathbf{R}_{\text{conv}}}, \quad (16)$$

$$\text{with } \mathbf{R}_{\text{conv}} = \frac{1}{\mathbf{hA}} \quad (17)$$

where \mathbf{R}_{conv} is the thermal resistance of the convection surface against heat or the thermal resistance of convection (K/W). It is worth noting that, regardless of the surface geometry, when the convective coefficient is very high, resistance $h \rightarrow \infty$ of convection is equal to zero, this means that the surface does not offer any resistance to convection, therefore, it does not hinder the passage of heat. This case is commonly observed on surfaces that boil and condense.

2.1.3 Radiation

Unlike transfer by conduction and convection, transfers that occur by radiation do not require the presence of a material medium. Radiation is the energy emitted by the matter through electromagnetic waves due to changing electron configurations of atoms or molecules.

For the study of heat transfer, what matters to us is thermal radiation, which differs from other forms of radiation that are unrelated to temperature such as electromagnetic radiation, gamma rays, x-rays, microwaves, radio and television waves. Thermal radiation is the energy emitted by matter at a non-zero temperature.

As the main energy source in the solar system, solar radiation, when crossing the Earth's atmosphere, can be absorbed, reflected or dispersed depending on the presence of particles and gases present in it. In the process of transmitting solar radiation, opaque materials absorb or reflect part of the received energy and transparent materials allow direct or diffuse transmission of the incident energy portion.

Solar Absorbance

According to Dornelles (2008), solar absorbance corresponds to the amount of radiant energy absorbed by a surface as a result of the total energy incident on it. This characteristic depends on variables such as absorptivity, surface color, roughness, geometric shape of the body, among others.

Also according to Dornelles (2008), solar absorbance has a direct effect on the temperatures reached by surfaces exposed to solar radiation, which influence the intensity of the thermal flux that permeates constructive systems. Thus, it is interesting to be aware of the characteristic whose objective is to mitigate heat gains in buildings and promote better thermoenergetic performance.

Relationship Between Absorbance, Reflectance and Transmittance

The relationship that defines the amount of radiant energy incident on the surface of a material transfigured by means of absorption, reflection and transmission could be expressed from the first law of thermodynamics (ASHRAE, 2017b):

$$\alpha + \rho + \tau = 1 \quad (18)$$

where α is the absorbance, absorbed portion from incident radiation (-); ρ is the reflectance, reflected portion from incident radiation (-); τ is the transmittance, transmitted portion from the incident radiation (-).

In opaque materials, the total radiant energy incident on surfaces is determined through the absorbance and reflectance portions. The transmittance, in this case, is null. In view of this, it is possible to determine any one of the properties based on the other (Dornelles, 2008).

$$\alpha = 1 - \rho \quad (19)$$

2.2 Energy Balance

The energy balance in the building envelope is based on the first law of thermodynamics, the law of energy conservation. This law establishes that the amount of thermal energy (heat) that enters a control volume—in this case the envelope (E_e), plus the amount of heat generated inside the volume (E_g), minus the amount of energy that leaves the volume (E_s) must equal the increase in the amount of stored energy (E_{ar}) in the control volume.

$$E_e - E_s + E_g = E_{ar} \quad (20)$$

2.3 Thermal Bridges

According to EN ISO 10211, thermal bridges could be defined as portions of the building envelope in which the thermal resistance changes significantly, due different thermal conductivities of the materials used, thickness and layers variations, differences in external and internal areas of the building, etc.

Some works such as presented by Freitas et al (2016) and Gioelli et al. (2015) reported the importance of including this mechanism in thermoenergy simulations, justified by the growing impact of energy consumption in buildings at different bioclimatic zones.

2.4 Building Performance

Social interest housing are buildings provided by actions of the federal government in partnership with states, municipalities, private companies and non-profit entities whose purpose is to guarantee subsidies to the low-income population that does not have access to formal housing or conditions for such. This federal program continues to expand and improve as technology advances and there are regulatory norms establishing limits to be respected for each necessary housing requirement. In accordance with this, it is common knowledge the precariousness in the quality in which these buildings were built. As a result of this, the NBR 15,575 (2013) standard emerged, aiming to recommend construction parameters for new housing buildings, with an emphasis on housing of social interest, and establish the responsibility between the agents involved in the civil construction field: builders, suppliers, designers and users. In this way, it is possible to guarantee urban development and reduce the housing deficit while maintaining decently acceptable housing conditions.

ISO 6241, which was developed in 1984, was a milestone in terms of the concept of performance, due the definition of fourteen basic requirements that should be met by construction products, including stability, fire safety, air purity and quality, acoustic comfort, visual comfort, safety in use, tactile comfort, among others.

Through the definition of qualitative requirements and quantitative premises or criteria, it could be established that performance is studied worldwide, through methods that allow understandable assessments of meeting the requirements made by the user, when the built unit is inhabited (NBR 15,575, 2013).

The standard makes it clear that for all the requirements and criteria that are available in it, there is a minimum level of performance that must be considered and, consequently, meted, considering basic health and safety needs, as well as the economic factor. In addition to it, the standard mentions intermediate and superior performance, the latter being optional (NBR15575-1, 2021). It is of great importance to emphasize how the thermal performance in buildings must be appreciable, especially in low-income buildings.

In accordance with this the thermal performance of a building depends on several factors that must be observed both in the building itself, such as the temperature, relative humidity, materials used, dimensions, the number of floors, etc. (CBIC, 2013).

For Siqueira (2005): “A building designed for the climate in which it is located becomes comfortable, in addition to saving energy”. What is quite satisfactory for the user, considering that in addition to providing comfort, the economic factor will be very beneficial.

In the computational simulation procedure, the normative method, established by NBR 15,575 (2013) is based on comparisons between the air temperature outside the building with the internal air temperature inside environments, criticized by the bioclimatic zone belonging to the building. These temperature values are referenced in typical summer and winter days that represent, respectively, the maximum and minimum annual temperature; the typical days should be determined according to the climatic data in which the building is located. In the thermal performance evaluation, it is defined that only prolonged stay environments, such as bedrooms and living rooms, must be evaluated, although the entire housing unit must be included in the simulation. The standard indicates the choice of the most critical pavement, thermally, in computer simulation, which tends to be the roof floor, as it has a larger area of exposure to radiation effects, and prescribes the choice of the most critical housing unit to represent the level of performance of the building. The service condition adopted in the simulation is based on the use of different room ventilation rates. These values should be equal to 1 air renewal per hour (1 rph); for cases, in summer situations, which did not meet the criteria of the typical day, NBR 15,575 (2013) recommends that a new computer simulation be carried out with the following changes: increase in ventilation to 5 air changes per hour (5 rph), consideration of shading on glazed surfaces (which can be configured as sun protection devices, external or internal, capable of mitigating, at least 50% of the incident direct solar radiation) with a ventilation rate of 1 rph and, finally, the combination of the two previous strategies.

On the other hand, the simulation model proposed by NBR 15,575 (2013) introduces a new simulation concept. In such a case, the housing unit is simulated based on comparisons between the real and reference models and allows the assessment of the units at the minimum, intermediate and higher levels.

This computer simulation procedure evaluates the annual thermal performance of the building envelope in relation to the reference model, which represents the building evaluated with changes (see Table 1) based on normative preconceptions that are both geometric and constructive, such as, for example, reconfiguration of the transparent elements of environments of prolonged stay and modifications in the constructive elements. For the computer simulation program, it is required to be in accordance with ASHRAE 140, able to model the effects of thermal inertia, consider heat exchanges between soil and building, calculate latent and sensitive thermal loads, capable of simulating shading effects, elements outside the thermal zones and cross ventilation in one or more rooms.

Table 1 Characteristics of the reference model

Thermal properties of the building elements for the reference model						
Element	Thermal conductivity W/mK	Specific heatJ/kgK	Solar radiation absorbance	Long wave emissivity	Density kg/m ³	
Outer walls	1.75	1000	0.58	0.9	2200	
Internal walls	1.75	1000	real model value	real model value	2200	
floors	1.75	1000	real model value	real model value	2200	
Tile (6 mm thick)	0.65	840	0.65	0.9	1700	
Slab (100 mm thick)	1.75	1000	real model value	real model value	2200	
Thermal properties of the roof insulation material for the reference model in the bioclimatic zone 8						
Element	Thermal resistance (m ² K)/W		Absorbance to solar radiation		Long wave emissivity	
Thermal insulation	1.75		0.7		0.9	
Characteristics of the transparent elements in the frames for the reference model						
Element	Solar factor		Thermal transmittance W/m ² K			
Transparent elements	0.87		5.7			
Percentage of opening for ventilation in the frames for the reference model						
Element	Percentage of opening for ventilation (%)					
Ventilation opening	7.65					

(continued)

Table 1 (continued)

Thermal properties of the building elements for the reference model			
Characteristics of frame profiles for the reference model			
Element	Absorbance to solar radiation	Long wave emissivity	Thermal conductance $W/m^2 K$
Frame profiles	0.58	0.9	56

Initially, an analysis of the climate file must be carried out to determine the parameters and normative criteria from the average of the external dry bulb temperatures. Therefore, it is possible to identify the operating temperature values used in the parameter percentage of hours occupied within an operating temperature range (PHFT). The parameters used to meet the minimum level of performance are the PHFT indicator and annual maximum or minimum operating temperatures during the occupation of extended stay environments, the analysis to determine the minimum level of thermal performance comprises computational models operating with natural ventilation.

In the numerical analyses whose purpose is to verify the service of the housing unit at the intermediate or higher level, the criteria used to determine the minimum level are replicated, with a difference in the PHFT parameter, which makes a difference between the values obtained in the real and reference model and compared with the normative minimum values. As the last parameter used in the evaluation of the intermediate or higher level, calculations are carried out for the reduction of the total thermal load (cooling and heating) between the real and reference models to compare with the minimum defined due to meeting each level of thermal performance. The calculations of total thermal load reduction (cooling and heating) are performed between the real and reference models to compare with the minimums defined in terms of meeting each level of thermal performance. The calculations of total thermal load reduction (cooling and heating) are performed between the real and reference models to compare with the minimums defined in terms of meeting each level of thermal performance.

3 Methodology

The methodology used to carry out this research was based on four main steps:

- Choice of two buildings: one house of social interest (HIS) and another framed in the high standard profile,
- Modeling the buildings through sketchup and computational numerical simulation using the EnergyPlus software,
- Numerical analysis of the results obtained from the numerical simulations.

3.1 Buildings Analysed

The buildings considered in this work were simulated, located in the city of Recife, capital of the state of Pernambuco, and are part of the bioclimatic zone 08, according to NBR 15,220-3 (2005). For the purposes of this research, housing units facing northwest were chosen as the object of study of the work, representing the critical condition for buildings located in hot climates.

The architectural project on the ground floor of the social housing and the high-end building with the environments considered in this analysis are represented in Figs. 4, 5, 6, 7. The HIS-type building has four floors that each have eight apartments; the high-end building is configured in a 20-story tower, having a total of 40 housing units (two per floor).

Tables 2 and 3 indicate the constructive composition of the opaque and translucent materials used in the analyzed buildings. The calculations performed to obtain the values of thermal transmittance and thermal capacity of opaque materials followed the recommendation of the NBR 15,220-2 (2005) standard.



Fig. 4 Sketch of the ground floor plan, from HIS, with representation of the evaluated environments



Fig. 5 Floor plan of the type and roof pavement, from HIS, with representation of the evaluated environments

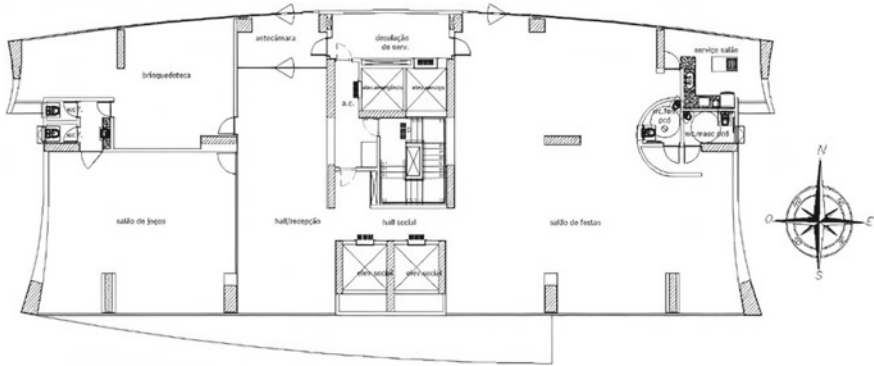


Fig. 6 Ground floor plan of the high-end building

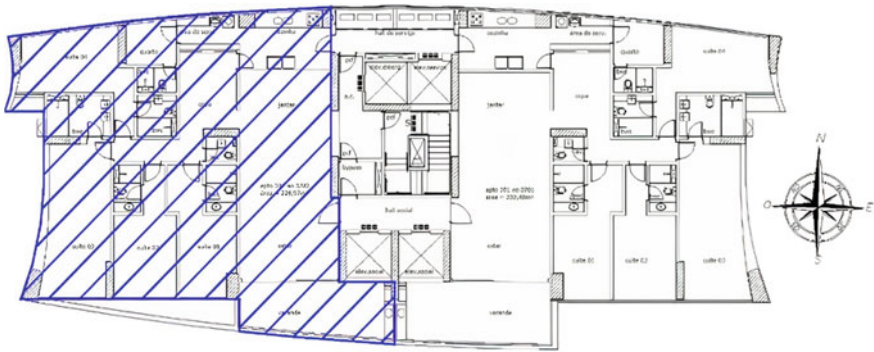


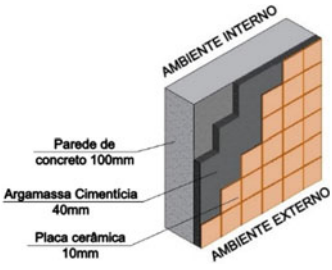
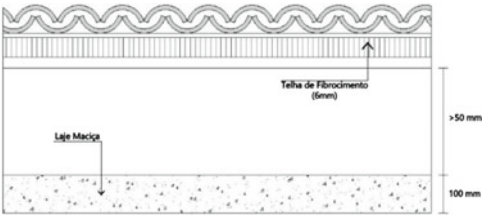
Fig. 7 Floor plan of the type and roof pavement of the high-end building, with representation of the evaluated environments

3.2 Computer Modeling and Simulation

As described in the previous sections, the three-dimensional modeling was performed in Sketchup software (see Figs. 8, 9), using the OpenStudio plugin that intercepts the modeling data for calculation in EnergyPlus.

EnergyPlus is a thermo-energetic simulation program, created from the BLAST and DOE-2 programs, the origin of which refers to concerns arising from the energy crisis that affected the United States in the 70 s, and had as target audience the designers who they wanted to dimension HVAC equipment (Heating, ventilation and air conditioning), to optimize the thermo-energetic performance of buildings, etc. EnergyPlus was developed by the Building Technologies Office (BTO), an agency linked to the DOE (United States Department of Energy), in partnership with the National Renewable Energy Laboratory (NREL), private sector companies and academic institutions (DOE, 2020 and NREL, 2020).

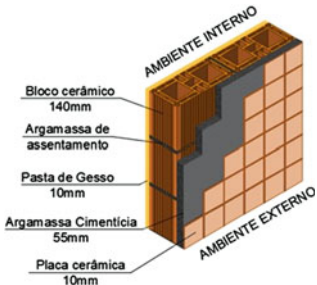
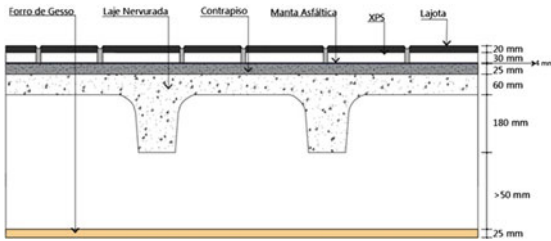
Table 2 Physical characteristics of the materials used in the housing envelope of the HIS type

Physical properties of opaque materials	
External vertical sealing system	Thermal characteristics
	Thermal transmittance (U) 3.66 W/m ² K
	Thermal capacity (CT) 338.4 kJ/m ² K
	Solar absorbance of the external coating (α) 0.3
Cover system	Thermal characteristics
	Thermal transmittance (U) 2.07 W/m ² K
	Solar absorbance of the external coating (α) 0.3
Thermoenergetic and luminous properties of translucent materials	
Thickness (mm)	4.00
Transmission to solar radiation (%)	83.0
Reflectance to solar radiation—external (%)	8.00
Solar radiation reflectance—internal (%)	8.00
Visible transmittance (%)	89.0
Visible radiation reflectance—external (%)	8.00
Visible radiation reflectance—internal (%)	8.00
Emissivity (%)	0.89
Thermal Conductivity (W/mK)	1.00

Widely used in Brazilian research (Santos, 2018). The EnergyPlus computational tool is certified “ASHRAE Standard 140” for the calculation of envelopes, as well as meeting the requirements of standards and regulations such as, for example, NBR 15,575 (2021), ASHRAE Standard 90.1 (2016), among others. Written in Fortran 90 language, EnergyPlus communicates easily with other programs as it presents a well-defined modular structure (LBNL, 2010).

EnergyPlus allows you to carry out simulations involving the interaction of the building in the environment of which it is inserted, soil-building interaction, consideration of internal loads such as people and their respective energy values of metabolic rates, energy consumption of lighting and equipment, cross ventilation

Table 3 Physical characteristics of the materials used in the envelope of the high-end housing

Physical properties of opaque materials	
External vertical sealing system	Thermal characteristics
	Thermal transmittance (U) 2.53 W/m ² K
	Thermal capacity (CT) 264 kJ/m ² K
	Solar absorbance of the external coating (α) 0.3
Cover system	Thermal characteristics
	Thermal transmittance (U) 0.76 W/m ² K
	Solar absorbance of the external coating (α) 0.6
Thermoenergetic and luminous properties of translucent materials	
Glasses used in frames exempt from safety requirements	
Thickness (mm)	4.00
Transmission to solar radiation (%)	44.0
Reflectance to solar radiation—external (%)	5.00
Solar radiation reflectance—internal (%)	5.00
Visible transmittance (%)	72.0
Visible radiation reflectance—external (%)	7.00
Visible radiation reflectance—internal (%)	7.00
Emissivity (%)	0.89
Thermal Conductivity (W/mK)	1.00
Glass used in frames that meet safety requirements	
Thickness (mm)	8.40
Transmission to solar radiation (%)	26.0
Reflectance to solar radiation—external (%)	5.00
Solar radiation reflectance—internal (%)	5.00
Visible transmittance (%)	57.0
Visible radiation reflectance—external (%)	6.00
Visible radiation reflectance—internal (%)	6.00
Emissivity (%)	0.89
Thermal Conductivity (W/mK)	1.00

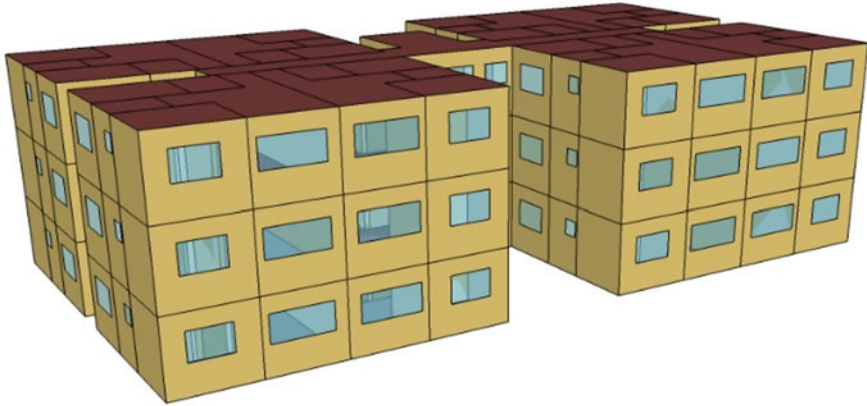


Fig. 8 HIS modeling, used in the analysis

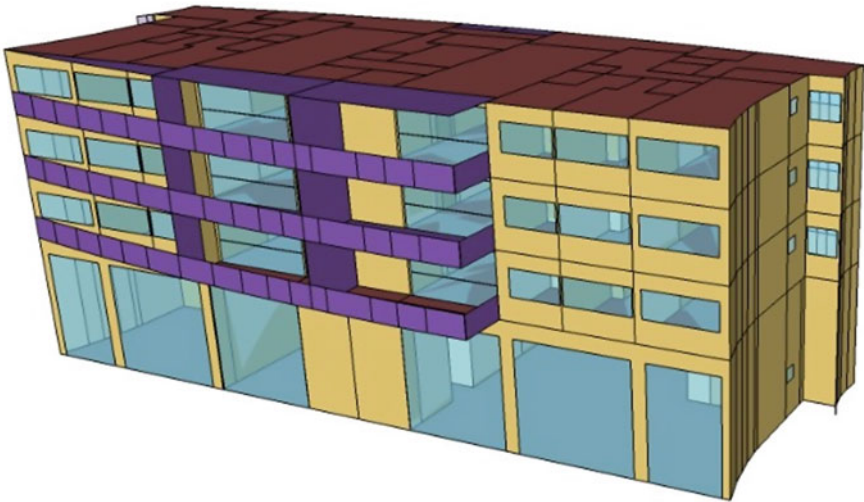


Fig. 9 High standard building modeling used in the analysis

effects, shading, insertion of HVAC systems in environments, photovoltaic systems etc. The software's calculation model is based on the fundamental principles of mass and energy balance, making it possible to determine the thermoenergetic behavior of a building, in the inserted climate, and its transient systems in an integrated and simultaneous manner, as well as to reproduce the inertia effects thermal. The program makes available data of great value, with regard to the investigation of energy efficiency and thermal performance of a building, for example, annual energy consumption by cooling or heating, internal temperature in simulated environments, surface temperature, etc. To provide this output data, EnergyPlus works with three modules:

simulation manager module (responsible for controlling the simulation process), heat and mass balance simulation module and building systems simulation module (DOE, 2020).

In this study, the buildings were modeled according to their architectural design and corresponding geographic north. The type of climate file adopted was the INMET file for the city of Recife/PE. The SLAB pre-processor method was used in order to calculate the thermal exchanges between the ground floor of the building and the ground, thus continuing the simulations and evaluating the buildings thermoenergetically.

4 Results and Discussion

4.1 Results According to NBR 15,575 (2013)

The numerical results represents the analyzes carried out in accordance with the parameters established by NBR 15,575 (2013). The criteria for buildings in bioclimatic zone 08 refers only the evaluation of the building for a typical summer day. So, the internal air temperature inside the rooms is less than or equal to the outside air temperature and is characterized as the requirement to meet the minimum level of thermal performance. It should be noted that the typical summer day considered for evaluation was February 22.

To meet the intermediate and higher levels, it is necessary that the internal temperatures of the environments have a decrease in the total value equivalent to that established by standard, in accordance with the corresponding bioclimatic zoning of the building. Thus, the established decrease, referring to bioclimatic zone 08, to service the intermediate and higher level is $-1\text{ }^{\circ}\text{C}$ and $-2\text{ }^{\circ}\text{C}$, respectively.

4.1.1 Building of Social Interest

Figure 10 shows results obtained for the maximum annual operating temperature are expressed for the typical summer day considered. Three lines are also represented that define the maximum criteria required for each level of performance investigated.

It is observed, from the Fig. 10, that the HIS-type building met the thermal performance requirement for all the environments evaluated, adopting a ventilation rate of 1 air change per hour, called the standard condition. The Room 02 environment served at an intermediate level of thermal performance, however, as the Living and Room 01 environments only respected the minimum level of service, the indicative profile that expresses the building's level of service is consistent with the minimum level of performance thermal.

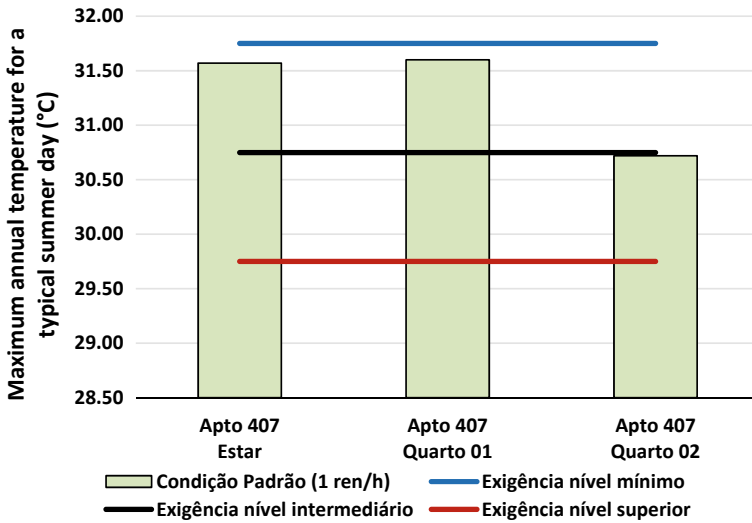


Fig. 10 Numerical results for the HIS-type building

4.1.2 High Standard Building

Figure 11 indicates the representation of the values obtained in the simulation of the high standard building for evaluating the compliance with the thermal performance requirement, as well as the ranges of requirements corresponding to each level of service.

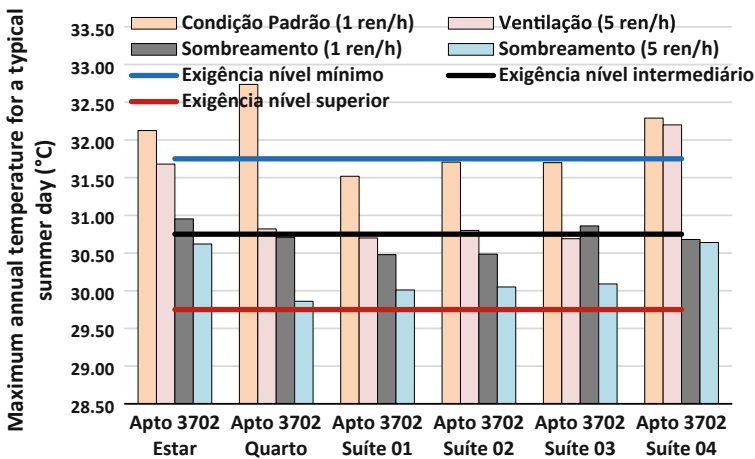


Fig. 11 Numerical results for the high standard building

According to Fig. 11, it is possible to observe that the numerical simulations with ventilation rates of 1 air change per hour (1 rph) and 5 air changes per hour (5 rph) did not meet the minimum level of thermal performance. There are environments as the living room, bedroom (all with 1 rph) and Suite 4 (1 rph and 5 rph), which exceeded the recommended limits to meet the requirement. However, when the simulation was carried out with the adoption of shading in the frames, the minimum level of thermal performance was met for the simulated condition considering a ventilation rate of 1 rph, at an intermediate level, when the ventilation rate of 5 rph.

4.2 Numerical Results According to NBR 15,575 (2021)

Below are the products of the simulations for thermal performance evaluation in accordance with NBR 15,575 (2021). The evaluation is divided into two parts: the first refers to the analysis for evaluating the project at the minimum level of thermal performance, which is the normative requirement, and the last one relates to the analysis for evaluating the intermediate and higher level.

Before carrying out the simulations, normative amendment 1 recommends the verification of the climate file as the average value of the external dry bulb temperature (TBSm) to determine the operating temperature values to be considered in the calculation of the parameter of the percentage of hours occupied within a comfort temperature range (PHFT). According to the simulations carried out, the TBSm value obtained for the climate file INMET Recife was 25.19 °C and, therefore, operating temperatures below 28 °C (interval 2) were the criterion adopted for calculating the PHFT. Figure 12 expresses the behavior of external temperatures of dry bulb in the city of Recife during the year.

Fulfilling the objective of generating comparative effects, only the simulations carried out in the high-end building will have shading adoptions in the frames. That said, the simulations in the HIS-type building will be carried out without the use of shading generator devices.

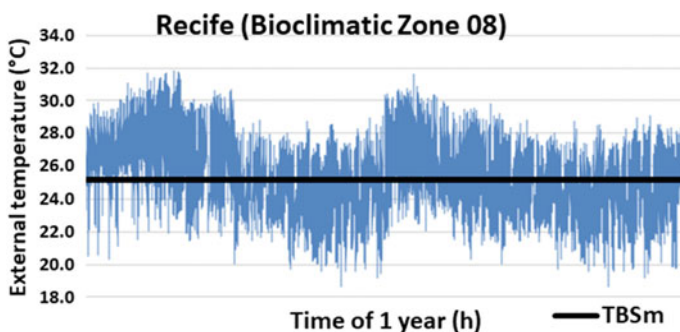


Fig. 12 Annual behavior of the external dry bulb temperature for the city of Recife/PE

4.2.1 Building of Social Interest

The following sections present the thermal performance evaluations for the minimum to the superior level of performance, based on the numerical results obtained from different simulations.

Assessment at the Minimum Level of Thermal Performance

In Fig. 13, the normative parameters used to verify the minimum level of thermal performance are illustrated, which are the percentage of hours occupied in the operating temperature range (PHFT) and the maximum annual operating temperature.

In view of the results obtained, it is observed that the HIS-type building provided an excellent distance margin, compared to the values obtained in the reference model. The criterion for minimum level was met in all floors, as the PHFT of the real model was greater than 90% of the PHFT belonging to the reference model. The criterion



Fig. 13 Numerical results for evaluating the minimum level of performance of the social building



Fig. 14 Numerical results for evaluating the intermediate and superior level of performance of the social building

of maximum annual operating temperatures was also met, taking into account that, on both floors, the maximum annual operating temperatures of the real model were lower than those obtained in the reference model with the respective increments.

Assessment at Intermediate and Upper Level of Thermal Performance

Data for investigating compliance with the attenuated regulatory conditions at the intermediate and higher levels are presented in Fig. 14. The established criteria are defined based on an analysis of the percentage increase of hours occupied in the operating temperature range (PHFT), maximum annual operating temperature, similarly to what is required in meeting the minimum level, and reduction of the total thermal load (RedCgTT).

In view of the results presented in the figure above, it is possible to verify that the intermediate level of the PHFT increment criterion was met, since the three floors analyzed had values greater than the minimum required. The minimum values for

the increment of the PHFT are determined when the calculation of the PHFT of the reference model is inferior to 70%. On the other hand, to meet the intermediate level of the total thermal load reduction criterion, the condition of compliance is given when the real model has lower energy consumption compared to the reference model; in the case in question, the intermediate floor does not meet the RedCgTT criterion and therefore implies that the HIS building does not meet the intermediate level of thermal performance.

In the analysis of the service of the building at the higher level, the criteria used in the maximum annual operating temperature and minimum increment of the PHFT are maintained, however, minimum values of thermal load reduction of the real model compared to the reference model are determined. Given the ratio of the total thermal load of the reference model to the sum of the areas of the long-stay environments, the minimum required reduction is 40, 50 and 40% for the ground, 3th and top floors, respectively.

4.2.2 High Standard Building

In this section, thermoenergetic simulations are presented to evaluate the thermal performance of the high-end building. These simulations are divided into two parts: without adopting shading in the frames and with admission of shading in the frames. A priori, the results obtained are verified regarding the attendance at the minimum level and later the evaluation of the attendance at the intermediate and higher level.

Simulation Without Shading in the Frames

Assessment at the Minimum Level of Thermal Performance

Figure 15 shows the results obtained in the simulation of the high standard building without the use of shading in the frames through graphics that will be used in the evaluation of the thermal performance at the minimum level.

In light of the above, it is noted that a high-end building met the PHFT criterion on the ground and intermediate floor, however the roof floor obtained lower values corresponding to the PHFT parameter of the real model when compared with a 10% reduction in the calculated PHFT in the reference model and provokes the disapproval of the high standard building at the minimum level of performance. However, the established criterion for evaluating the maximum annual operating temperatures was respected in all analyzed pavements.

Assessment at Intermediate and Superior Level of Thermal Performance

Taking the assessment of the minimum level of thermal performance as an example, it is to be expected that the building under analysis does not meet the intermediate or higher level. In this way, from the Fig. 16 it can be seen that the analyzed building does



Fig. 15 Numerical results for evaluating the minimum level of performance of the high standard building

not meet the intermediate or superior level of thermal performance, as the roof floor obtained negative values in the difference in PHFT between the real and reference model and thermal load reduction; and the real model of the ground floor also proved to be less efficient than the real model in terms of thermal load reduction. As a result of these data, both the intermediate level and the upper level cannot be reached.

Simulation with Shading in the Frames

Assessment at the Minimum Level of Thermal Performance

As the last simulation condition, the high-end building was simulated with additions of devices that cause shading in the frames, capable of reducing, at least, 50% of the direct solar radiation. Figure 17 shows the numerical results obtained from the building in question to assess compliance with the minimum level of thermal performance.



Fig. 16 Numerical results for evaluating the intermediate and superior level of performance of the high standard building

According to the results expressed in Fig. 17, it is possible to notice the gain achieved in the real model in the PHFT indicator with shading admission in such a way that the strategy allowed the reaching of the high standard building to the minimum level of performance. Despite having met in the simulation situation without the use of shading devices, a decrease in annual maximum operating temperature values was also verified and the parameter remained met.

Assessment at Intermediate and Superior Level of Thermal Performance

Finally, the project was simulated with the admission of shading in the frames to assess the service at the intermediate or higher level. The results obtained in the numerical simulations are presented in Fig. 18, that represents the building’s efficiency in terms of the PHFT indicator and thermal load reduction compared to the reference model.

According to the efficiency level of the parameters, represented by Fig. 18, the successful advance in thermal performance indicators is evidenced by the real model



Fig. 17 Numerical results for evaluating the minimum level of performance of the high-end building

of the high-end building when comparing it with the reference model. Investigating the data to check the service at the intermediate level, the PHFT values of the real model were sufficient to meet the normative criteria required for both conditions imposed on the PHFT value of the reference model. According to the total thermal load reduction table (RedCgTT), the ground and intermediate floors met the established minimum, 0 and 25%, respectively, but the roof floor did not have a satisfactory percentage of RedCgTT to meet the minimum required which should be greater than 20%

The parameters required to service the higher level are the same as those for the intermediate level, with the exception of the criteria used in the minimum values for RedCgTT, which are more rigorous. Similarly, because the building does not meet the RedCgTT criteria required for the intermediate level, the studied building does not meet the higher level. To achieve this service, the percentage of RedCgTT should be greater than 40% for the ground floor, 50% reduction for the intermediate floor and 40% for the roof floor.



Fig. 18 Numerical results for evaluating the intermediate and superior level of performance of the high-end building

5 Conclusions

Based on the simulations performed, some considerations could be presented about this work:

- The characteristic profile of the level of performance between the buildings studied was maintained, despite the different procedures between the two normative methods;
- The building framed in the HIS class met the minimum level of performance with some clearance. Because of having construction systems and glazed areas similar to the reference model, buildings of type HIS with solar upper-bodies smaller than the reference model follow a strong tendency to meet the minimum level of performance in hot climate regions.
- To achieve the minimum level of thermal performance, buildings with large glazed areas, as was the case with the high standard building, can follow a trend with higher requirements of the thermal properties of the materials that compose them;

- The analysis, promoted by the new method, represents a progress in the elaboration of the computational methodology of thermal performance, taking into account the annual simulation of the building and withdrawal of the analysis criteria considered of typical summer and winter days. Thus, it is possible to optimize strategies to obtain better thermos-energetic indices of a building;
- The PHFT indicator allows for more significant analyses, especially with regard to the thermal behavior of housing units during the year;
- The thermal load analysis, required to meet the intermediate and higher levels, affects the normative advance in the study of energy efficiency in buildings.

Finally, some future recommendations:

- Comparison between models with high and low values of thermal inertia, for different values of external solar absorbance;
- Feasibility study encompassing energy efficiency between alternative scenarios with more efficient construction systems thermos-energetically than those presented in the real model;
- Comparative simulation between projects contemplated in regions with different bioclimatic zoning.

Acknowledgments This study was financed by the Base Funding - UIDB/04708/2020 and Programmatic Funding - UIDP/04708/2020 of the CONSTRUCT - Instituto de I&D em Estruturas e Construções - funded by national funds through the FCT/MCTES (PIDDAC).

References

- ALMEIDA, L. S. S. (2014). Influência de parâmetros físicos e geométricos no desempenho termoenergético de habitações unifamiliares. Dissertação (Mestrado em Engenharia Civil)—UFSC.
- AMERICAN SOCIETY OF HEATING, REFRIGERATING AND AIR-CONDITIONING ENGINEERS—ASHRAE. (2016). ANSI/ASHRAE/IESNA Standard 90.1—2016: “Energy Standard for Buildings Except Low-Rise Residential Buildings”. Atlanta.
- AMERICAN SOCIETY OF HEATING, REFRIGERATING AND AIR-CONDITIONING ENGINEERS—ASHRAE. ASHRAE Handbook—Fundamentals (SI). (2017a). Mark S. Owen (Ed.), American Society of Heating, Refrigerating and Air-Conditioning Engineers (ASHRAE), Atlanta, Georgia, USA.
- AMERICAN SOCIETY OF HEATING, REFRIGERATING AND AIR-CONDITIONING ENGINEERS—ASHRAE. (2017b). ANSI/ASHRAE Standard 55—2017: Thermal environmental conditions for human occupancy. American Society of Heating, Refrigerating and Air-Conditioning Engineers, Inc. Atlanta, EUA.
- ASSOCIAÇÃO BRASILEIRA DE NORMAS TÉCNICAS (ABNT). (2005a). NBR 15.220—1: Desempenho térmico de edificações: parte 1: Definições, símbolos e unidades. Rio de Janeiro.
- ASSOCIAÇÃO BRASILEIRA DE NORMAS TÉCNICAS (ABNT). (2005b). NBR 15.220—2: Desempenho térmico de edificações: parte 2: Métodos de cálculo da transmitância térmica, da capacidade térmica, do atraso térmico e do fator solar de elementos e componentes de edificações. Rio de Janeiro.

- ASSOCIAÇÃO BRASILEIRA DE NORMAS TÉCNICAS (ABNT). (2005c). NBR 15.220–3: Desempenho térmico de edificações: parte 3: Zoneamento bioclimático brasileiro e diretrizes construtivas para habitações unifamiliares de interesse social. Rio de Janeiro.
- ASSOCIAÇÃO BRASILEIRA DE NORMAS TÉCNICAS (ABNT). (2013). NBR 15.575: Edificações habitacionais—Desempenho. Rio de Janeiro.
- ASSOCIAÇÃO BRASILEIRA DE NORMAS TÉCNICAS (ABNT). (2013). NBR 15.575: Edificações habitacionais—Desempenho: parte 1: Requisitos gerais. Rio de Janeiro
- ASSOCIAÇÃO BRASILEIRA DE NORMAS TÉCNICAS (ABNT). (2021). NBR 15.575: Edificações habitacionais—Desempenho: parte 1: Requisitos gerais. Em. 1. Rio de Janeiro.
- ÇENGEL, Yunus A., & GHAJAR, Afshin J. (2012). Transferência de Calor e Massa: Uma Abordagem Prática. 4. ed. Porto Alegre: Editora McGrawHill.
- DOE—UNITED STATES DEPARTMENT OF ENERGY. (2021). EnergyPlus: Version 8.1.0. Disponível em: <https://energyplus.net/>. Acesso em: 05 mai.
- DOE—UNITED STATES DEPARTMENT OF ENERGY. (2020). Getting Started—EnergyPlus™ Version 9.4.0 Documentation.
- DORNELLES, Kelen Almeida. (2008). Absortância solar se superfícies opacas: método de determinação e base de dados para tinta látex acrílica e PVA. Tese (Doutorado em Engenharia Civil) —Programa de Pós-graduação da Faculdade de Engenharia Civil, Arquitetura e Urbanismo, Universidade Estadual de Campinas. Campinas.
- EMPRESA DE PESQUISA ENERGÉTICA (EPE). (2021). Consumo de energia elétrica: consumo mensal de energia elétrica por classe (regiões e subsistemas)—1995–2018. Rio de Janeiro: EPE, 2021. Disponível em: <https://www.epe.gov.br/pt/publicacoes-dados-abertos/publicacoes/Consumo-mensal-de-energia-eletrica-por-classe-regioes-e-subsistemas>. Acesso em: 18 abr.
- EMPRESA DE PESQUISA ENERGÉTICA (EPE). (2021). Uso de Ar Condicionado no Setor Residencial Brasileiro: Perspectivas e contribuições para o avanço em eficiência energética. Rio de Janeiro: EPE, 2018. Disponível em: <http://www.epe.gov.br/pt/publicacoes-dados-abertos/publicacoes/nota-tecnica-epe-030-2018>. Acesso em: 18 abr.
- FAJKUS, M. Superficial Skins? Super Skins? Shading Structures and Thermal Impact Analysis. Advanced building skins—energy forum, Bressanone, 2013.
- FREITAS, J. M. R., LEITZKE, R. K., GIOIELLI, B. I., & CUNHA, E. G. (2016, Dez). Análise da influência das pontes térmicas na simulação de eficiência energética nas paredes de edificações residenciais. Revista de Arquitetura IMED, Passo Fundo, vol. 5, no. 2, pp. 24–41. ISSN 2318–1109.
- GIOIELLI, B., ALMEIDA, A., CUNHA, E., & FERRUGEM, A. (2015). Estudo do Efeito de Pontes Térmicas em Estruturas de Concreto Armado no Desempenho Energético de Edifício Hoteleiro Para 4 Zonas Bioclimáticas Brasileiras. XV Encontro Nacional de Tecnologia do Ambiente Construído. Anais do evento. Alagoas.
- INCROPERA, F. P., & DEWITT, D. P. (2008). Fundamentos da Transferência de Calor e de Massa. 6. ed. Rio de Janeiro: LTC.
- INTERNACIONAL ORGANIZATION FOR STANDARDIZATION. (1984). ISO 6241: 1984 Performance standards in bulding: Principles for their preparation and factors to be considered. USA.
- Ioannou, A., & Itard, L. C. M. (2015). Energy performance and comfort in residential buildings: Sensitivity for building parameters and occupancy. *Energy and Buildings*, 92, 216–233.
- ISO 10211. (2017b). Thermal bridges in building construction—Heat flows and surface temperatures—Detailed calculations. International Organization for standardization.
- JARDIM, Patrícia R. S. A. (2011). Desempenho térmico de coberturas: um estudo comparativo entre as telhas de material reciclado, de fibra e betume, fibrocimento e cerâmica. 2011. 124p. Dissertação (Mestrado)—Universidade Federal do Rio Grande do Norte, Natal.
- LAMBERTS, R., DUTRA, L., & PEREIRA, F. O. R. (2014). Eficiência Energética na Arquitetura. 3. ed. São Paulo.
- LBNL. (2010). Getting started With EnergyPlus. US Department of Energy, Version 5.0, USA.

- NOVAIS, J. W. Z., OLIVEIRA, E. V., JOAQUIM, T. D., LEAL, L. A., NOGUEIRA, M. C. J. A., & SANCHES, L. (2014, November). Comparação do Desempenho Térmico de Painéis em EPS como Alternativa aos Tijolos Cerâmicos no Conforto Térmico de Residências em Cuiabá-MT. UNOPAR Científica Exatas Tecnológica, Londrina, vol. 13, no. 1, pp. 39–43.
- NREL. (2021). National Renewable Energy Laboratory. Disponível em: <https://www.nrel.gov/>. Acesso em: 08 mai.
- SANTOS, A. C., LIMA, J. V. S., J. R. G., M. S. G. C. (2018). Uso do EnergyPlus em pesquisas brasileiras. XVII ENCONTRO NACIONAL DE TECNOLOGIA DO AMBIENTE CONSTRUÍDO—ENTAC 2018. Foz do Iguaçu.
- Silva, A. S., & Ghisi, E. (2014). Análise comparativa dos resultados do desempenho térmico da envoltória de uma edificação residencial pelos métodos de simulação do RTQ-R e da NBR 15575-1. *Ambiente Construído*, 14, 213–230.
- SIQUEIRA, Tulio C. P. A., et al. (2005) Dados Climáticos para avaliação de desempenho térmico de edificações. Esc. Minas, Ouro Preto, MG.
- SORGATO, M., MELO, A., & LAMBERTS, R. (2013). Análise do método de simulação de desempenho térmico da norma NBR 15575. ENCAC 2013.
- SPECHT L. P., BORGES P. A. P., RUPP, R. F., & VARNIER, R. (2010). Análise da transferência de calor em paredes compostas por diferentes materiais. *Revista Ambiente construído*, porto alegre.
- TRIMBLE INC. SketchUp: Versão 8.0.15158. 2012.
- YOSHINO, H., HONG, T., & NORD, N. (2017, March). IEA EBC Annex 53: total energy use in buildings, analysis and evaluation methods. *Energy and Buildings*, 152, 124–136.